Surgical treatment of meniscal extrusion associated with medial meniscus posterior root tears: An in-vitro biomechanical study comparing centralization techniques

A DISSERTATION SUBMITTED TO THE UNIVERSITY OF BIRMINGHAM IN FULFILMENT OF THE REQUIRMENTS FOR THE DEGREE OF

Masters by Research in Mechanical Engineering, University of Birmingham

Author: Khalis Ahmed Boksh
Student ID: [redacted]
Academic Year: 2023-24
Word count: 22,289 (excluding acknowledgements, abstract, list of contents, figures, tables, and references)

Abstract

Background

Medial meniscus posterior root tears (MMPRTs) are associated with meniscal extrusion and can alter tibiofemoral contact mechanics. This accelerates chondral injury, leading to early degeneration of the knee joint. Despite the success of root repairs, post-operative extrusion can persist, with suboptimal healing and progressive osteoarthritis. Centralization techniques as an adjunct to root repair have recently emerged to counter extrusion. This includes the transtibial and suture anchor techniques. However, biomechanical comparison between the two are required to determine the most suitable technique.

Purpose

To quantitatively compare the tibiofemoral contact mechanics and extent of meniscal extrusion between an isolated root repair, and a repair in conjunction with a transtibial or suture anchor centralization technique to determine which method closely restores the normal loading profile of the knee.

Methods

Twelve porcine knee joints were used and underwent testing under the following conditions: (1) intact state; (2) MMPRT; (3) anatomical transtibial pull-through repair (ATPR); (4) ATPR and transtibial centralization (TTC); and (5) ATPR and two-anchor centralization (2AC). The testing protocol loaded knees with a 200 N axial compressive force at 4 flexion angles (30°, 45°, 60° and 90°). Two-dimensional motion analysis using digital photography and imaging software was used to measure extrusion. Peak contact pressure and contact area were analysed in a customized MATLAB program.

Results

Medial meniscus extrusion was significantly reduced after ATPR + TTC than after ATPR or ATPR + 2AC at 60° (2.68 mm vs. 4.39 mm vs. 4.09 mm, $p < 0.001$), and 90° (2.99 mm vs. 4.75 mm vs. 4.36 mm, $p < 0.001$). The contact area was significantly greater with ATPR + TTC compared to ATPR + 2AC at 60° (693.31 mm^2 vs. 603.13 mm^2, $p = 0.011$), and with ATPR at 60° (693.31 mm^2 vs. 601.01 mm^2, $p = 0.008$) and 90° (619.68 mm^2 vs 563.97 mm^2, $p = 0.037$). ATPR + TTC significantly reduced peak contact pressure compared to ATPR at 45° (4.97 MPa vs. 5.60 MPa, $p = 0.02$), and 60° (5.20 MPa vs. 5.99 MPa, $p = 0.03$), whilst ATPR + 2AC only reduced such pressure at 60° (5.23 MPa vs 5.99 MPa, $p = 0.03$). Both centralization techniques showed similar peak contact pressure at all angles.

Discussion

The ATPR + TTC best restored extrusion and contact mechanics of the knee when compared to other fixation methods. Except for contact pressure at 60°, there were no differences between ATPR and ATPR + 2AC. Future comparative trials are required to determine the true clinical efficacy between the techniques.

Acknowledgements

I am incredibly grateful to my supervisors Professor Duncan Shepherd and Dr. Daniel Espino for their willingness to guide me through this project, enabling me to develop my ideas freely and productively. Despite coming from a medical background, their advice and support helped to facilitate my understanding in basic concepts in engineering, whilst also developing the skills required to run independent work in the biomedical laboratory both safely and effectively.

I am grateful to Mr. Lee Gauntlett, a key stalwart in the Engineering centre, for allowing my ideas to become a reality, and helping me to solve challenges faced with the design and properties of testing materials.

I am thankful to Mr. Tarek Boutefnouchet, consultant orthopaedic surgeon at the University Hospitals of Birmingham NHS Trust. His role as clinical supervisor played an essential role in my expertise to carry out the 'surgical' side of the experiment, and his teaching allowed me to perform the experiments to a high standard.

I am indebted to the Royal College of Surgeons and Orthopaedic Research UK, who provided a 1-year research fellowship to support my work. Without your help, this research may not have been possible, and so I thank you for your role in allowing this important topic to come to fruition.

I thank you, the reader, for sharing a fondness in developing techniques to improve the daily lives of our patients. I hope when you are reading this, more innovative ideas surface, so that future avenues can be explored to further optimize treatments for patients.

I would like to thank my parents for helping me to maximise my potential. My father for the sacrifices he made for me to be where I am today, and my mother for helping me to deal with setbacks and challenges I have gone through during my education.

And finally, I would like to show my appreciation to my wife Shanaz, my daughter Hana, and the new member of the family this December. Their unwavering support and patience played a pivotal role in helping me to achieve my goals, whilst driving me to constantly keep achieving. I send my apologies to the late nights working, and I hope to always keep them proud.

Funding Statement

This Masters by Research was funded jointly by the Royal College of Surgeons of Edinburgh and Orthopaedic Research United Kingdom. The funding was provided over a 1-year period.

TABLE OF CONTENTS

LIST OF FIGURES

LIST OF TABLES

ACRONYMS

2AC: two-anchor centralization

ACL: Anterior cruciate ligament

ATPR: anatomical transtibial pull through repair

IKDC: International Knee Documentation Committee score

KOOS: Knee Injury and Osteoarthritis Outcome Score

LCL: lateral collateral ligament

LMPRT: Lateral meniscus posterior root tears

MCL: meniscofemoral ligament

MM: medial meniscus

MMA: modified Mason-Allen

MME: Medial meniscal extrusion

MMPRT: Medial meniscus posterior root tears

MTE: medial tibial eminence

NATPR: non-anatomical transtibial pull through repair

PCL: Posterior cruciate ligament

PCP: peak contact pressure

POL: posterior oblique ligament

TFCM: tibiofemoral contact mechanics

TSS: two simple stitches

TTC: transtibial centralization

UHMWPE: Ultra High Molecular Weight Polyethylene

CHAPTER 1

1. Introduction

The meniscal roots for both the medial and lateral meniscus of the knee are responsible for its anchorage on the tibial plateau. On loading, they convert axial loads to circumferential hoop stresses across the meniscus (Andrews et al., 2017), helping to preventing meniscal extrusion and maintain normal knee kinematics (Kennedy et al., 2020; Pache et al., 2018).

Meniscal root tears are either complete radial tears within 1 cm of its tibial attachment point or bony or soft tissue avulsion injuries (LaPrade CM et al., 2015a). Medial meniscus posterior root tears (MMPRT) are becoming increasingly recognized, with it accounting for up to 30% of all medial meniscus tears (Bin et al., 2004). Furthermore, they are more susceptible to injury than lateral meniscus posterior root tears (LMPRT) as they bear more load and are less mobile than their counterpart (Bonasia et al., 2015). Often, they are degenerative injuries resulting from low energy mechanisms, and present commonly in the middle-aged population (Carreau et al., 2017; Hwang et al., 2012)

In the presence of a meniscal root tear, axial compressive forces are no longer distributed intrinsically as tensile hoop stresses within the meniscus (Banovetz et al., 2022). This can subsequently force the meniscus to extrude out of the joint space (Costa et al., 2004; Johannsen et al., 2012; LaPrade et al., 2015b; LaPrade et al., 2015c), leading to a decrease in contact area over which the tibiofemoral compressive loads are distributed, and an increase in tibiofemoral contact pressures (LaPrade et al., 2014; LaPrade CM et al., 2015b; LaPrade et al., 2021; Marzo et al., 2009; Mueller et al., 2016). A landmark paper revealed that meniscal root tears are equivalent to total meniscectomies in the resulting biomechanical function of the knee (Allaire et al., 2008).

Meniscal extrusion, defined as the excursion and subluxation of the meniscus outside of the meniscotibial compartment (Crema et al., 2012; Kim et al., 2020), will eventually defunctionalize the meniscus. The link between extrusion and progression of degenerative joint disease is well established in the literature. Numerous studies have identified extrusion as an independent predictor of tibiofemoral cartilage loss, joint space narrowing and osteoarthritis (OA) in the knee (Adams et al., 1999; Berthiaume et al., 2005; Gale et al., 1999; Wang et al., 2010). Extrusion can however be seen in healthy knees on weightbearing, where values less than 3mm between the outer edge of the meniscus and tibial plateau are considered 'physiological' (Patel et al., 2016). Values greater than 3 mm show high sensitivity to chondral injury, bone marrow lesions and OA and are deemed 'pathological' (Svensson et al., 2019).

Prognosis is generally poor with meniscal root tears associated with pathological extrusion. Non-operative treatment has shown to negatively impact joint longevity, with poor clinical outcomes, progressive OA, and high conversion to total knee arthroplasty (Krych et al., 2017; Neogi et al., 2013; Tagliero et al., 2021). Despite patients experiencing initial symptomatic relief, partial meniscectomy demonstrates similar outcomes to non-operative treatment, providing no benefit in halting arthritic progression (Krych et al., 2018; Salata et al., 2010). In view of these findings, there is growing interest in its surgical repair, particularly for medial meniscus posterior root tears (Chung et al., 2016; Feucht et al., 2014; Pache et al., 2018). Biomechanical models of meniscal root repair have demonstrated that techniques returning the meniscus to its native orientation restores several key metrics of the loading profile, namely tibiofemoral contact area and pressure, to values indistinguishable from the root intact state (Johanssen et al., 2012; LaPrade et al 2015b; LaPrade et al., 2021a).

The commonest repair techniques described in the literature are the transtibial pull-through repair (TPR) and suture anchor repair (SAR). The transtibial method involves suture passage through the meniscal tissue adjacent to the root tear, which is then pulled through a drilled tibial tunnel and secured over the tibia with a fixation device (Figure 1).

Figure 1. Anatomical transtibial root repair (Reprinted from 'Biomechanical evaluation of the transtibial pull-out technique for posterior medial meniscal root repairs using 1 and 2 transtibial bone tunnels' by LaPrade et al. (2015). Reproduced with permission from SAGE)

Suture anchor repairs are an all inside arthroscopic technique that require the standard anterolateral and anteromedial portal, and a more technically challenging posteromedial portal. However, they do not require bone tunnels, making it useful in patients with concomitant multi-ligamentous pathology or skeletal immaturity (Engelsohn et al., 2007; Lee et al., 2018). Following the insertion of two number 0 polydioxanone (PDS) sutures adjacent to the torn edge, two suture anchors with their own suture strands are placed at the same location. The latter is through the posteromedial portal. One suture strand of each anchor is coupled with one limb of the number 0 PDS. Following this, a shuttle relay occurs by pulling on the remaining limb of the number 0 PDS, which subsequently pulls the suture of the anchor through the meniscus, and the 0 PDS out of the knee. The suture strands can be tied securely, and the same step is repeated for the second anchor (Figure 2).

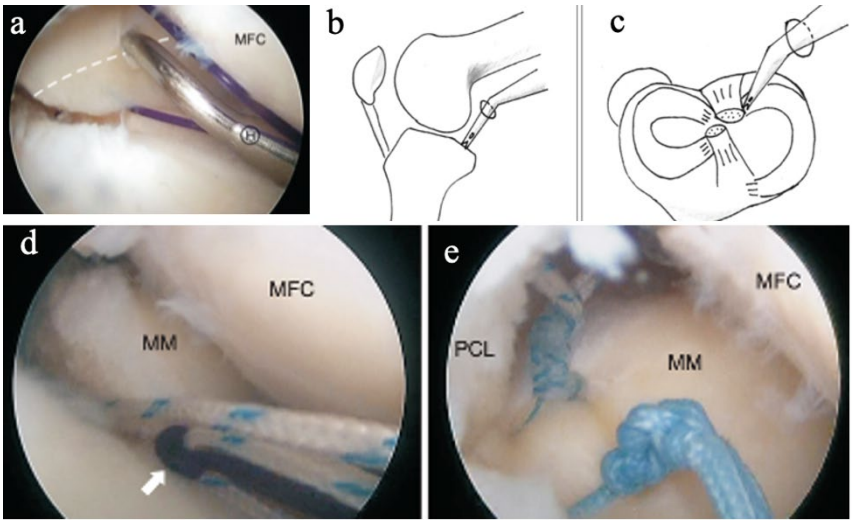

Figure 2. Suture anchor repair. **a.** Following penetration of the posterior 1/3 of the meniscus adjacent to root edge with Number 0 PDS, the anterior 1/3 of the meniscus (white dotted line) is penetrated in the same manner **b & c.** Schematic diagram showing the knee position and insertion of a curved guide through the posteromedial portal for the insertion of suture anchors **d.** Following coupling of one suture strand within anchor and one limb of Number 0 PDS, the remaining limb of Number 0 PDS (white arrow) is pulled, creating a shuttle relay allowing the suture strand of anchor to pass through the meniscus and then be tied **e.** Two suture anchors with sutures tied securely, with posterior root of the medial meniscus repaired to the insertion site (Reprinted from 'Medial meniscal root repair using curved guide and soft suture anchor' by Lee et al. (2018). Reproduced with permission from Clinics in Orthopaedic Surgery)

Whilst both techniques are well-established with equivalent outcomes regarding reduction in meniscal extrusion and rate of complete healing (Kim et al., 2011), the transtibial approach represents a more pragmatic approach as it is less technically demanding, omits the need for posterior portals adjacent to critical neurovascular structures and does not require dedicated suture passing devices. In view of this, the transtibial fixation is advocated with an established record of positive mid-term to long-term results (Ahn et al., 2007; Lee et al., 2014; Peterson et al., 2014).

Despite numerous clinical results showing successful clinical outcomes following transtibial repair, post-operative extrusion can persist, and in such a scenario the meniscus is unlikely to remain chondroprotective. A recent systematic review found that although there was improvement in post-operative clinical scores, there was progressive osteoarthritis with

pathological extrusion and suboptimal healing at three years (Chang et al., 2022). It is likely the extrusion led to these pathological conditions, and the improved clinical results have been influenced more by the relatively older age of patients (mean age, 57.1 years) at which point high impact activity and competitive sports would be expected to decline. One potential explanation for persistent extrusion despite repair is the chronic scarring of the meniscal body to the capsule in a non-anatomical position, either due to delayed repair or a root tear that's remained undetected for a period of time (Homan et al., 2023).

Advances in surgical techniques have been made to optimise the transtibial root repair to maintain the normal loading profile of the knee and reduce pathological extrusion. This includes investigating the position and number of transtibial tunnels (LaPrade et al., 2015b; LaPrade et al., 2015b; Padalecki et al., 2014), number and type of sutures (Feucht et al., 2015a; Matthews et al., 2020; Nakama et al., 2019; Okimura et al., 2019; Robinson et al., 2018; Rosslenbroich et al., 2013), suture configuration (LaPrade et al. 2015d), location of sutures (Kim et al., 2016; Robinson et al., 2018) and fixation devices on the tibial side (Robinson et al., 2020; Wu et al., 2020). Despite this, meniscus extrusion is not fully addressed by isolated repair of the medial meniscus posterior root tear (Chung et al., 2017). Based on these implications, a focus on newer surgical techniques to reduce meniscal extrusion has emerged.

One technique includes centralization. This is the process of re-attaching the meniscal midbody complex just central to the peripheral rim of the tibial plateau (Koga et al., 2012). Several techniques have been described. This includes the insertion of suture anchors at the edge of the tibial plateau and, following the passage of sutures under the extruded meniscus and through the meniscocapsular junction; the centralization stitch is subsequently tensioned down to reduce the extruded meniscus and tied (Koga et al., 2012; Koga et al., 2017). More recently, this has been refined for the use of knotless fixation (Koga et al., 2021, Leafblad et al., 2021).

It is thought knotless fixation helps to better facilitate anchorage at the most extruded locations of the tibial plateau, whilst also increasing the contact area between the meniscocapsular attachments and edge of the tibial plateau (Koga et al., 2021). Theoretically this can lead to a better reduction in meniscal extrusion. In addition, knotless anchors can avoid knot impingement, control suture tension without knot tying, and eliminate the possibility of rigid material loose bodies in the joint. Another centralization technique includes the use of a transtibial stitch. This involves the passage of a peripheral stabilization suture on the extruded meniscus, and through a transtibial tunnel that is independent of the tunnel for the conventional meniscal root tear repair. Once pulled through the tunnel, appropriate tension is applied to the suture to centralize the meniscus, and it is then tied over a tibial cortical button (Daney et al., 2019; Dean et al., 2020). Compared to anchor-based centralization, it may enhance meniscal healing and maintain a better reduction through the transosseous drilling and extent of tissue-bone interface it incorporates. Furthermore, posterior portals are not required, reducing the risk of neurovascular injury (Feucht et al., 2014). A recent systematic review by the author found biomechanical studies investigating centralization techniques for meniscus extrusion to restore the load-distribution function of the meniscus to the native state (Boksh et al., 2024a). However, the review identified key limitations with avenues for potential exploration. In particular, this included no comparison between the centralization techniques used, nor the extent to which biomechanical outcomes were attributed to centralization itself rather than a root repair.

Consequently, the aim of this thesis was to biomechanically compare the anchor-based and transtibial centralization techniques following transtibial pull-through repair of a medial meniscus posterior root tear in porcine knees.

The primary objectives were to a) investigate which technique better restores both the tibiofemoral contact mechanics of the knee, to include contact area and pressure, and b) which technique better reduces pathological extrusion under loading over a range of flexion angles. It is expected the results of this study to subsequently enable the performance of novel clinical trials to evaluate patient outcomes using the biomechanically optimum centralization technique in combination with root repair to fully determine its efficacy. This would be of immense benefit to both patient and surgeon for the provision of alternative treatment options to salvage the native knee joint.

1.1 Thesis overview

Chapter 2 acts as the foundation of the thesis and outlines the background information to understand the subsequent chapters in the thesis. The background details the anatomy and function of the meniscus to include the similarity and differences between human and porcine knees, the appropriate techniques to optimise the transtibial pull through repair, and a review of the development of meniscus centralization with detailed explanation of the centralization methods to be compared.

Chapter 3 focuses on the materials and methods that have been used. Information on the development of a testing rig for the knee joints and surgical technique are discussed here. Furthermore, measurements for tibiofemoral contact mechanics with the use of Fujifilm Prescale film (Tokyo, Japan) and its analysis on the custom MATLAB program (MathWorks, Natick, Massachusetts) are included. In addition, the measurement of meniscal extrusion with its calibration on ImageJ software are also discussed. In essence, the method section provides knowledge of the experiments and data analysis.

Chapter 4 describes the results of the study, in particular the contact area and pressure and meniscus extrusion between the techniques described.

Chapter 5 presents the overall discussion, including the future work the findings in the thesis could be applied to, and final conclusions.

CHAPTER 2

2. Background

2.1 Chapter Introduction

This chapter discusses the meniscal tissue including its structural and physiological properties, as a principal focus for the biomechanical exploration presented in this thesis. To begin, its anatomy in human and porcine knees is discussed in Section 2.2. Pictures from anatomical dissection of the porcine knees within the thesis are provided in this section to clarify the similarity and differences between the two species. The structure, composition, and function of the meniscus is described in Section 2.3. Following this, literature on the conventional techniques to optimise repair of a medial meniscus root tear is critically analysed in Section 2.4. Section 2.5 outlines the recent history and emergence of centralization techniques, with its application in surgical practice. Section 2.6 details the methods that have been used to assess tibiofemoral contact mechanics in meniscus root-torn and repaired knees. Section 2.7 provides the chapter summary.

2.2 Anatomy of the meniscus and root

The medial (MM) and lateral (LM) meniscus are two C-shaped borders filling the triangular space between the tibial and femoral articular cartilage surfaces and joint capsule. Both menisci have anterior and posterior segments of their curvature, referred to individually as a 'horn', and a central portion of their curvature, referred to as the 'body' (Figure 3).

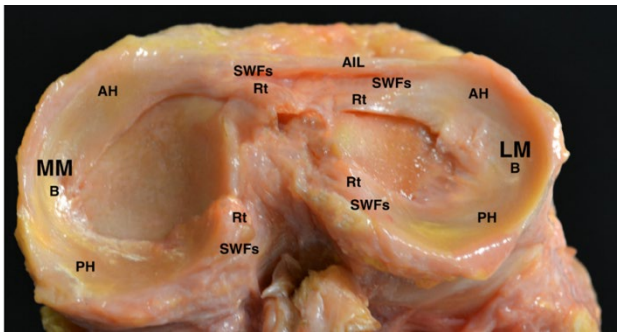

Figure 3. Photograph of a superoposterior view of the meniscus and its anatomy in a cadaveric right knee. MM, medial meniscus; LM, lateral meniscus; B, body; AH, anterior horn; PH, posterior horn; Rt, root; SWFs, shiny white fibers; AIL, anterior intermeniscal ligament (Reprinted from 'Meniscal Root Tears: A Decade of Research on their Relevant Anatomy, Biomechanics, Diagnosis, and Treatment' by Banovetz et al. (2022). Reproduced with permission from Archives of Bone and Joint Surgery).

The medial meniscus can be divided into five anteroposterior zones (Hathila et al., 2019; Smigielski et al., 2014). This includes the anterior root attachment (zone 1), the anteromedial zone between the posterior border of the anterior root and anterior border of the superficial medial collateral ligament (MCL) (zone 3), the posterior horn (zone 4) and the posterior root (zone 5). The lateral meniscus can be divided into six anteroposterior zones (Zdanowicz et al., 2016). These include the anterior root (zone 1), the anterolateral zone between the anterior root and the anterior border of the popliteal hiatus (zone 2), the popliteal hiatus (zone 3), the posteroinferior popliteomeniscal fascicle (zone 4), the ligamentous zone (zone 5), and the posterior root (zone 6) (Figure 4).

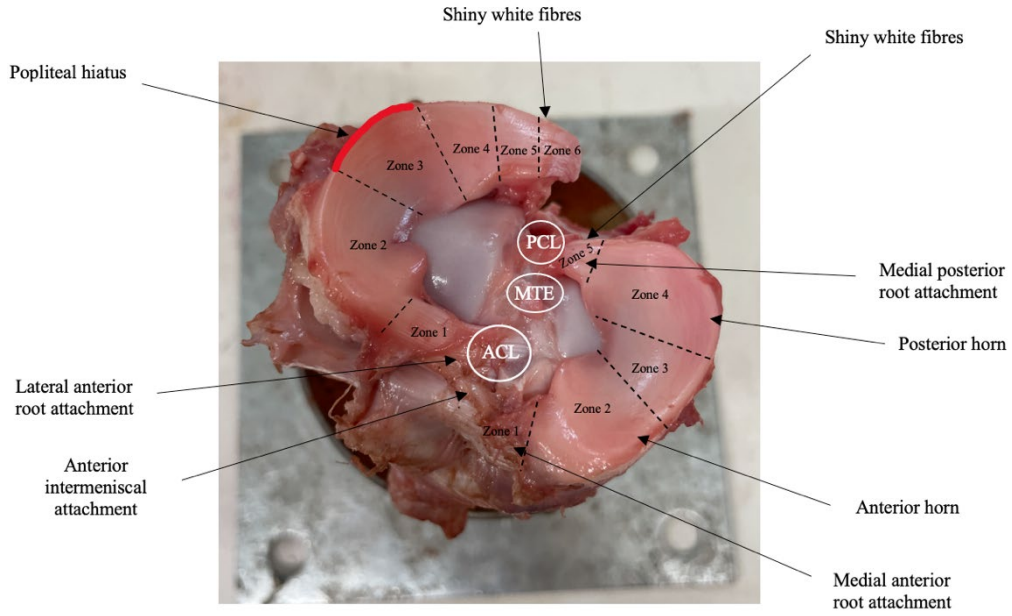

Figure 4. Photographic illustration of a dissected porcine right knee within this study. Medial and lateral zones and relevant anatomical relations. ACL, anterior cruciate ligament; PCL, posterior cruciate ligament; MTE, medial tibial eminence

The anterior and posterior roots of both medial and lateral menisci contain a dense central fibre attachment with surrounding 'supplementary' fibres, known as shiny white fibres (LaPrade et al., 2010). The posteromedial and posterolateral attachments of the root attachments for both

posterior roots make up 46.5% of the attachment surface area and contribute 37.4% of the strength of the native root attachment (Ellman et al., 2014). Incorporating these fibres within the root repair can potentially enhance the biomechanical properties of the repair technique (Ellman MB et al., 2014). In human knees, the anterior and posterior roots of both menisci attach to the tibial plateau. Furthermore, the posteromedial aspect of the lateral meniscus posterior horn is additionally attached onto the medial femoral condyle via the meniscofemoral ligament (MFL) (Figure 5). This structure is of clinical importance as it acts as a secondary stabilizer to excessive anterior tibial translation and internal rotation of the knee in an anterior cruciate ligament (ACL) deficient knee (Frank et al., 2017). The anterior meniscal root attachments in both medial and lateral menisci for porcine knees are similar to humans, running horizontally from the body to their insertion sites on the tibial plateau, with thin layers of transparent septa surrounding the bundles (Figure 6). However, the posterolateral horn root attachment differs to human knees. In porcine knees, they solely attach to the medial femoral condyle without any connection to the tibial plateau and hang freely after separation from the condyle (Figure 4, 5 & 7). Furthermore, although the anterior root of the lateral menisci attaches to the tibial plateau, it splits the anteromedial and posterolateral bundles of the anterior cruciate ligament, a feature not observed in human knees (Proffen et al., 2012) (Figure 8).

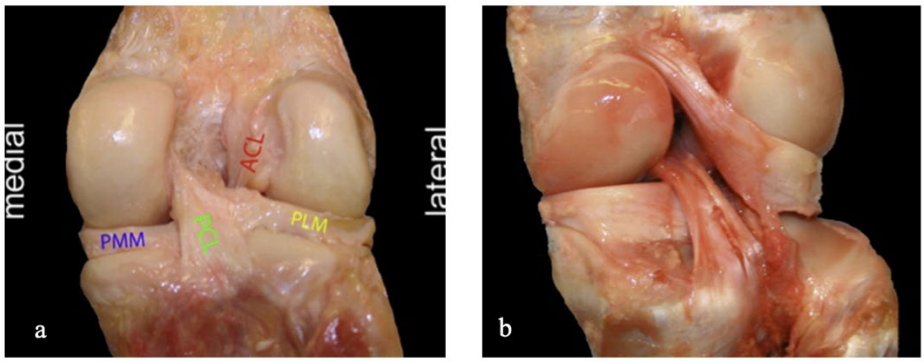

Figure 5. Photograph of the posterior right knee in a. human and b. porcine specimen. The posterior root of the lateral meniscus **partly inserts** on the medial femoral condyle in human knees, whilst it **fully inserts** at the condyle in porcine knees (Reprinted from 'A comparative anatomical study of the human knee and six animal species' by Proffen et al (2012). Reproduced with permission from Elsevier)

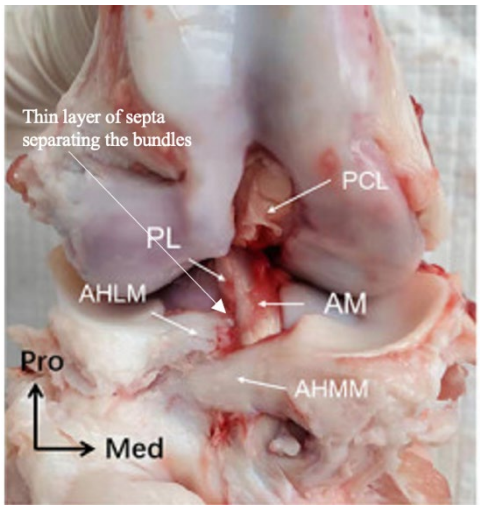

Figure 6. Photographic illustration of a right porcine knee with its anterior root attachments and septa surround the ACL. (Reprinted from 'Comparison of the morphology of the anterior cruciate ligament and related bony structures between pigs and humans' by Shi et al (2022). Reproduced with permission from Frontiers). AHMM, Anterior horn of medial meniscus; AM, anteromedial bundle of ACL; PCL, posterior cruciate ligament; PL, posterolateral bundle of ACL

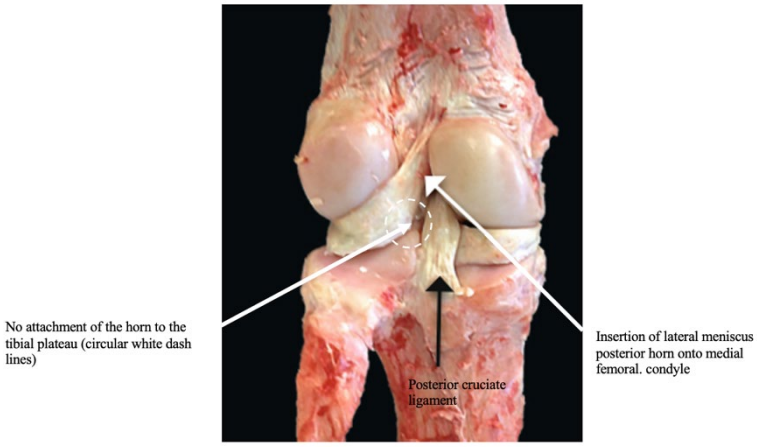

Figure 7. Photographic illustration of a left porcine knee with the attachment side of the lateral meniscus posterior horn (Reprinted from 'Anatomical study: comparing the human, sheep and pig knee meniscus' by Takroni et al (2016). Reproduced with permission from Springer Open)

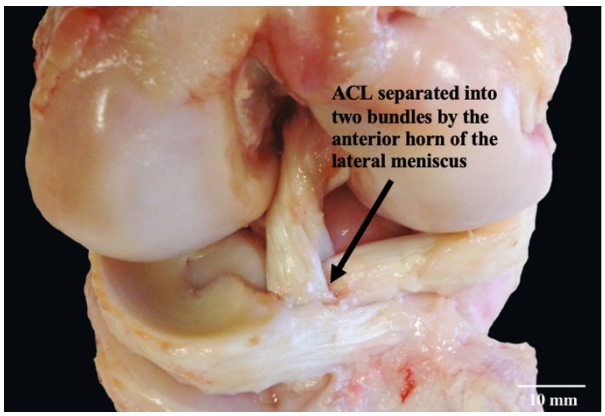

Figure 8. Photographic illustration of a left porcine knee with ACL bundle separation by the lateral meniscus. (Reprinted from 'Anatomical study: comparing the human, sheep and pig knee meniscus' by Takroni et al (2016). Reproduced with permission from Springer Open)

Despite the differences for the posterior root of the lateral meniscus, the focus of the thesis is on the posterior root of the medial meniscus. Cadaveric and porcine specimens both denote the posterior root attachment on the tibial plateau to be located posterolateral to the medial tibial eminence, and anterior to the superior tibial attachment of the posterior cruciate ligament (Johannson et al., 2012; Proffen et al., 2012; Takroni et al., 2016) (Figure 4 and 9). Based on these observational features, surgical repair techniques for medial meniscus posterior root tears in porcine knees are appropriate proxy models for biomechanical investigation prior to the translation of such techniques into clinical practice in humans.

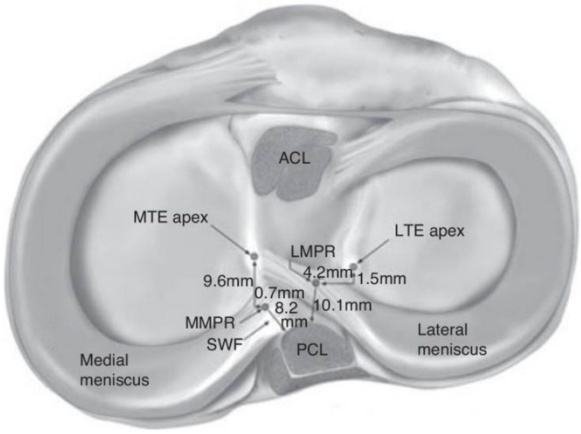

Figure 9. Illustration of the attachment of the medial meniscus posterior root. It is located 9.6mm posterior and 0.7mm lateral to the apex of the medial tibial eminence. It is also 9.2 mm anterior to the tibial attachment of the PCL (Reprinted from 'Understanding posterior medial meniscus root lesions: from basic science to treatment' by Cruz et al. (2017). Reproduced with permission from Elsevier)

The anatomical features of the medial meniscus posterior root in humans are complex. It consists of a ligamentous mid-substance (root ligament), a transition zone between the meniscal body and root ligament, and bony insertion of the root ligament onto the tibial plateau (Figure 10a). A recent biomechanical study noted that the strength of a medial meniscal posterior root repair may vary with the position of the suture repair within the root itself. The strongest repairs were found for insertion within the body of the meniscus and either side of the central part of the transition zone (Robinson et al., 2018) This can be explained by the

orientation of the collagen fibres which are discussed in detail in Section 2.3. Such landmarks can be also delineated in porcine knees (Figure 10b)

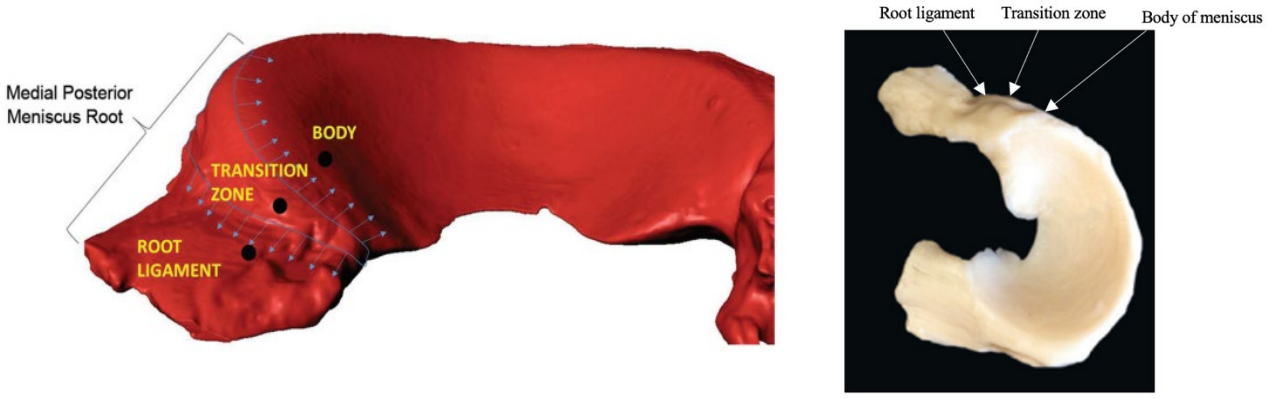

Figure 10 (a). 3D from a micro-computed tomography scan of a representative meniscus showing the meniscal root and its landmarks **(**Reprinted from 'The Strength of Transosseous Medial Meniscal Root Repair Using a Simple Suture Technique Is Dependent on Suture Material and Position by Robinson et al. (2018). Reproduced with permission from SAGE) **(b).** Photographic illustration of a porcine right knee medial meniscus with these corresponding features (Reprinted from 'Anatomical study: comparing the human, sheep and pig knee meniscus' by Takroni et al (2016). Reproduced with permission from Springer Open

Other similarities between both species are noted for the rest of the medial meniscus. This includes the anterior horn being more anterior than that of the lateral meniscus (Figure 8), and the body of the MM becoming wider posteriorly. Although the medial meniscus is connected to the medial collateral ligament medially in both species, the body and posterior horn in porcine knees are more tightly attached to the capsule throughout its peripheral border, which can further restrict its mobility (Figure 11a). However, the body of the lateral meniscus in both specimens has a small area located at the middle third devoid of capsular attachment, and the capsule itself is more elastic (LaPrade et al., 2021b) (Figure 11b). Additionally, the popliteus tendon partially disrupts the capsular circumferential attachment. These properties allow the lateral meniscus to have more mobility relative to the more static medial meniscus (Simonian et al., 1997).

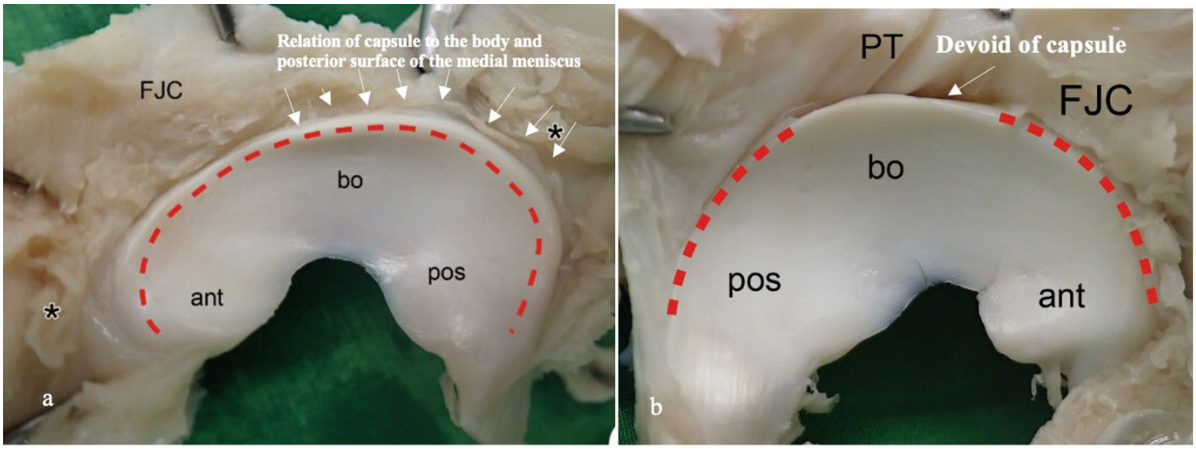

Figure 11 (a) Photographic illustration of a medial meniscus on the femoral side of a porcine knee. The capsule is tightly attached to the body of the medial meniscus within its peripheral border (see white arrows). **(b).** Photographic illustration of a lateral meniscus on the femoral side of a porcine knee. A small area devoid of capsule is noted in the middle third of the peripheral border. (Reprinted from 'The continuous structure of the joint capsule and meniscus in the pig knee' by Natsuyama et al (2013). Reproduced with permission from Wiley. FJC, femoral joint capsule; PT, popliteal tendon.

Anatomical understanding of the posterior medial meniscal attachments is imperative, as posteromedial arthrotomies within this region was performed for the study. This was so Fujifilm prescale film (Tokyo, Japan) could be inserted under the medial meniscus for the measurement of tibiofemoral contact mechanics in various testing scenarios (see section 2.6). The key anatomical attachments leading to its rigid meniscocapsular structure include the posterior meniscocapsular attachment, posterior meniscotibial ligament, the posterior oblique ligament, the deep medial collateral ligament (dMCL) and the semi-membranosus muscle (Mameri et al., 2022). The posterior meniscotibial ligament joins and blends within the posteromedial capsule on its internal surface, forming a conjoined attachment onto the posterior horn and root of the medial meniscus (Figure 12a) (LaPrade et al., 2021b). The

superficial medial collateral ligament (sMCL) blends with the capsule externally (Figure 12b), and the posterior oblique ligament (POL) is located posterior to this structure. The POL consists of two elements – the POL meniscofemoral ligament that attaches the meniscus to the femur and the POL meniscotibial ligament, attaching the medial meniscus to the tibia (DePhillipo et al., 2019). Blended with the POL meniscofemoral ligament is the deep MCL, which is clearly visualised following cut-down of the sMCL. It consists of a meniscotibial and meniscofemoral ligament. The oblique popliteal ligament, arising from the semimembranosus runs superolaterally, attaching to the lateral femoral condyle. This is an important landmark as it marks the medial border of the posteromedial arthrotomy, as described in earlier studies (Allaire et al., 2008; Muriuki et al., 2011). In view of these posteromedial attachments, previous biomechanical studies on porcine knees advocate for the incision of the described meniscotibial ligaments in order for insertion of pressure sensors under the medial meniscus for measurement of tibiofemoral contact mechanics (Allaire et al., 2008; Amano et al., 2023; Chung et al., 2018; Muriuki et al., 2011; Seo et al., 2009). Anteromedial capsulotomy was also required to ensure the Fujfilm prescale film (Tokyo, Japan) was fully seated under the meniscus (see section 2.6). As there is much fewer complex meniscocapsular attachment here, the arthrotomy was made between the patellar tendon and anterior border of sMCL (Figure 13), in keeping with previous biomechanical studies (Allaire et al., 2008; Daney et al., 2019; Muriuki et al., 2011; LaPrade et al., 2015b; Padalecki et al., 2015; Park et al., 2023; Saltzman et al., 2020).

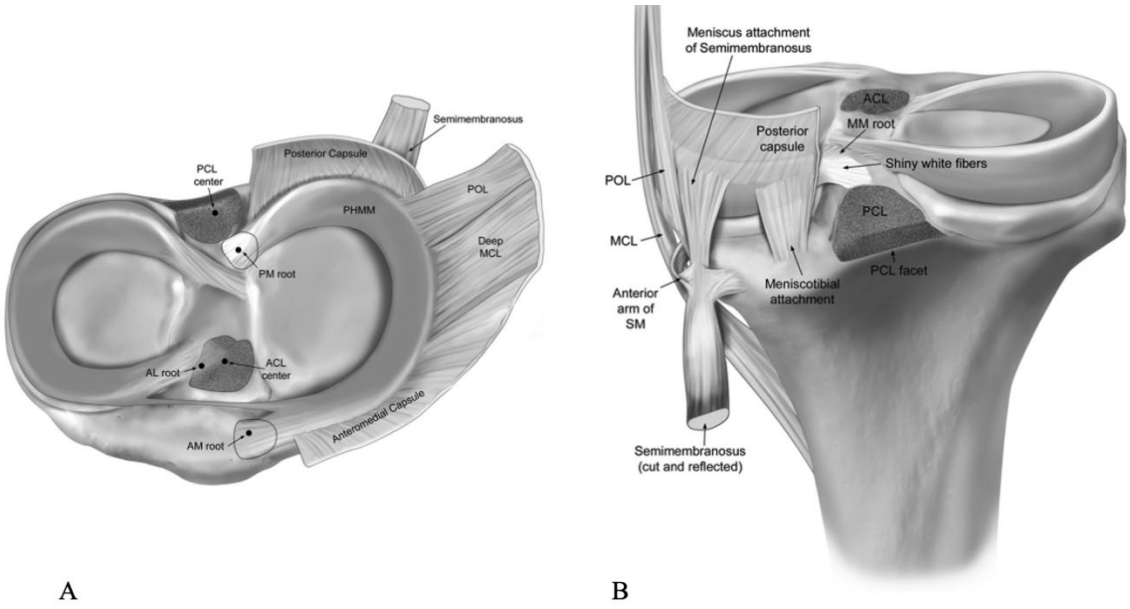

Figure 12. (A) Axial view illustration of the anatomic relationships of the posterior horn of the medial meniscus, posterior capsule, posterior oblique ligament (POL), deep medial collateral ligament (MCL) and semimembranosus tendon. **(B)** Posterior medial anatomy with the posterior capsule reflected. This figure illustrates the intimate relationship of the static and dynamic structures of the posteromedial corner, including the semimembranosus tendon fascial expansion that attached directly to the posterior horn of the medial meniscus. ACL, anterior cruciate ligament; AM, anteromedial; SM, semimembranosus PCL, posterior cruciate ligament; PM, posteromedial (Reprinted from 'Quantitative and Qualitative Assessment of the Posterior Medial Meniscus Anatomy' by DePhillipo et al (2018). Reproduced with permission from Sage)

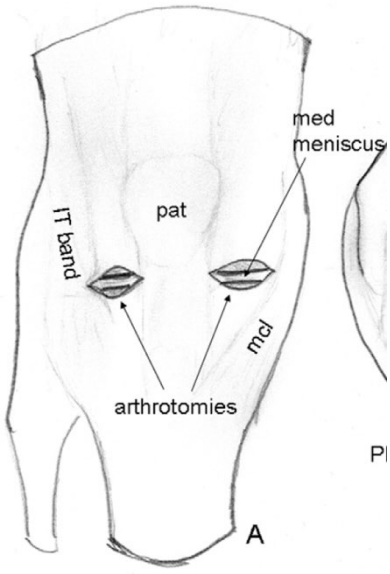

Figure 13. Anterior schematic of a dissected knee, showing the anteromedial arthrotomy of interest preserving the patellar tendon and superficial medial collateral ligament (mcl). Reprinted from 'Biomechanical consequences of a tear of the posterior root of the medial meniscus: similar to total meniscectomy' By Allaire et al. Reproduced with permission from JBJS)

2.3 Structure, composition and biomechanics of the meniscus and its roots

2.3.1 Structure and composition

The meniscus is a dense extracellular matrix composed primarily of water (72%) and collagen (22%), interposed with cells. Proteoglycans, non-collagenous proteins, and glycoproteins account for the remaining dry weight (Arnoczky et al., 1992; Brindle et al., 2001). Water composition is greatest at the posterior horns, generating a drag force during axial loading (Markes et al., 2020).

Collagen composes 75% of the dry weight of the menisci (Gee et al., 2021) and are primarily responsible for the tensile strength of the meniscus, with type 1 predominating and providing the primary structural framework of the meniscus. The arrangement of the fibres is ideal in transferring axial compressive load into circumferential hoop stresses during weight bearing (Ghosh et al., 1975). In the most superficial layer, the type I fibres are orientated radially, whilst a circumferential arrangement is present in the deeper layers. Radially oriented "tie" fibres are also present in the deep zone and are interspersed or woven between the circumferential fibres to provide structural integrity (Peterson et al., 1998), which helps to prevents longitudinal splitting (Markes et al., 2020) (Figure 14). As described in section 2.2, the meniscal root consists of a complex structure of root ligament, transition zone and body. In the root ligament, only circumferential fibres are present which are parallel to its direction (Smith et al., 2015). The transition zone contains predominantly parallel fibres, whilst the body contains a mixture of radial and circumferential fibres (Bullough et al. 1970). This fibre orientation likely contributed to the increased ultimate yield load for medial meniscus posterior root repairs when suture location was in the substance of the meniscus body rather than the root ligament and transition zone (Robinson et al. 2018).

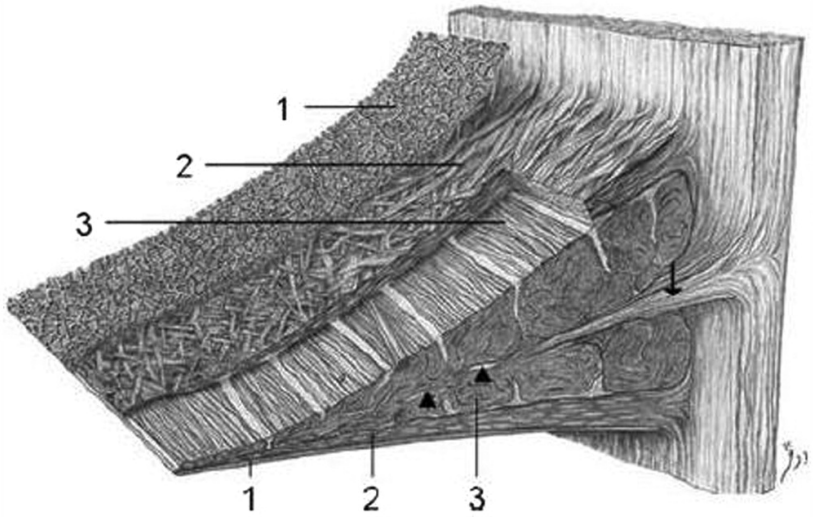

Figure 14. Schematic diagram demonstrating the collagen fibre ultrastructure and orientation within the meniscus: 1, superficial network; 2, lamellar layer; 3, central main layer. Arrowheads, radial interwoven fibres; arrow, loose connective tissue. (Reprinted from 'Collagenous fibril texture of the human knee joint menisci' by. Peterson et al. (1998). Reproduced with permission from Springer)

Proteoglycans are located within a fine meshwork of collagen fibrils. The proteoglycan consists of a hyaluronic acid backbone (Figure 15). Off this, they are connected to a protein core through link proteins. Within the protein core are the keratin sulphate and chondroitin sulphate (Muir et al., 1969). The proteoglycan provides the meniscus its compressive strength by trapping water, and its concentration is greatest in the meniscal horns due to their weight bearing nature (Fox et al., 2012)

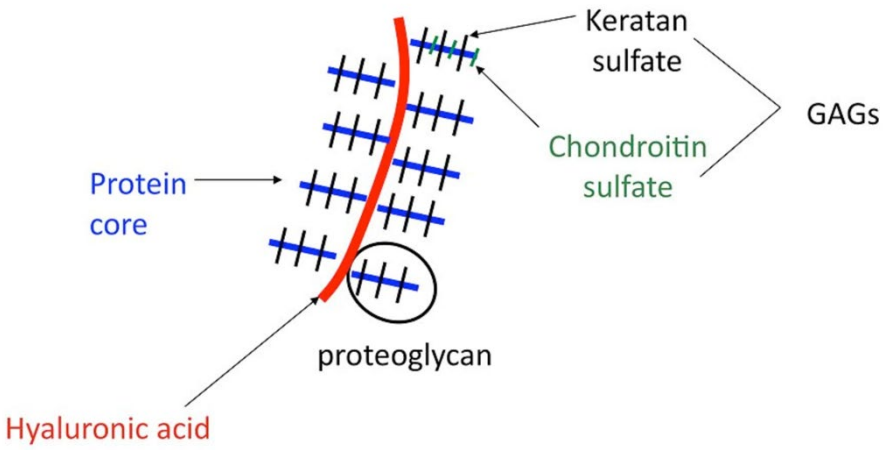

Figure 15. Schematic drawing of a proteoglycan

2.3.2 Vascularity

The meniscus is a relatively avascular structure with a limited peripheral blood supply, which thereby has important implications in its ability to heal. The medial, lateral, and middle geniculate arteries (which branch off the popliteal artery) provide the major vascularization to the inferior and superior aspects of each meniscus (Figure 16). A peri-meniscal capillary plexus arises from these branches that penetrate the meniscal stroma in a radial fashion at a depth of 2-3 mm. This is roughly 10-30% of the periphery of the medial meniscus border, and 10-25% of the lateral meniscus border (Kean et al., 2017; Perreira et al., 2019). A second distinct vascular fringe provides vascularity in the anterior horns of both menisci, and to the posterior horn to a lesser degree (Arnoczky et al., 1992). The central meniscus is avascular and receives nutrition through diffusion of the synovial fluid (Gee et al., 2021), or mechanical pumping (i.e. joint motion) (Mow et al., 1989).

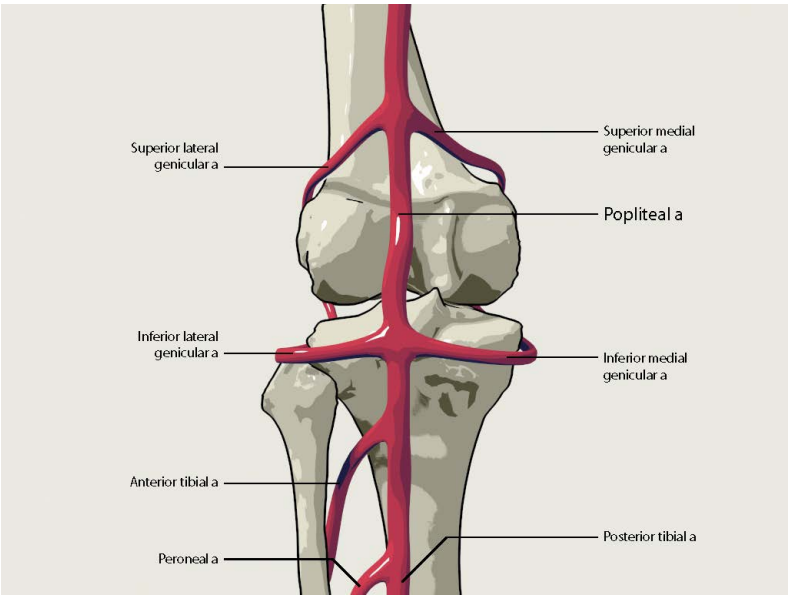

Figure 16. Confluence of geniculate arteries (posterior view), a, artery

The relative avascular nature of the meniscus has led to the categorization of the meniscus into three zones based on the Cooper classification (Cooper et al.,1991). This includes the red-red, red-white and white-white zones. These zones were calculated by dividing the distance

between the meniscocapsular junction and the most centrally located blood vessel in cross section of the meniscus by the total width of the meniscus, multiplied by 100 (Figure17).

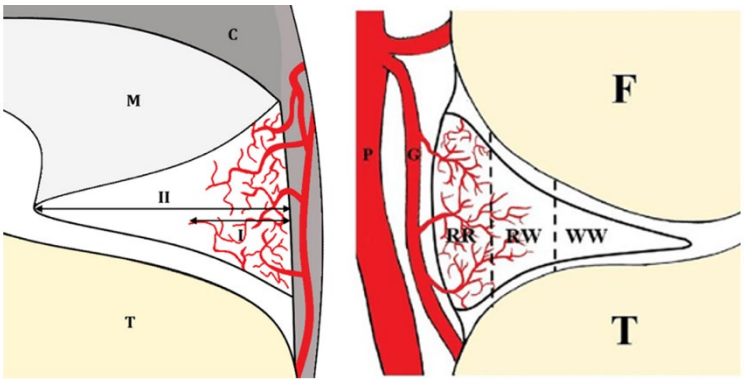

Figure 17. A schematic cross-section of the meniscus. The extent of vascularization is calculated by dividing the distance between the meniscocapsular junction and the most centrally located blood vessel (I) by the total width of the meniscus (II) multiplied by 100%. 1 = Zone 1 or ‘‘Red-red” zone, 2 = Zone 2 or ‘‘Red-white” zone, 3 = Zone 3 or ‘‘White-white” zone, C = Capsule, T = Tibia, M = Meniscus. (Reprinted from ‘The role of patient characteristics and the effects of angiogenic therapies on the microvasculature of the meniscus: A systematic review’ by van der Lelij et al (2022). Reproduced with permission from Elsevier)

The red-red zone represents the vascular peripheral region supplied directly by the peri-meniscal capillary plexus. The white-white zone is avascular and represents the thin concave, cartilaginous region of central menisci with unattached free edges. The red-white zone is located between the two and has characteristics of the other two zones (Kean et al., 2017). In clinical practice, meniscal tears will have different healing potential according to the involved vascular region (Crawford et al., 2020). Red-red zone tears, and to some extent red-white zone tears, have acceptable healing potential so repair is indicated. White-white zone tears are avascular with poor healing potential and are thus amenable to partial meniscectomy.

2.3.3 Biomechanics – meniscus kinematics

As described, the medial meniscus is less mobile than the lateral meniscus. Kinematic studies report 2-3 mm anteroposterior movement of the medial meniscus during flexion compared to 9-10 mm for the lateral meniscus (Brantigan et al., 1941; DePalma. 1954). A landmark cadaveric study reported the mean medial excursion to be 5.1 mm compared to 11.2 mm for

the mean lateral excursion (Thompson et al., 1991). These were taken from the average of the movement of both the anterior and posterior horns for each meniscus. Furthermore, the excursion of the anterior and posterior horn of the lateral meniscus was similar, suggesting the meniscus to move more as a single unit. In contrast, the anterior horn excursion for the medial meniscus was 2.2 times greater than that of the posterior horn (Figure 18). This suggests the posterior horn to be constrained, and as described in section 2.2, is largely down to its rigid posteromedial attachments to include the posterior meniscotibial ligament, posterior oblique ligament, and deep MCL. Biomechanically, a reduction in both the motion of the posterior horn and greater differential between the anterior and posterior horn of the medial meniscus is a potential mechanism for meniscal body and root tears with a resultant "trapping" of the fibrocartilage between the femoral condyle and the tibial plateau during full flexion. This can explain why medial meniscus posterior root tears are more susceptible to injury than its lateral counterpart and underlines the focus of the medial side in this thesis.

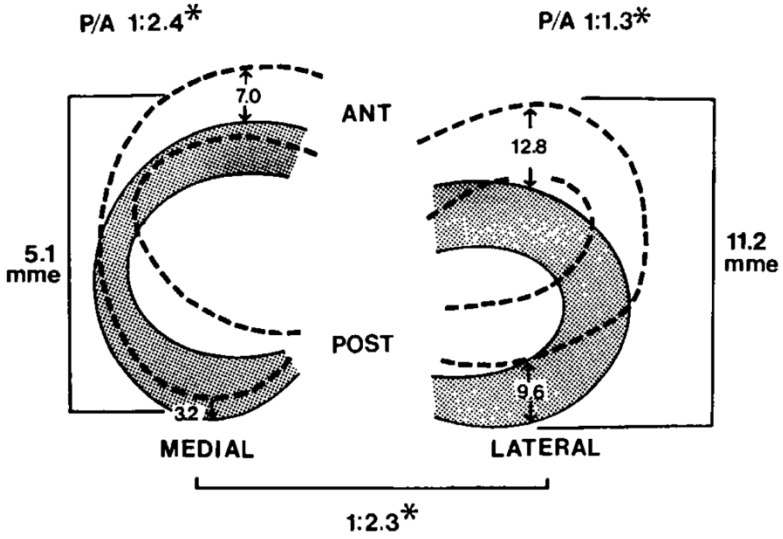

Figure 18. A schematic diagram showing the mean movement (mm) in each meniscus during flexion (shaded) and extension (hashed). ANT, anterior; POST, posterior; mme, mean meniscal excursion; P/A, ratio of posterior to anterior meniscal translation during flexion (Reprinted from 'Tibial meniscal dynamics using three-dimensional reconstruction of magnetic resonance imaging' by Thompson et al. (1991). Reproduced with permission from SAGE)

2.3.4 Biomechanics – load transmission

Seventy percent of the load in the lateral compartment and 50% of the load in the medial compartment is transmitted through the menisci (Seedhom et al., 1979). The medial meniscus bears a higher load, usually around 50-70% of the compressive load during weight bearing, whilst the lateral meniscus bears less, typically around 30-50%. The posterior horn is involved in 50% and 85% transmission of compressive load at 0 and 90° flexion respectively (Walker et al., 1975). As the femur compresses the meniscus during loading, the vertical component is resisted by a reaction force from the tibial plateau (Figure 19). The horizontal force component, however, can potentially cause the meniscus to deform radially and extrude out the joint. However, in response to the radial deformation in normal knees, the axial load is converted to circumferential 'hoop' stresses (Aspden et al., 1985; Fox et al., 2012; Peterson et al., 1998). The hoop stresses then exert tensile stresses along the circumferential collagen fibrils of the meniscus. Ultimately, this reduces the compressive loads experienced by the chondral cartilage of the knee. However, for this circular traction (tensile stress) to be initiated or maintained, it requires the meniscus to be anchored to the tibial plateau via its roots (Krause et al., 1976). Therefore, from a biomechanical perspective, if the integrity of the collagen bundles is damaged from a meniscal tear, or the root is detached (meniscal root tear), then circular traction is compromised. Radial deformation can subsequently occur, with resultant extrusion.

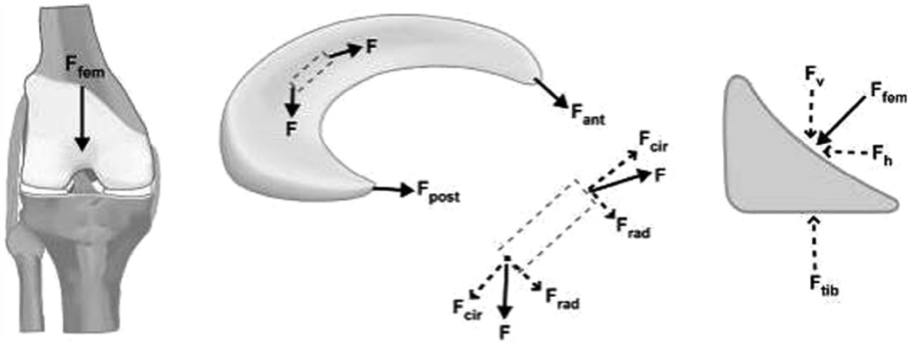

Figure 19. Free body diagram of forces acting on the meniscus during joint compression. Radial deformation upon loading is countered by the circumferential hoop stress (F_{cir}) generated in the menisci. This is maintained by the anchorage of meniscus to the plateau via the roots. Vertical component of axial load (F_v) is counted by reaction

force from tibia (F_{tib}). (Reprinted from 'Engineering the Knee Meniscus' by Athanasiou et al. (2009). Reproduced with permission).

Following meniscus extrusion from a root tear, the biomechanical profile of the meniscal-root deficient knee is equivalent to a knee that has received a total meniscectomy (Allaire et al., 2008; LaPrade et al., 2015e; Padalecki et al., 2014). Allaire et al (2008) reported a 25% increase in peak contact pressures following a medial meniscus root tear, with a 50% increase reported following a lateral root tear (Schillhammer et al., 2012). Therefore, the integrity of the meniscal roots is of paramount importance to preserve the knee kinematics of the joint and prevent degenerative changes (Han et al., 2012; McDermott et al.. 2006; Ozkoc et al., 2008).

2.4 Conventional methods to optimize medial meniscus posterior root repair

The deleterious changes in tibiofemoral contact mechanics in patients with meniscal extrusion following MMPRT are well established in the literature. Accelerated chondral injury and early osteoarthritis have been noted in clinical studies (Berthiaume et al., 2005; Krych et al., 2017; Krych et al., 2018). Early identification and appropriate treatment can theoretically be important in preventing these pathological sequelae of events. Arthroscopic transtibial pull through repair is considered the gold-standard treatment by many investigators (Feucht et al., 2015b). However, despite the advances in surgical techniques to optimise the biomechanical and clinical outcomes of transtibial root repair, post-operative extrusion can persist.

It is important one selects the appropriate combination of techniques available in the transtibial repair stage to provide the best biomechanical and clinical construct possible prior to entering the centralization phase. This subsection will focus on the options available to understand the root repair technique that was performed in chapter 3.

2.4.1 Number of transtibial tunnels

The transtibial method involves passage of sutures through the meniscal tissue adjacent to the root tear, pulled through a single tunnel to then be securely tied over the tibia (Figures 1 and 20). However, several studies have demonstrated significant displacement to compromise the meniscal function following cyclical loading with a single tunnel (Cerminara et al., 2014; Feucht et al., 2014). It was thought this may not have incorporated the shiny white fibres, which provides 37.4% of the strength of the native root attachment (Ellman et al., 2014). It was proposed that multiple bone tunnels may be necessary to account for these fibres and improve the biomechanical properties of the transtibial pull-out technique. However, only one study investigated this (one vs two tunnels) and found that there were no difference between the two techniques regarding displacement under cyclical loading (1, 100, 500 and 1000 cycles) and ultimate load to failure (LaPrade et al. 2015c) (Figure 20). Theoretically the addition of extra bone tunnels could stimulate more healing at the tissue-bone interface with a torn meniscal root held down over a wider surface area. However, there are no clinical studies to date to compare this between the two techniques.

Figure 20. Two transtibial bone tunnels. First tunnel (conventional tunnel) placed at the middle of the central main attachment fibres of the MMPRT. A second tunnel (new tunnel) reamed parallel and 5mm posterior to the first to capture the shiny white fibres (Reprinted from 'Biomechanical evaluation of the transtibial pull-out technique for posterior medial meniscal root repairs using 1 and 2 transtibial bone tunnels' by LaPrade et al. (2015c). Reproduced with permission from SAGE.

2.4.2 Position of transtibial tunnel

The position of the transtibial tunnel within the tibial plateau has important implications on the biomechanical properties of the root repair. Starke et al. (2010) reported non-anatomical positioning of the root attachment had a significant effect on hoop tension. Their model demonstrated that lower levels of meniscus hoop tension caused increased cartilage deformation, indicating increased local stress. Preservation of meniscus tension is important as decreased meniscal tension impairs the ability of the meniscus to support hoop stresses (Seo et al., 2009). One cadaveric biomechanical study compared an anatomical repair with the tunnel at the root insertion site with a non-anatomical repair. The tunnel for the latter was 5 mm posteromedial to the root insertion site, synonymous to the position where a MMPRT generally extrudes to if it remains undetected or undergoes delayed repair (Lerer et al., 2004; Magee et al., 2008). The anatomical tunnel position was 9.6 mm posterior and 0.7 mm lateral to the apex of the medial tibial eminence. It was also 9.2 mm anterior to the tibial attachment of the PCL (figure 9). The study found that both native medial meniscus posterior root and the one that was repaired anatomically had significantly greater contact area and lower contact pressure than for the non-anatomical tunnel across all flexion angles (0 – 90°). Furthermore, the non – anatomical tunnel performed only slightly better than a root tear.

2.4.3 Suture configuration

The meniscus-suture interface has been identified as the primary source in eliminating TPR displacement (Cerminara et al., 2014), and whilst one cannot enhance the structural property of the injured root, the properties at the interface can be targeted. Several suture techniques have been developed to identify the optimum method to gain a strong-hold in the meniscus. Feucht et al. (2013) compared the biomechanical properties of meniscus-suture constructs

among four different suture techniques currently used for transtibial pull-out repair of posterior meniscus root tears (Figure 21). In this study, the modified Mason-Allen (MMA) suture technique provided superior biomechanical properties of the meniscus-suture construct compared to the others.

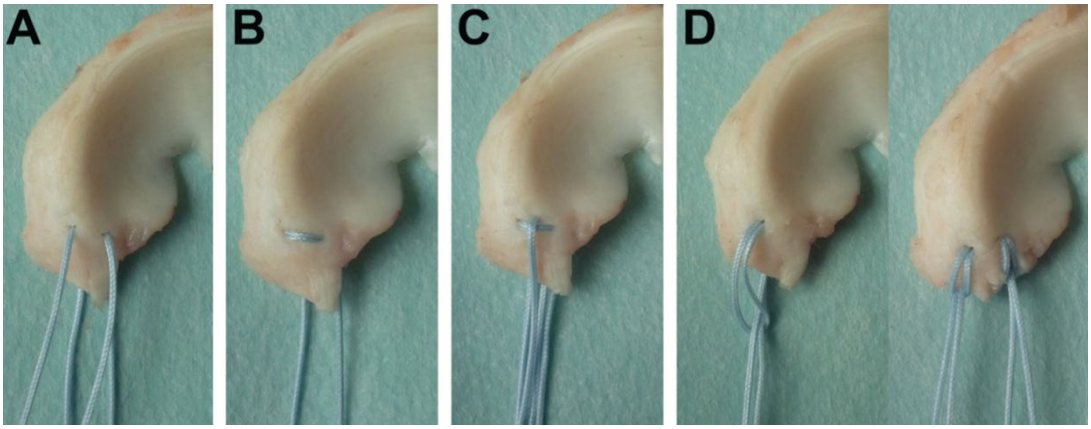

Figure 21. (a) Two simple sutures (TSS). 2 sutures placed 5mm medial to lateral edge of posterior meniscal horn. One suture placed next to meniscosynovial junction and the other 5mm more anteriorly **(b) Horizontal mattress suture.** 1 suture passed twice through the meniscus, creating horizontal loop on superior surface. Suture penetration same location as TSS technique **(c) Modified Mason Allen.** Horizontal mattress suture created first. A second suture passed through meniscus immediately medial to and in centre of horizontal loop **(d) Two modified loop stitches**. A folded suture passed through meniscus so that the loop of the suture placed at the superior surface of the meniscus. Free ends of suture passed through the loop, creating new loop. Loop stitch tightened. Second loop stitch in the same fashion. Suture penetration same location as TSS. (Reprinted from 'Biomechanical evaluation of different suture techniques for arthroscopic transtibial pull-out repair of posterior medial meniscus root tears' by Feucht et al. (2013) Reproduced with permission from SAGE)

In contrast, however, LaPrade et al (2015D) found no difference biomechanically between the MMA and the simpler two simple stitch (TSS) technique (LaPrade RF et al. 2015). In fact, they found the TSS was less prone to displacement after cyclical loading. Furthermore, the MMA is technically more challenging and entails a longer surgical time. In view of these findings, the two simple stitch technique was concluded to be a more feasible and appropriate option for posterior meniscal root repairs. This was further underlined in a systematic review by the author who found TSS performed just as well as the MMA technique at one year follow-up, regarding patient reported outcome measures, meniscal extrusion, and healing (Boksh et al. 2024b).

2.4.4 Type of suture

In recent years, the influence suture material has at the meniscus-suture interface have been evaluated. The ideal material should provide low displacement, high stiffness, and maximum load to failure to keep the re-attached root in place during healing (Burgess et al., 2010). Various materials are available, from conventional braided polyesters (Kim et al., 2011a; Kim et al., 2011b), to the stronger and stiffer ultra-high molecular weight polyethylene (UHWMPE) sutures (Nicholas et al., 2009). The common UHMWPE sutures used in practice include FiberWire (Arthrex, Naples, Florida, USA) and UltraBraid (Smith and Nephew, Andover, Massachusetts, USA) (Figure 22). FiberWire is made of a multi-strand, long-chain UHMWPE core with a braided polyester jacket. UltraBraid consists of an UHMWPE jacket, but this is absent in its central core.

More recently, UHMWPE tapes have become popular, with the 2 mm FiberTape (Arthrex, Naples, Florida, USA) and 2 mm UltraTape (Smith and Nephew, Andover, Massachusetts, USA) commonly used in practice. Unlike their suture counterparts, both the core and jacket contain the UHMWPE construct, and it is theorized that this provides it superior biomechanical properties (Figure 22). Furthermore, its wider structure is thought to fill the hole created for suture passage through the meniscus more effectively and distributes load over a broader area (Ahn et al., 2009). In theory, this should increase the load required for failure at the meniscus-suture interface and promote meniscal healing. Suture tapes have an established practice in rotator cuff injuries, with a recent systematic review by the author showing it to have superior biomechanical properties to that of conventional sutures (Boksh et al., 2022). This was regarding contact pressure, load to failure, stiffness and gap formation. Several biomechanical studies on the use of UHMWPE Tapes over sutures have shown superior biomechanical properties, particularly in relation to load to failure, stiffness and elongation at failure

(Bachmaier et al., 2024; Matthews et al., 2020; Nakama et al., 2019; Robinson et al., 2018; Takahashi et al., 2023). To date, only one clinical study has compared the two materials, with greater meniscal healing observed at one year with the Tape construct (Hiranaka et al., 2022)

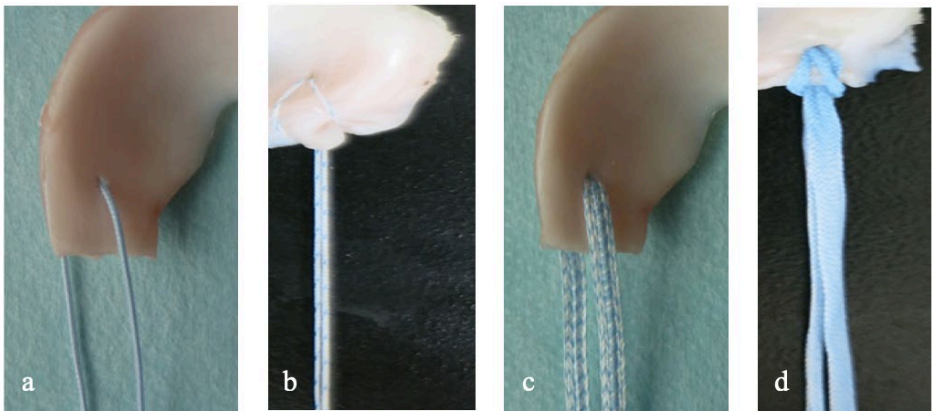

Figure 22. (a) Number 2 FiberWire **(b)** Number 2 UltraBraid **(c)** 2mm FiberTape **(d)** 2mm UltraTape
(Reprinted from 'Biomechanical evaluation of different suture materials for arthroscopic transtibial pull-out repair of posterior meniscus root tears' by Feucht et al. 2015, and 'Biomechanical Comparison of Two Different Sutures for the Tensile Strength of the Pullout Repair of Posterior Meniscal Root Tear' by Takahashi et al. (2023). Reproduced with permission from Springer)

2.4.5 Number of sutures

As previous described in section 2.4.1, capturing the shiny white fibres following repair of the posterior medial meniscus root tear is thought to enhance the transtibial root repair (Ellman et al., 2014). Furthermore, the red-red zone and meniscocapsular junction tissues are not torn as easily when the suture material is pulled through the tunnel, and out of the proximal tibia for tying (Kim et al., 2016). The insertion of two or more sutures compared to one is likely to ensure these factors are accounted for. Only one biomechanical study has investigated this, albeit on the lateral posterior meniscal root (Rosslenbroich et al., 2013). They found using two stitches with the simple stitch technique had greater stiffness, greater load to failure and lower displacement after cyclical loading compared to one stitch. Furthermore, it performed similarly to an intact root.

2.4.6 Fixation on the tibial side

From the evidence described in subsections 2.4.3 to 2.4.5 it can be suggested that the use of two UHMWPE tapes in a simple stitch manner will optimise the repair strength at the meniscus-suture interface, minimising repair displacement. However, to have appropriate fixation to withstand physiological loading, adequate fixation is required on the anterior aspect of the tibia following its passage through the tibial tunnel.

There is currently no consensus on MMPRT tibial fixation techniques. Different techniques have been described based on surgeons' preference. This includes the use of a cortical button (Lee et al., 2013), screw and washer (Vyas et al., 2012), transosseous suture (Ahn et al., 2009), and anchors (Moon et al., 2012) (Figure 23). Two biomechanical studies have compared these fixation techniques (Robinson et al., 2020; Wu et al., 2020) and found cortical fixation devices (screws and buttons) to perform better than anchors, particular regarding load to failure and construct stiffness. However, this should not be interpreted as anchors perform poorly when used for centralization, the main scope of thid thesis. Centralization involves the insertion of anchors directly within the plateau, whilst the anchors fixed in the tibial bone for transtibial repair have tapes passing through it which have shuttled through a tunnel. It is possible these tapes to become coated with bone marrow fat, reducing the friction co-efficient between the tape, bone and anchor. Ultimately, this can lead to tape slippage and lower load to failure (Wieser et al., 2012). Despite buttons and screws performing similarly, cortical buttons have a lower profile meaning the need for implant removal and likelihood of knot-induced skin irritation will be lower.

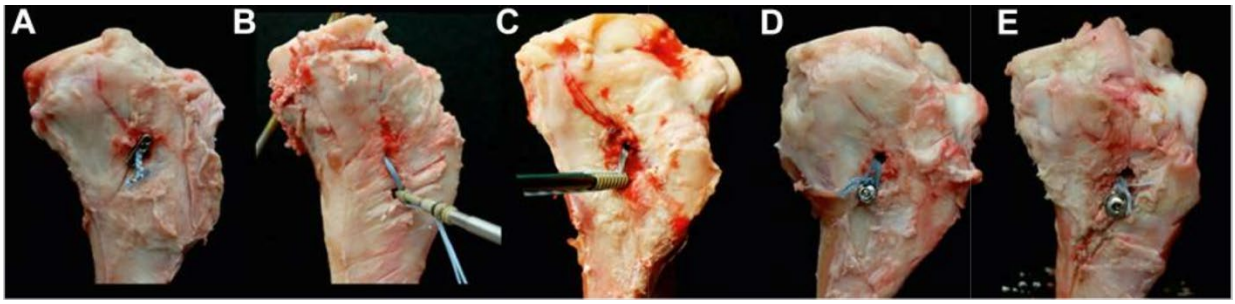

Figure 23. Fixation techniques on the tibial side **(a)** Endocortical fixation button **(b & c)** suture anchors **(d)** cortex screw **(e)** cortex screw with washer. (Reprinted from 'Knotless Anchor Fixation for Transosseous Meniscal Root Repair Using Suture Tape Is Inferior Compared With Button or Screw Fixation: A Biomechanical Study' by Robinson et al. (2018). Reproduced with permission from SAGE)

2.4.7 Suture position following meniscal root tear

The position of the suture within the medial meniscus posterior root tear partly depends on the tear morphology. Two-thirds of root tears are radial tears within 0 – 9 mm from the root attachment site (Type 2 tears) (Figure 24). In over fifty percent of such cases, these are within 0 – 3 mm (Type 2a tears). A biomechanical study performed by Padalecki et al. (2014) reported that the position of the transtibial tunnel within the plateau should be directly under the torn root. That is, if the tear is at the tibial attachment site, 3 or 6 mm from the attachment site, then the tunnels should also be at these corresponding positions. This will ensure the meniscus tension is kept constant, otherwise its ability to absorb hoop stresses becomes impaired (Starke et al., 2010). Section 2.4.2 describes the benefits of an anatomical tunnel, that is, immediately under the root insertion site. Therefore, in this thesis creating the root tear at its insertion site would be appropriate. The additional benefit in doing this includes it being the commonest tear type as described, thereby closely reflecting the study population.

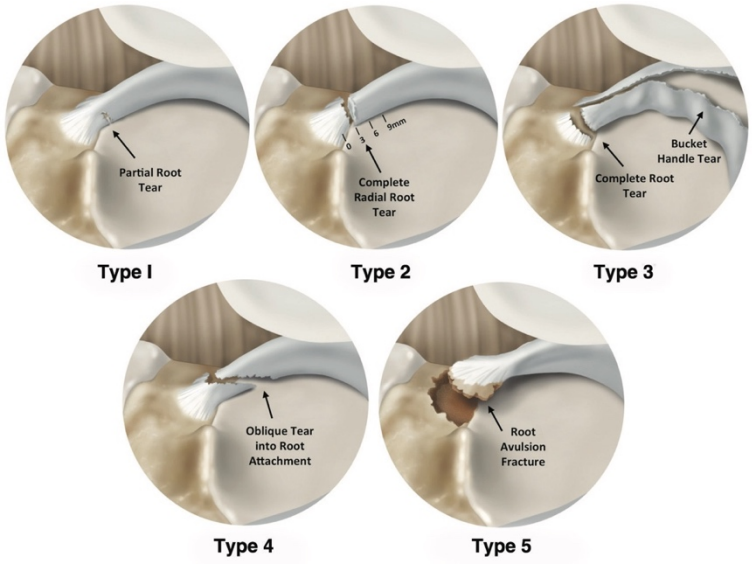

Figure 24. Meniscal root tear classification **Type 1.** Stable partial lesion within 9mm of the root attachment (7%) **Type 2.** Complete radial tears within 9 mm of root attachment (67.6%). Separated into: 2A: 0 – 3 mm (38%); 2B: 3 – 6 mm (16.9%); 2C: 6 – 9 mm (12.7%). **Type 3.** Complete root detachment with bucket handle tear (5.6%) **Type 4.** Complete root detachment with oblique tear (9.9%) **Type 5.** Bony avulsion fracture at root attachment site (9.9%). (Reprinted from 'Meniscal root tears: a classification system based on tear morphology' by LaPrade CM et al. (2015). Reproduced with permission from SAGE)

The position of the suture can now be explored. Very close proximity to the torn edge may result in suture cut out, loss of fixation, and failure of the root repair. Alternatively, capturing the horn at a distance may lead to excessive tension on the meniscal body. One biomechanical study reported the strongest repairs to be within the body of the meniscus or on either side of the central part of the transition zone of the root ligament (Figure 10a) (Robinson et al., 2018). A further two biomechanical studies reported that following a medial meniscus posterior root tear, the load to failure and tibiofemoral contact mechanics was markedly improved if the suture construct was positioned 5 – 8 mm from the root attachment site (Kim et al., 2016; Padalecki et al., 2014). Many studies have adopted this approach (Marzo et al., 2008; Chung et al., 2018; Park et al., 2023; Saengpetch et al., 2023; Seo et al., 2009).

2.4.8 Summary of surgical options in transtibial pull through repair for MMPRT

It is important one selects the best combination of techniques to construct the transtibial repair for MMPRT. This is to limit its potential in deranging the extrusion value or tibiofemoral contact mechanics prior to performing the centralization procedures. Furthermore, it will also provide context in some of the constructs selected for centralization.

In summary from the evidence provided, a single tunnel anatomical transtibial pull through repair with two UHMWPE tapes in a simple stitch configuration was used for this thesis. The root tear was created at the insertion site and the tapes were passed 5 – 8 mm from the torn edge. Once passed through the tunnel they were tied over a cortical button.

2.5 Centralization

Numerous studies have shown successful clinical outcomes after a transtibial meniscal root repair (Kim et al., 2011; LaPrade et al., 2017; Lee et al., 2009; Moon et al., 2012). However, the presence of pathological extrusion and osteoarthritis progression may worsen even if the technique is performed well. This is particularly the case at two-to-three-year follow-up post-operatively (Kaplan et al., 2018; Chung et al., 2022), suggesting that although clinical outcomes in the short-term are optimistic, long-term outcomes regarding progression of OA may not be as predictable. Therefore, concomitant techniques are required to anchor the periphery of the meniscus to the rim of the tibial plateau following root repair to provide additional protection to pathological extrusion.

This stabilization technique is known as centralization. Its history, evolution and application will now be explored, with a view to support our aims and objectives of the thesis. It will also help to understand the surgical technique that was performed in the methodology.

2.5.1 Knotted anchor-based centralization

Centralization was first introduced by Koga for repairing lateral meniscus extrusion secondary to a discoid lateral meniscus (Koga et al., 2012). This was with the use of a knotted anchor system. Arthroscopically, the meniscal extrusion would be confirmed with a probe (Figure 25a). The meniscotibial capsule would be released from the tibia using a rasp to improve the meniscal mobility to aid the restoration of the anatomical position of the meniscus (Feucht et al., 2015b). A Jugger Knot soft anchor with two suture strands (Biomet, Warsaw, Indiana, USA) is placed on the lateral edge of the lateral tibial plateau anterior to the popliteal hiatus (Figure 25b & c; Figure 26a). A specialised instrument with a nitinol wire loop (Figure 26b) called a Micro Suture lasso small curve is then inserted to penetrate the capsule from a superior to inferior direction (Figure 25d). This passes between the meniscus and capsule. One suture strand from the anchor is then placed into this nitinol wire loop underneath the extruded meniscus. The other limb of the wire loop is pulled to pass the suture from an inferior to superior direction through the capsule (Figure 25e; Figure 27). The same procedure is performed again for the remaining suture of the anchor. Both strands are then tied to create a mattress configuration and secured with a sliding locking knot, helping to tighten the capsule. It is this tightening of the capsule that helps to ‘push’ the extruded body of the lateral meniscus back to its anatomical position (Figure 25f).

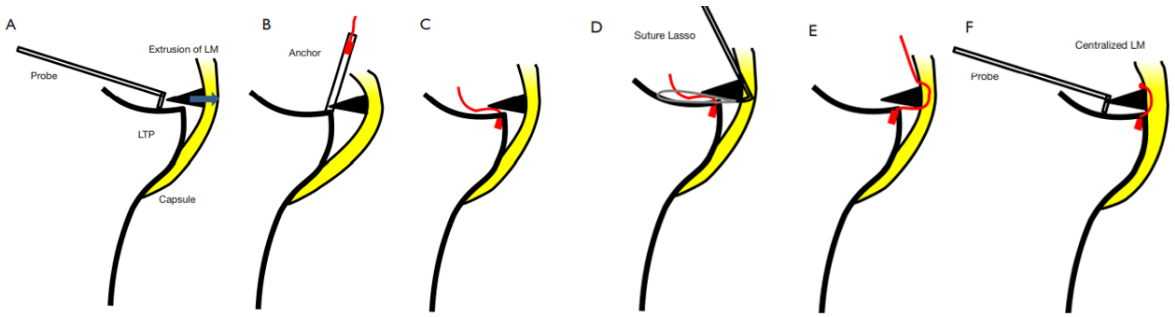

Figure 25 Schematic drawing of the knotted arthroscopic centralization procedure **(a)** meniscal extrusion confirmation with prob **(b & c)** anchor insertion lateral edge of tibial plateau **(d)** insertion of nitinol wire loop between meniscocapsular junction (**e)** both strands of the anchor passed through capsule from an inferior to superior direction with help of nitinol wire loop **(f)** suture strands tied, tightening capsule and bringing extruded meniscus back into position (Reprinted from 'A narrative review of lateral meniscus root tears and extrusion: techniques and outcomes' by Nakagawa et al. (2022). Reproduced with permission)

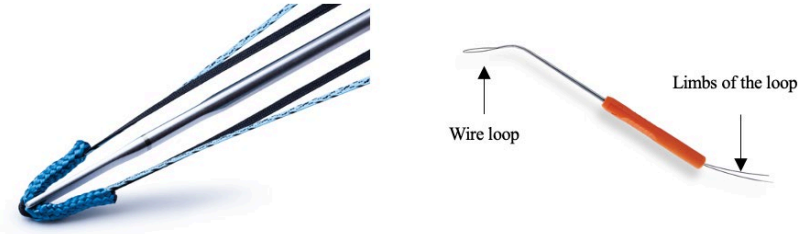

Figure 26 (a) Jugger knot soft anchor – the U-curved anchor is placed into the tibial plateau. The two suture strands will in turn go through the nitinol wire loop. **(b)** Micro SutureLasso Small Curve (Arthrex). Pulling on one of the limbs of the loop will close the loop containing the suture strand from anchor, and pull it through the capsule in inferior to superior direction (Reprinted with permission from Zimmer Biomet and Arthrex website)

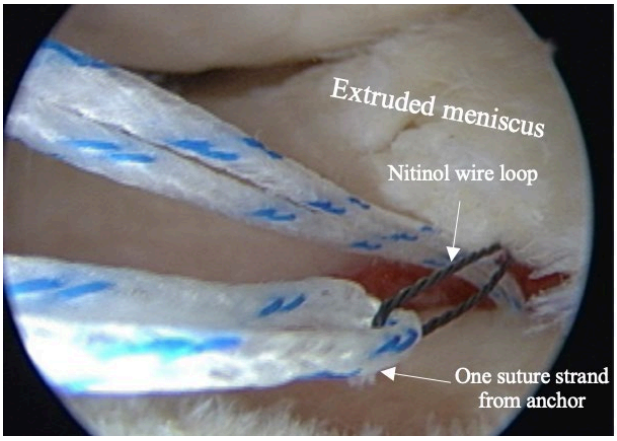

Figure 27. Arthroscopic view of a lateral meniscus extrusion. Nitinol wire loop seen under the extruded meniscus. One suture strand from anchor passed through the wire loop. Following this, the limb of the wire loop will be pulled, closing the loop hole and pulling the suture strand from and inferior to superior direction through the capsule. (Reprinted from 'A narrative review of lateral meniscus root tears and extrusion: techniques and outcomes' by Nakagawa et al. (2022). Reproduced with permission)

Three biomechanical studies investigated this technique for lateral meniscus extrusion following a lateral meniscus posterior root tear (Ozeki et al., 2020; Kohno et al., 2022; Kubota et al.m 2020) No root repair was performed in these studies. The overall findings were that knotted centralization significantly improved tibiofemoral contact mechanics and reduced extrusion, with values restored to the intact state. Clinical results with this centralization technique for lateral meniscus extrusion were promising, with two-year post-operative results showing significant improvement in patient-reported outcome measures (Lysholm and Knee Injury and Osteoarthritis Outcome Scores (KOOS)), full range of motion and maintenance of extrusion to physiological values (less than 3 mm) (Koga et al., 2016; Koga et al, 2020)

Following this, Koga et al (2017) then described the same technique but for centralization of the medial meniscus, particularly in conjunction with transtibial repair for medial meniscus posterior root tear. It is advised to perform the centralization technique prior to the root repair (Lee et al., 2022). Two biomechanical studies have investigated knotted repair for MMPRT, but no root repair was performed. Both showed significant improvement of tibiofemoral contact mechanics with reduced extrusion, with values restored to the intact state (Debieux et al., 2020; Ueki et al., 2023). Clinical results with this technique for MMPRT in conjunction with a root repair are promising, with improved Lysholm and KOOS scores at 2.5 years post-operatively with maintenance of extrusion to physiological values (less than 3 mm) (Mochizuki et al., 2021).

2.5.2 Knotless anchor-based centralization

Centralization with a knotted suture has potential pitfalls. The knot stack can cause impingement, and if is over-tensioned it can potentially over constrain the knee. In contrast,

sub-optimal tensioning can undo the knot and loosen the capsule, leading to re-extrusion of the meniscus. Furthermore, this can leave loose bodies in the joint, causing pain.

As discussed in subsection 2.4.2, the medial meniscus is most vulnerable to extrusion posteromedially. Placing an anchor here arthroscopically through a posteromedial portal may achieve more effective centralization and augmentation. This is best achieved with a knotless system.

Koga et al. (2021) described such a system using a 1.8mm Knotless FiberTak Soft Anchor (Figure 28). This consists of the following strands – a repair suture (blue and white), and a two ended Fiberlink (black) with one looped end. The looped end is called the shuttling loop and non-looped end the shuttling suture.

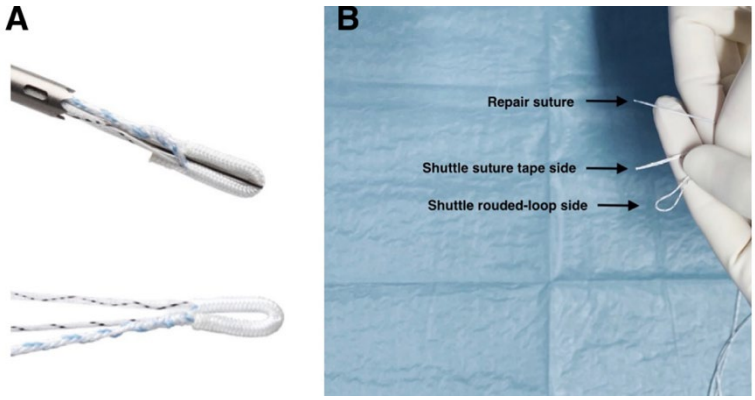

Figure 28. (A) A single suture knotless 1.8-mm FiberTak Arthrex anchor **(B)** The end of the repair suture and the 2 different ends of the shuttle suture. (Reprinted from 'Arthroscopic Superior Capsular Reconstruction (ASCR): All Soft Anchors Technique' by Avanzi et al. (2023). Reproduced with permission from Elsevier)

Following meniscotibial capsular release to mobilise the medial meniscus, the knotless anchor is inserted on the edge of the medial tibial plateau, as posterior as possible. A position 10 mm posterior to the posterior border of superficial MCL is acceptable. The repair suture passes

between the meniscus and capsule from an inferior to superior direction through the capsule and then back down to create a mattress configuration. The end of the repair suture is then loaded into the fiberlink looped end (Figure 29). The shuttling suture (the other end of the fiberlink) is then pulled, and the repair suture is then shuttled into the anchor's locking mechanism ('Chinese finger trap') (Figure 29). The tension is controlled under direction vision, and an appropriate amount can be applied to re-tighten the capsule and bring the meniscus back to its anatomical position.

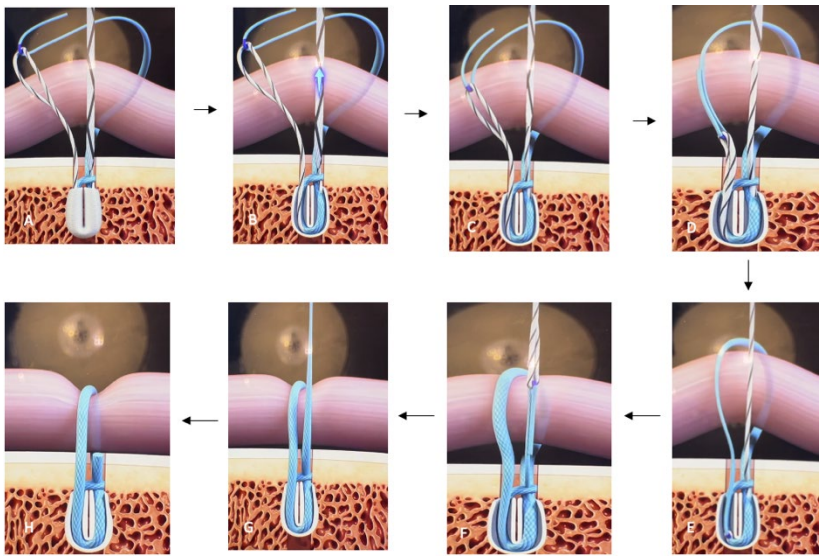

Figure 29. Schematic diagram of Knotless FiberTak anchor technique on an extruded meniscus **(A – D):** The repair suture loaded within the looped end, and at same time the shuttling suture is pulled upwards. This brings the repair suture down onto meniscus. **(E – G):** Capsule and meniscus tightened and held down by the repair suture. **(G – H)** Note how fiberlink suture after being pulled leaves the knee joint

Koga et al. (2021) described this system but with the use of three anchors. The first anchor was placed as described. The second anchor was 10 mm anterior to the first (at the posterior border of the MCL) and third anchor 10 mm anterior to the second (Figure 30). Once all three anchors were inserted, the repair suture of each anchor, having passed through the meniscocapsular junction, was passed into the shuttling loop of the next anchor. When the shuttling suture of its

own anchor is then pulled, the repair suture from the previous anchor then interlinks with this anchor (see Figure 30). This is known as horizontal plane centralization and allows extensive centralization across the meniscus.

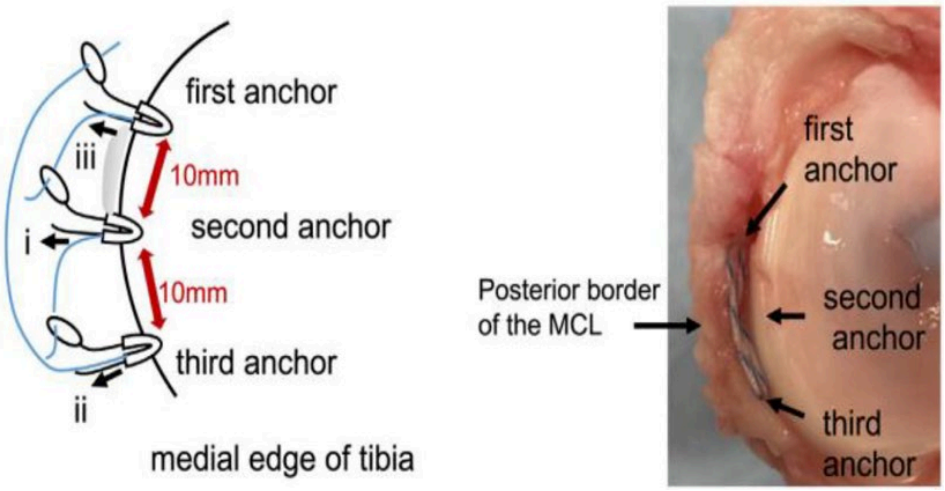

Figure 30. Repair suture from first anchor enters shuttling loop of second anchor. Repair suture from second anchor enters shuttling loop of third anchor. Repair suture from third anchor enters shuttling loop of first anchor. After pulling the shuttling suture of first anchor, the repair suture from third anchor interlinks with first anchor. After pulling shuttling suture of second anchor, the repair suture from first anchor interlinks with second anchor. After pulling shuttling suture of third anchor, the repair suture from second anchor interlinks with third anchor. (Reprinted from 'Augmentation of a Nonanatomical Repair of a Medial Meniscus Posterior Root Tear With Centralization Using Three Knotless Anchors May Be Associated With Less Meniscal Extrusion and Better Compressive Load Distribution in Mid-Flexion Compared With Non-Anatomical Root Repair Alone in a Porcine Knee Model' by Amano et al. (2023). Reproduced with permission from Elsevier.

Around the same time, two other authors reported similar methods, albeit they used a mattress suture technique for the repair suture of each anchor rather than the horizontal interlinkage described in Figure 30 (Leafblad et al., 2021; Wu et al., 2022). To date, only one biomechanical study has investigated the effects of this knotless centralization construct in medial meniscus posterior root tears. This was performed also in the presence of a root repair (Amano et al., 2023). The results of this study showed that not only did the knotless construct significantly improve tibiofemoral contact mechanics and reduce extrusion in comparison to the root torn state, but it also reduced it to the intact state and performed better than a root repair on its own

throughout knee flexion (0 - 90°). Clinical results with this technique for MMPRT in conjunction with a root repair are promising, with significant improvement in a number of patient-reported outcome measures at two-years post-operatively to include subjective International Knee Documentation Committee score (IKDC), KOOS, Tegner score and subjective pain (Krych et al., 2024)

2.5.3 Transtibial centralization

Dean et al (2020) reported on a centralization technique for medial meniscus posterior root tears without anchors, but with a tibial tunnel created at the posteromedial edge using the drill guiding system used for the transtibial repair. This tunnel is created once the conventional tunnel for the meniscal root repair has been performed and the repair sutures are passed through it, pulling the root tear into place. A suture tape is placed for the peripheral stabilization of the extruded meniscus. Its location is at the apex of the posterior horn of the medial meniscus from the tibial to femoral side (Figure 31). This tape will pass through the meniscus from the tibial to femoral side, and then back through the femoral to tibial side to create a double loaded construct. Both suture tapes are then fixed to their own cortical fixation device.

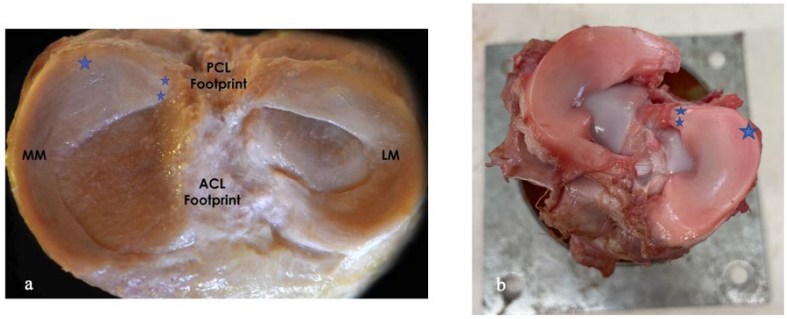

Figure 31. Axial view looking down a **(a)** cadaveric and **(b)** porcine dissection in a right and left knee respectively. The porcine dissection is from the experimental work presented in this thesis. The 2 small stars represent he location of the sutures to pass through the conventional transtibial tunnel. The large star at the apex of the posterior horn of the medial meniscus represents the location of the peripheral stabilization suture and the respective transtibial tunnel (28 a reprinted from 'Peripheral Stabilization Suture to Address Meniscal Extrusion in a Revision Meniscal Root Repair: Surgical Technique and Rehabilitation Protocol' by Dean et al. (2020). Reproduced with permission from. Elsevier.

To date, there is one biomechanical study that investigated the effects of transtibial centralization for medial meniscus posterior root tears in the present of a transtibial repair (Daney et al., 2019). They found adding the centralization stitch was beneficial in reduction extrusion and restoring tibiofemoral contact mechanics to the native state. There are no clinical studies to date.

2.5.4 Anchor based centralization vs Transtibial centralization for medial meniscus posterior root tears

As outlined, multiple biomechanical and clinical studies have shown centralization to play a beneficial role in improving meniscal extrusion, tibiofemoral contact mechanics and patient reported outcomes in those with medial meniscus posterior root tears. This is further supported by a recent systematic review by the author (Boksh et al., 2024a).

However, to date there is no study identifying the optimal centralization technique. There is insufficient evidence to evaluate the extent to which improved biomechanical outcomes are attributed to centralization itself. Knotless anchor-based and transtibial centralization are routinely now used in practice, yet no biomechanical comparison exists to determine the superiority of either technique. Transtibial centralization has its potential pitfalls; an additional tunnel and suture fixation device is needed, which can increase the risk of intra-operative fracture and cause increased irritation. It is also technically challenging. Knotless anchors require a posteromedial portal and thus are near critical neurovascular structures. The arthroscopic instruments required such as the Microsuture Lasso, rasp and curved guide can cause chondral injury if not handled carefully. Furthermore, if the meniscal body is penetrated rather than the meniscocapsular junction, this will over constrain the medial meniscus, impairing its hoop stress function.

In view of these pitfalls, it is paramount to understand which technique would better restore both the tibiofemoral contact mechanics of the knee, to include contact area and pressure, and pathological extrusion following a medial meniscus posterior root repair. These results can potentially direct appropriate treatment to salvage the native knee joint.

2.6 Assessment of tibiofemoral contact mechanics

2.6.1 History

Tibiofemoral contact mechanics (TFCM), in particular contact area and pressure, provide an understanding in the development of chondral injury, and are accepted biomechanical metrics for the evaluation of the menisci in its intact, torn, and repaired state (Frank et al., 2017; Krych et al., 2020). Knowledge of the patterns of TFCM in these conditions will determine the approach one takes to restore knee joint function (Martinelle et al., 2006). Pressure sensors and and films are increasingly being used to quantify contact area and pressure (Allaire et al., 2008; Becher et al., 2008; Lee SJ et al., 2006; Ostermeier et al., 2007; Wirz et al., 2002), with importance placed on appropriate and correct utilization, as such outcomes in biomechanical research can influence clinical practice and patient care.

Historically, the systems used included casting techniques such as silicone rubber (Xantropen Blau) (Kurosawa et al., 1980; Walker et al., 1970) and silicon carbon powder suspensions (Yao et al., 1991). The silicone rubber method involves the mixture of two liquid components which following its solidification is placed on top of the meniscus. Its deformation under load provides a contact area measurement. However, a limitation to this is that the minimum time required to indicate contact areas clearly is at least one order of magnitude longer than the physiological loading period. The contact area thus obtained is, therefore, much larger than the actual one under the physiological joint loading, due to the viscoelastic nature of articular

cartilage. Yao et al. (1991) described the 3S technique, a form of carbon powder suspension. Silicon oil with a small quantity of Xerox V Toner photocopy carbon black powder is mixed, then applied onto the contact surface of the meniscus and following loading, the suspension squeezes out of the contact region. After unloading, the contact area is outlined on the surface and measurement can be made. However, its main limitations include the inability to measure pressure, and that the suspension requires constant wiping down from the meniscus surface, thus posing a particular problem at different flexion angles. This risks overestimating the area at each new test protocol.

2.6.2 Fujifilm Prescale film

Fujifilm prescale film (Fuji Ltd, Tokyo, Japan) is a pressure sensitive paper technique first described by Fukubayashi and Hurosawa (1980). There are two types of films: a mono-sheet, measuring pressure between 10 to 300 MPa and a two-sheet film, which measures pressure between 50 KPa to 50 MPa. The latter can be further separated into sheets with different measuring ranges: ultra-extreme low (5LW), extreme low (4LW), ultra-super low (LLLW), super low (LLW), low (LW) and medium pressure (MW) (Figure 32).

The two sheets consist of a colour forming layer (A film) and colour developing layer (C film). Both sheets are cut to the dimensions of the knee and meniscus. The rough surfaces of each film are opposed to each other and inserted under the meniscus. Pressure can then be applied onto the films in either one of two ways: a) gradually increasing the pressure to required level in two minutes and maintaining at that pressure for another two minutes. This is known as continuous pressure or b) applying pressure for five seconds and maintain pressure for another five seconds. This is known as momentary pressure. For ± 10% precision, the recommended temperature and room humidity range is 20°C-35°C and 35% - 80% respectively. Upon

pressure application, micro-capsules on A film break down and interact with the C film (Figure 33). A red colour will present on the C film, with its intensity proportional to the applied load. Patchy areas are suggestive of uneven pressure distribution. To roughly determine the pressure values, one should correlate the colour intensity to a standard colour calibration key, and then select the appropriate standard pressure densitometer chart.

An example of this is provided with the super-low-pressure sheet in Figure 34.

Types	Measurable pressure range [MPa] 1MPa≒10.2kgf/cm² (0.006 0.05 0.2 0.5 0.6 2.5 10 50 130 300)	Prescale Product size width(mm) x length(m)	Prescale Sheets Product size width(mm) x length(mm)	Classification
Ultra Extreme Low Pressure (5LW)		320 x 2	–	Two-Sheet Type
Extreme Low Pressure (4LW)		320 x 3	–	Two-Sheet Type
Ultra Super Low Pressure (LLLW)		270 x 5	270X200 (5 Sheets)	Two-Sheet Type
Super Low Pressure (LLW)		270 x 6	270X200 (5 Sheets)	Two-Sheet Type
Low Pressure (LW)		270 x 10	270X200 (5 Sheets)	Two-Sheet Type
Medium Pressure (MW)		270 x 10	–	Two-Sheet Type
Medium Pressure (MS)		270 x 10	270X200 (5 Sheets)	Mono-Sheet Type
High Pressure (HS)		270 x 10	270X200 (5 Sheets)	Mono-Sheet Type
Super High Pressure (HHS)		270 x 10	270X200 (5 Sheets)	Mono-Sheet Type

Figure 32. Table of the various Fujfilm prescale sheets. There are different sheets accustomed to measure different pressure ranges. **5LW**: PSI, 0.87 – 7.25; MPA, 0.006 – 0.05. **4LW**: PSI, 7.25 – 29, MPA, 0.05 – 0.2. **LLLW**: PSI, 28 – 85; MPA, 0.2 – 0.59. **LLW:** PSI, 71 – 355; MPA, 0.49 – 2.4. **LW**: PSI, 355 – 1420; MPA, 2.4 – 9.8. **MS & MW:** PSI, 1420 – 7110; MPA, 9.8 – 49. **High Pressure (HS):** PSI, 7100 – 18500; MPA, 49.0 – 127.6. **Super High Pressure (HHS):** PSI, 18500 – 43500; MPA, 127.6 – 300. (Reproduced with permission from Fujifilm prescale film website)

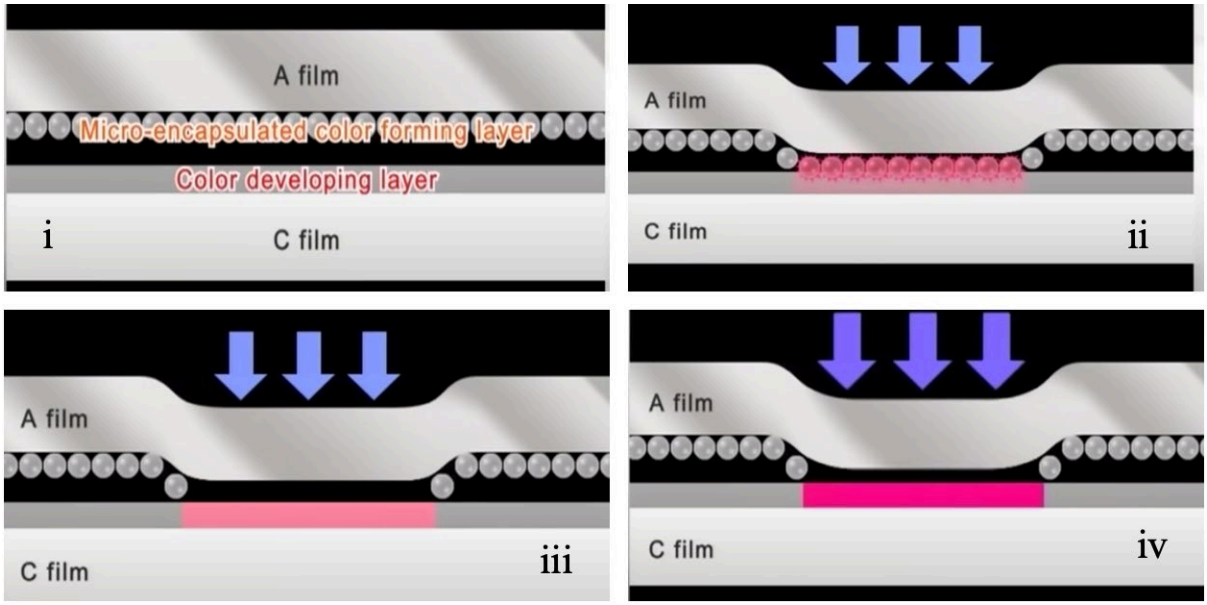

Figure 33. (i) Colour developing layers. **(ii)** upon load application, A capsules disperse colour layer on C film **(iii & iv)** the lighter and darker red colour proportional to the amount of load exerted.

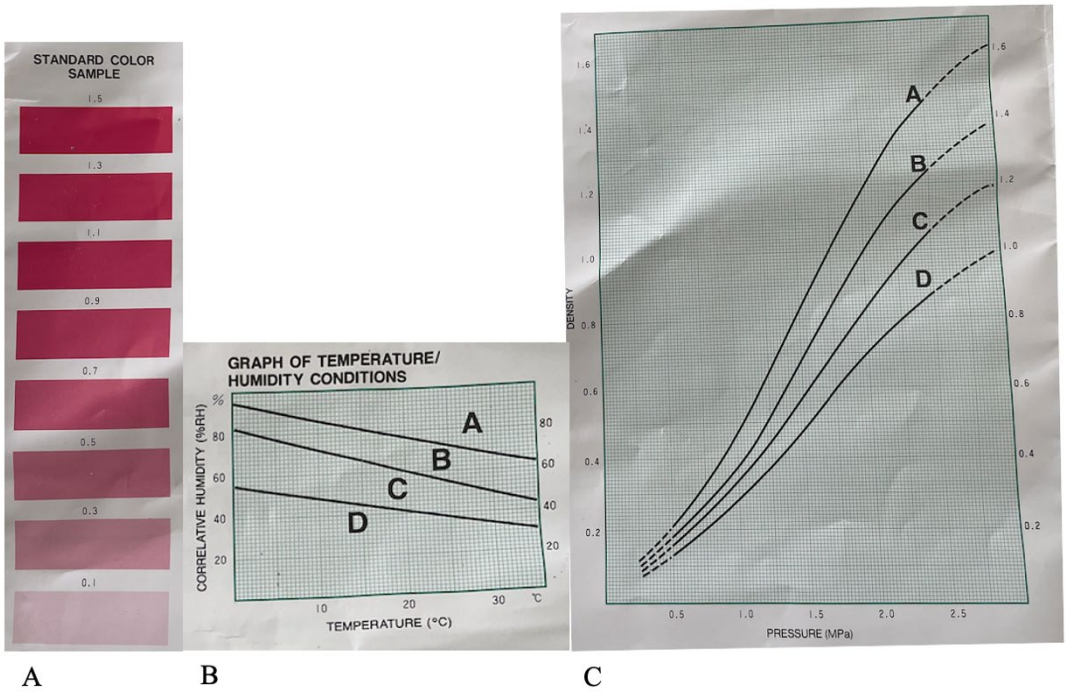

Figure 34. Estimating the pressure following application of load on a super-low Fujifilm sheet. Following the coordination of the colour density on the chart (A) and the label to choose based on the temperature and humidity of the surroundings (B), one can then estimate the pressure value on the densitometer graph (C)

2.6.3 Advantages and applicability of Fujifilm within study

Although it only provides a measure of TFCM at one time under one set of circumstances (Bertsch et al., 2001; Rosenbaum et al., 2003), its use with instantaneous loads can help to avoid the redistribution of fluid in articular cartilage, and in turn, pressure distributions, that occur when testing a joint with a static load (Brown et al. 1984). The film is also thin and pliable (0.4 mm thickness), allowing it to be inserted beneath the meniscus with minimal disruption of joint ligaments and capsule, and also adaptable to the concave and convex shape of the tibiofemoral joint. There are various ranges of films available as described, all of which operate under different load levels to ensure pressure maps can be created without the film becoming fully saturated. This may limit the acquisition of data based on the load applied. However, the super-low (0.5 – 2.5 MPa) and to an extent the low range films (2.5 – 10 MPa) have greater pressure resolutions compared to their counterparts (Liggins et al., 1995). Martens et al. (1997) noted a load of 1.75 times body weight provides accurate pressure maps under these circumstances. This was further underlined in studies that used Fujifilm to assess meniscal root tear repairs (Allaire et al., 2008; Baratz et al., 1986; Muriuki et al., 2011). All provided appropriate pressure maps and contact area with the low and super-low film at loads between 1000 – 1800N, reflecting the calculated target described by Martens et al (1997). Harris et al (1999) reported that although Fujifilm may under-estimate contact area across all flexion angles of 0 – 90°, this difference is much reduced with the lower range films. Furthermore, the under-estimation of TFCM with Fujifilm will occur across all testing conditions, therefore, minimizing the potential difference between the intact, torn and repaired meniscal root states. In fact, all 3 studies using these lower range films had shown similar conclusions (Allaire et al., 2008; Baratz et al., 1986; Muriuki et al., 2011). In this context, low and super-low Fujifilm, which is both cheap and readily accessible, is an appropriate measurement source within the thesis to assess tibiofemoral contact mechanics.

2.7 Chapter summary

This background chapter summarizes the function and anatomy of the meniscal root, its similarity and differences between human and porcine knees, and the pathological consequences following its injury. The chapter also focused on optimizing the conventional repair technique, and how despite this, suboptimal biomechanical performance can persist. Newer techniques, under the term centralization, have emerged, but it is not fully understood which of these provide the best biomechanical outcomes following a medial meniscus posterior root tear repair. This requires investigating, particularly its effects on a) tibiofemoral contact area and pressure with the use of Fujifilm prescale, and b) on meniscal extrusion at various degrees of flexion. The next chapter will present the materials and methods used in this study.

CHAPTER 3

3. Materials and Methods

3.1 Chapter overview

This chapter will present the materials and methods used in biomechanically comparing the knotless and transtibial centralization techniques for medial meniscus posterior root tears in porcine knee joints. To begin, porcine knee storage, handling and dissection will be discussed in section 3.2. The design of a testing rig for mechanically loading the knee at various flexion angles will be discussed in section 3.3 Section 3.4 will describe the key surgical instruments required for each testing state, the latter of which will be described step by step in section 3.5. Sections 3.6 and 3.7 focuses on the measurement of meniscal extrusion and tibiofemoral contact mechanics, respectively, along with their analysis on appropriate software. Section 3.8 presents the statistical methodology implemented.

3.2 Porcine knee storage, handling, and dissection

Fresh-frozen knee joints of approximately 90 kg, six-month-old commercially slaughtered pigs were obtained from a supplier (breed of Large White, Landrace and Duroc bloodlines; The Grassy Shire, Black Horse farm Partners, Slawston, Leicestershire, UK). As this was material generated for food production, no ethical approval was required.

Two hindlegs were used in the preliminary phase of the investigation, to understand the relevant dissection required and the working dimensions for the creation of the testing rig (section 3.3). Twelve hindlegs were used for the main body of research. This sample size was appropriate based on power calculations described in section 3.8. No gross evidence of meniscal damage, ligament tears, fractures, or cartilage degeneration greater than Outerbridge grade 1 classification were observed in any of the knees.

On arrival in the laboratory, the specimens were sealed in plastic sheathing, stored in a freezer at – 40 °C until they were required for testing (Li W et al., 2020; Mahmood et al., 2018). The specimens were thawed for 24 hours preceding dissection and testing. Specimens were dissected free of skin and subcutaneous tissue. Once down to the patella, the dissection continued anteriorly with a supra-patellar incision that extended inferiorly on both sides to remove the patella, patellar tendon and surrounding fat pad. Removal of the patella allowed for clear visualization of the anterior joint structures. Then, the dissection was carried out posteriorly to remove the popliteal blood vessels and all adherent soft tissue. The knee-stabilizing structures were preserved in order to simulate the biomechanical properties of the knee joint as closely as possible (Figure 35). This included the anterior cruciate ligaments (ACL), posterior cruciate ligaments (PCL), and lateral collateral ligament (LCL). Sub-meniscal arthrotomies were performed anteromedially and posteromedially for insertion of the Fujifilm prescale films. These were kept within the boundaries described in Section 2.2 and Figures 12a and 13. When performing the arthrotomies, the POL meniscotibial ligament and meniscotibial ligament within the deep medial collateral ligament (MCL) were carefully preserved for the intact testing condition. As the subsequent testing conditions were to investigate for pathological extrusion, these meniscotibial ligaments were resected.

Initially the medial collateral ligament (MCL) was also preserved, but it was noted during the experiment that it required resection for insertion of the pressure film, in keeping with previous studies (Amano et al., 2023). As the focus of the thesis was on surgical techniques for medial meniscus posterior root tears, the medial compartments were used for the analysis.

The waste generated from dissection was stored in a double heat-sealed plastic bag and taken to the autoclave for disinfection and sterilization prior to its collection by an approved

transporter for disposal. Samples that would be used again were covered in tissue paper, coated with Ringer's solution prepared to a full-strength mass concentration by dissolving 4.83g of Ringer's tablets (Oxoid Ltd, Hampshire, UK), per 500 ml of distilled water and separately stored in a double heat-sealed plastic bag.

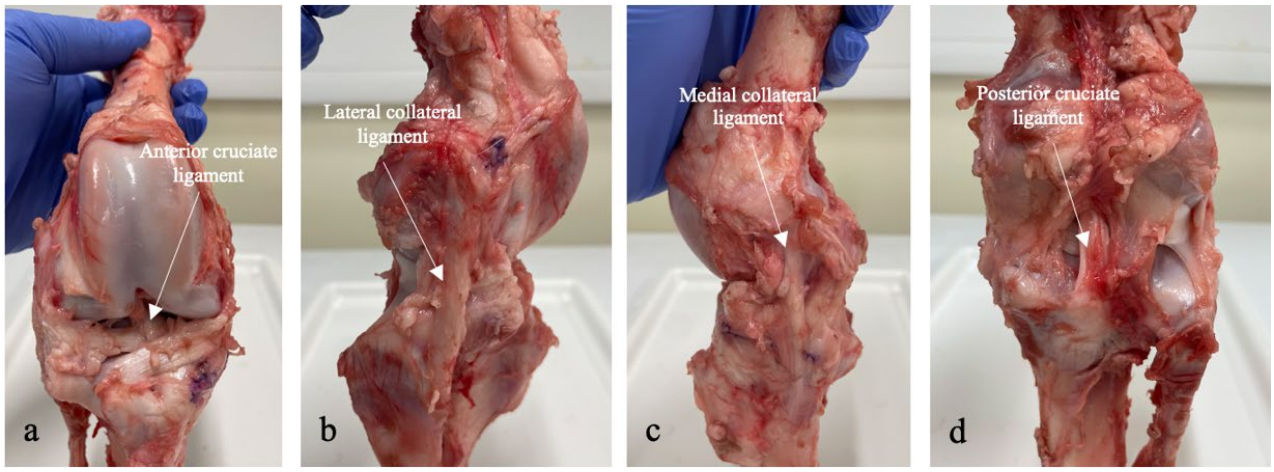

Figure 35. Dissection of a right porcine knee **(a)** anterior view with intact ACL **(b)** lateral view with intact LCL **(c)** medial view with intact MCL **(d)** posterior view with intact PCL

With a saw, the femur was cut 10 cm proximal and the tibia and fibula 12 cm distal from the joint line. Previous studies performed such cuts between 15 – 20 cm (Morales-Avalos et al., 2023; Chung et al., 2018; Saengpetch et al., 2023; Seo et al., 2009). The length chosen here was to keep the specimen within the confinements of the testing rig (see section 3.3).

A galvanised bolt down circular round post support base was bought from an appliance store and underwent refinement in the lab to pot the tibia and fibula (Figure 36). The total height was reduced by 6 cm with a cut and several holes at different levels across the steel cylinder was created for two to three M5.5 head self-tapping screws (60 mm in length) to insert into (Figure 37a & b). The screws were then drilled perpendicular to the bone shaft, engaging both cortices for secure fixation of the tibia and fibula (Figure 37c), with the tibial plateau orientated parallel to the testing surface. Engaging the screws at multiplanar level helped to fix the tibia

rigidly from multiple radial directions and at multiple superior-inferior levels (Koh et al., 2016). Additional fixation of the tibia and fibula was provided with the use of Petrobond casting sand (Blackbarn Design, UK), which can hold its shape and resist smaller rotatory motions at the tibia (Figure 37d).

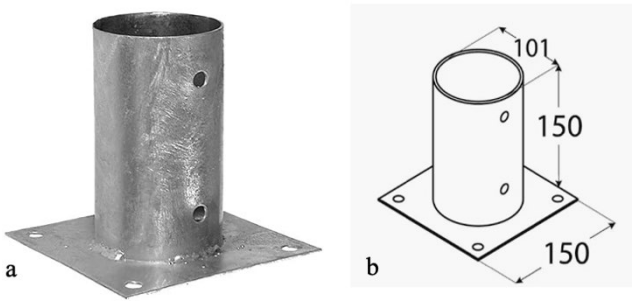

Figure 36 (a) Galvanised bolt down circular round post **(b)** Length 150 mm, cut down to 60mm and a number of holes added onto it at multiplanar level

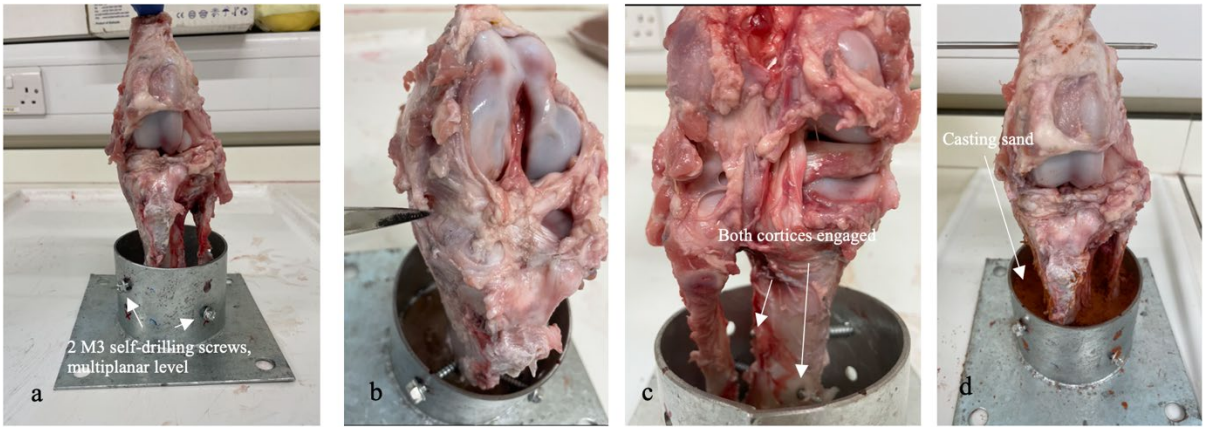

Figure 37 (a - c) Tibia and fibula potted in a steel cylinder and secured at multi-planar direction with screws **(d)** Petrobond casting sand to augment the fixation

3.3 Test rig

3.3.1 Overview

The primary objective of this study was to investigate which centralization technique (knotless anchor vs transtibial centralization) better restores both the tibiofemoral contact mechanics of the knee, to include contact area and pressure, and pathological extrusion under axial load over a range of flexion angles. In this respect, the potted dissected knee needs to be mounted onto a test rig that will not only allow an axial load to be placed across the tibiofemoral joint, but can also allow a selection of angles to be chosen.

3.3.2 Choice of load application

Previous biomechanical porcine studies examining tibiofemoral contact mechanics in the meniscal root and following various repair techniques advocate a single axial load of 200 N (Amano et al., 2023; Kohno et al., 2022; Kubota et al., 2020; Morales-Avalos et al., 2023; Ozeki et al., 2020). The general mass of pigs from which their knees are used are approximately 80 – 100 kg. Their centre of gravity is near the forelegs and load on the hind legs is lower than that of the forelegs. When standing on a quadruped, the load on a single hind leg is approximately 160 – 200 N (Conte et al., 2014). Although 200. N may be small as an axial compressive force compared to the 1000 N used in human cadaveric specimens (Daney et al., 2019; Debieux et al., 2021; Saltzman et al., 2020), previous biomechanical studies have shown this to be sufficient to examine the effects of meniscus extrusion and tibiofemoral contact mechanics following root repair and centralization, and large enough to yield clinically significant findings (Amano et al., 2023; Nakamura et al., 2019). In view of these findings, 200 N load was selected for this study.

3.3.3 Selection of flexion angles

At higher angles of flexion, the contact pressure on the meniscus increases (Ahmed et al., 1993; Thambyah et al., 2005). This is because at these angles, the area of contact of the femur and tibia with the meniscus increases (Yao et al., 2008). This causes the meniscus to bear more weight, particularly in the posterior direction and thus shows posterior movement (Yamamoto et al., 2021) (Figure 38). In this respect, range of motion has an influence on the distribution of load on the meniscus. Therefore, it is imperative to assess the centralization techniques on a range of flexion angles to see which one better restores the meniscal kinematics across the full range of motion to the native state.

Unlike human knees, the maximal extension of porcine knees corresponds to a human flexion of 30 degrees (Fuss et al., 1991). In view of these findings, a range of flexion angles to include 30°, 45°, 60° and 90° was selected for this study.

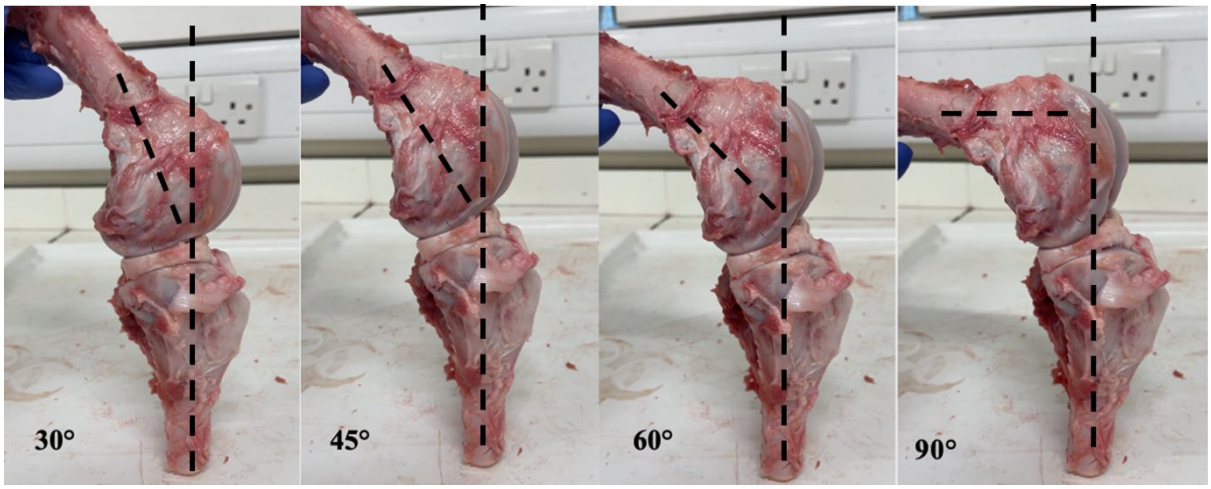

Figure 38. Medial view of left porcine knee used in the preliminary phase at varying degrees of knee flexion. Note the greater contact between the femur and medial menisci, and tibia plateau and medial menisci with deepening flexion. This causes the meniscus to move posteriorly and continue to do so as flexion deepens.
virtual lines along the longitudinal axes of the femur and tibia, respectively, to visualize the knee flexion angles illustrated.

3.3.4 Creation of the test rig

Previous biomechanical studies secured the potted knee by drilling transversely two parallel tunnels through the femur to which rods were then passed through and into a custom-made jig, which was then fixed onto a materials testing machine that applied axial compressive load (Geeslin et al., 2016; LaPrade et al., 2014a; Padalecki et al., 2014; Pasic et al., 2023). The distal tunnel was drilled through the femoral condyles (transepicondylar axis) and parallel to the tibial plateau to act as a load-bearing site and pivot point. The proximal tunnel was drilled through the proximal aspect of the femur parallel to the distal tunnel, acting to select and maintain the angle of knee flexion (Figure 39a). One study performed something similar, but the load was applied through two vertical threaded rods, one on the medial and one on the lateral side of the knee, transmitting the axial load to the transepicondylar rod (Figure 39b) (Koh et al., 2016). The advantage of this was that the threaded rods could be adjusted in the anteroposterior and superior-inferior directions to apply a balanced load to the medial and lateral sides of the transepicondylar rod and to the femur. In view of these findings, a similar test rig was created to conduct this experiment.

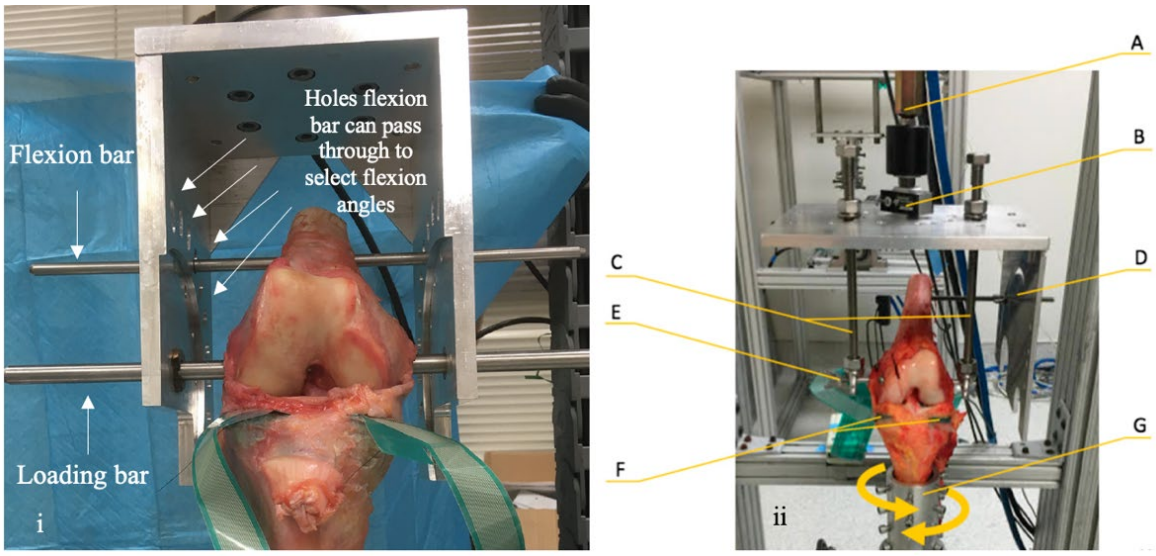

Figure 39. Custom made jigs to secure the femur onto the testing machine **(i)** Distal rod passing through transepicondylar axis acting as load pivot axis, and proximal rod passing through femur into various holes in the jig which coordinate with varying flexion angles **(ii)** Similar to (a), but the load pivot comes from the vertical threaded rods that transmit the axial load onto the transepicondylar rod (see label c). (Reprinted from 'A Biomechanical Comparison of All-Inside Versus Transtibial Meniscus Root Repair Techniques' by Pasic et al. (2023), and 'Tibiofemoral Contact Mechanics with Horizontal Cleavage Tear and Resection of the Medial Meniscus in the Human Knee' by Koh et al. (2016). Both reproduced with permission from SAGE and Wolters Kluwer)

A test rig from previous experiments was re-designed so that its structural properties could conform with the previously described studies to load the tibiofemoral joint at various angles (Figure 40). After preliminary dissection of one of the three 'practice' porcine knees, it was noted the following changes in the rig was required and thus performed:

a. The four 25 mm diameter mild steel support columns of 100 mm length were increased to 300 mm (so that the 220 mm length of total femur and tibia could sit within the rig) (Figure 41a & c).
b. The 30 mm linear bearing compression shaft through the flanged 30 mm linear bearing slide was welded with a mild steel platform. As a result, a 200 N load was now able to be applied (Figure 41a & b)

c. Two thin metal sheets were drilled to create 4.6 mm holes at 30°, 45°, 60° and 90° for a 4.5 mm pin to pass through. Multiple holes were created at each angle across a linear line, with the use of a goniometer to aid accuracy. These were then welded onto the sides of the support column (Figure 42a & b).

d. On the inferior surface of the compression shaft, a 30 mm circular locking collar was engaged on to it with an 8mm locking grub screw (Figure 43a & b). Two steel extension arms (horizontal bars) were welded onto the collar on either side with oval holes within them to allow a vertical M12 x 1.75 mild steel threaded rod of 200mm length to pass through. This was secured to the horizontal bar using M12 x 1.75 mild steel nuts on either side (Figure 43b). As per Koh et al. (2016) study, this vertical rod could be adjusted in the antero-posterior and superior-inferior directions.

e. The distal end of the vertical threaded rods had multiple holes of 7.0 mm diameter created. This was so a 6.5mm transfix pin could pass through this, into the femoral condyle, and out through the threaded rod on the other side (Figure 43 a).

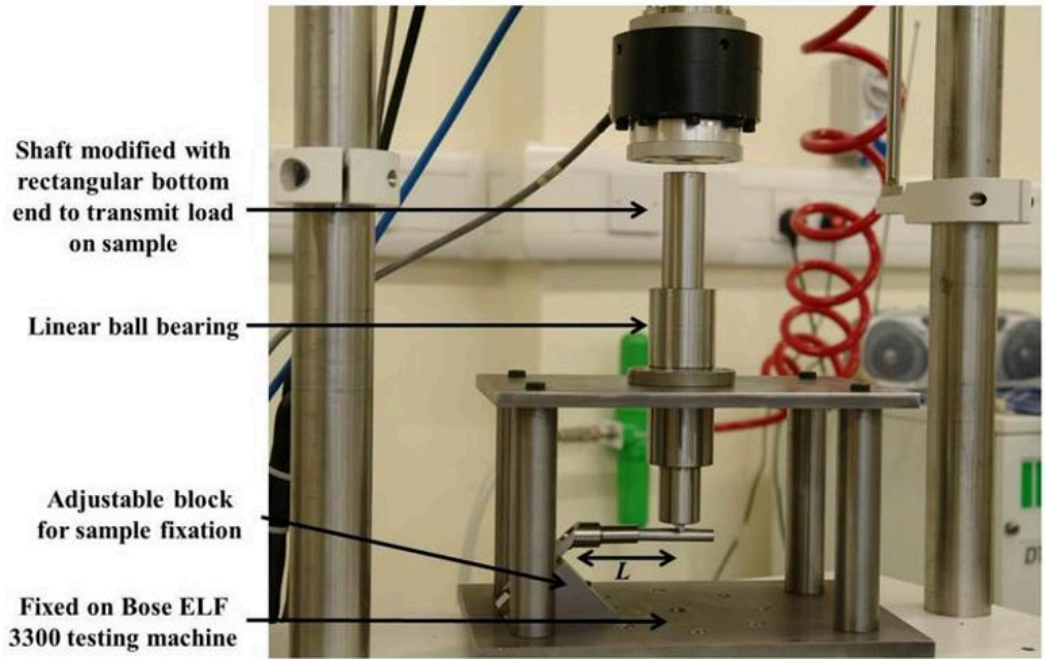

Figure 40. Testing rig taken from previous experiments and re-designed to create a suitable rig for mechanical testing of the knee joints

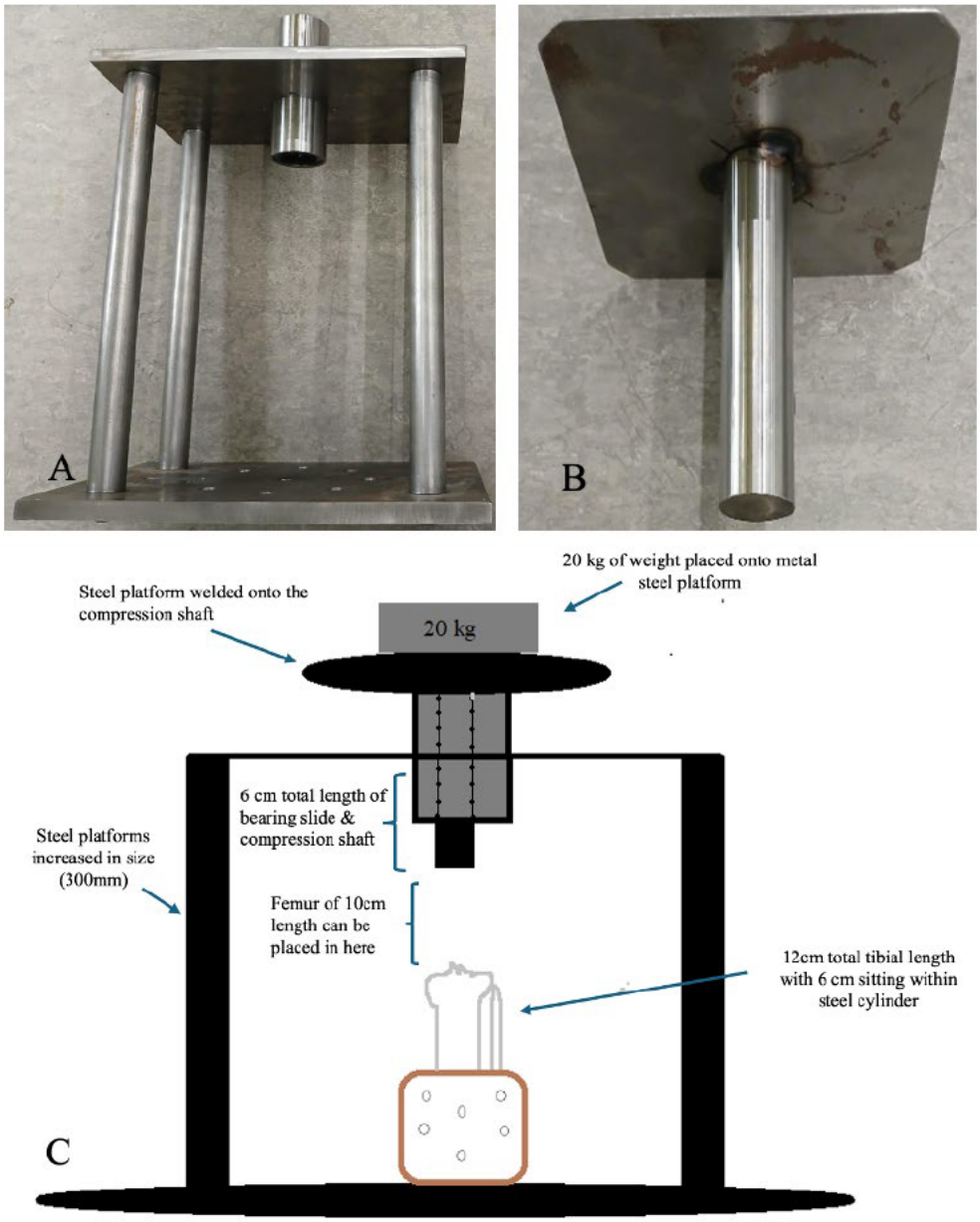

Figure 41 (a) Stainless steel column increased in length to 300mm **(b)** Metal platform welded onto the linear bearing compression shaft **(c)** Schematic diagram of the working length now provided within the rig

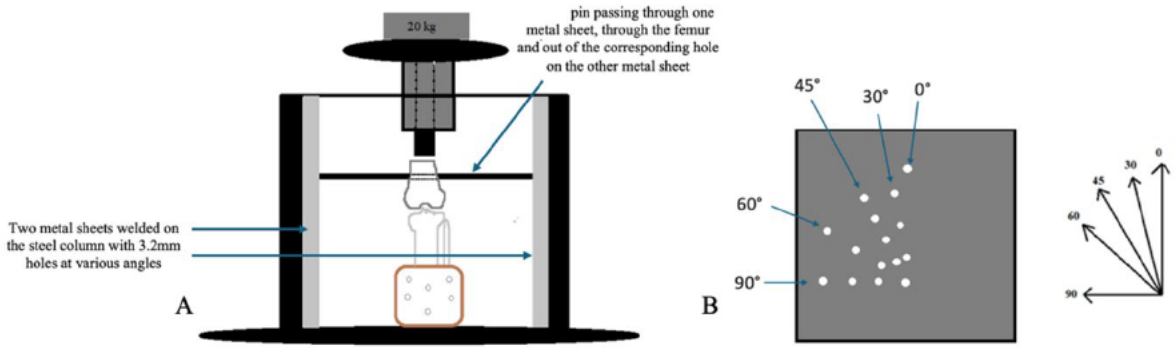

Figure 42 (a) Schematic diagram of the welded metal sheets with holes at multiple flexion angles. **(b)** Flexion angle holes

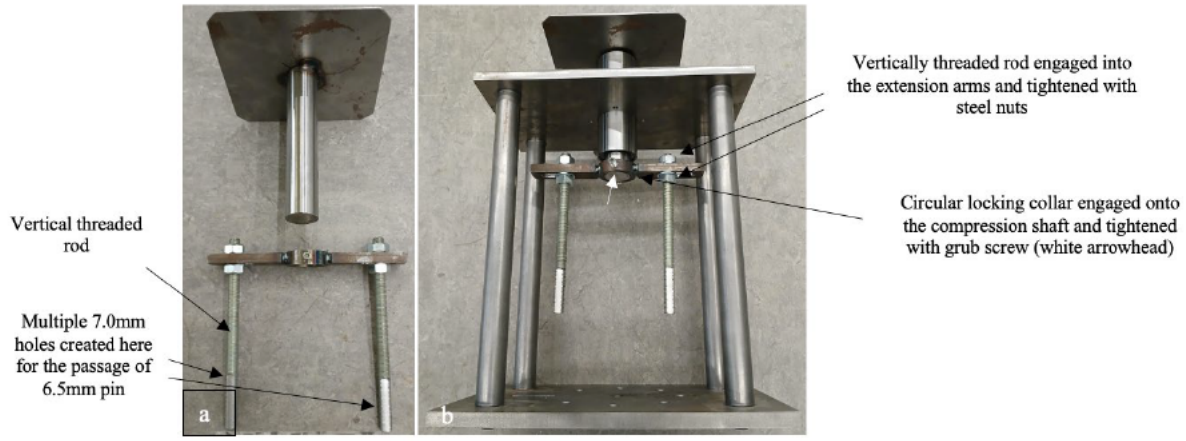

Figure 43. Mounting the circular locking collar onto the compression shaft **(a)** the collar with its extension bars and the vertical threaded rods running through it **(b)** the collar engages with the compression shaft through a grub screw. The vertical threaded rods tightened to the extension bar with nuts.

The final set up of the testing rig with a knee joint with the transmission of load is shown illustratively in Figure 44. Preliminary testing of a porcine knee within the rig at various flexion angles are shown in Figure 45 & 46.

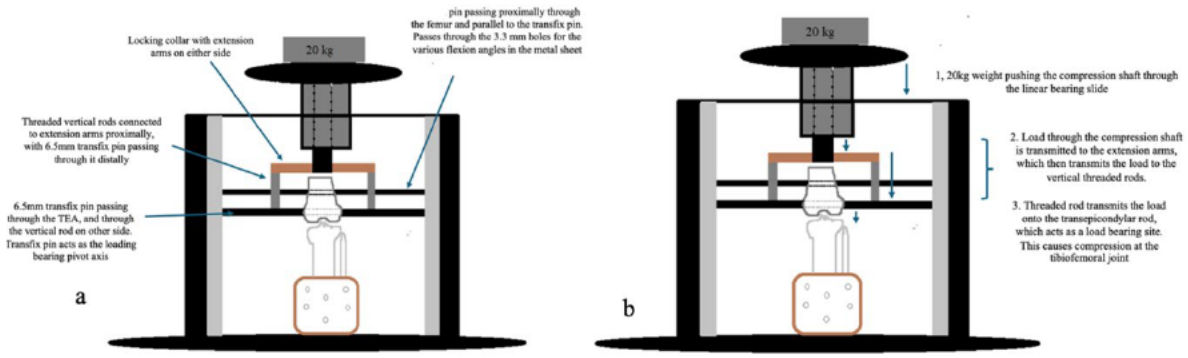

Figure 44. Schematic diagram of the final testing set up of the porcine knee joint within the testing rig. **(a)** All the key components of the rig are shown here **(b)** How load transmits through the rig and on to the tibiofemoral joint

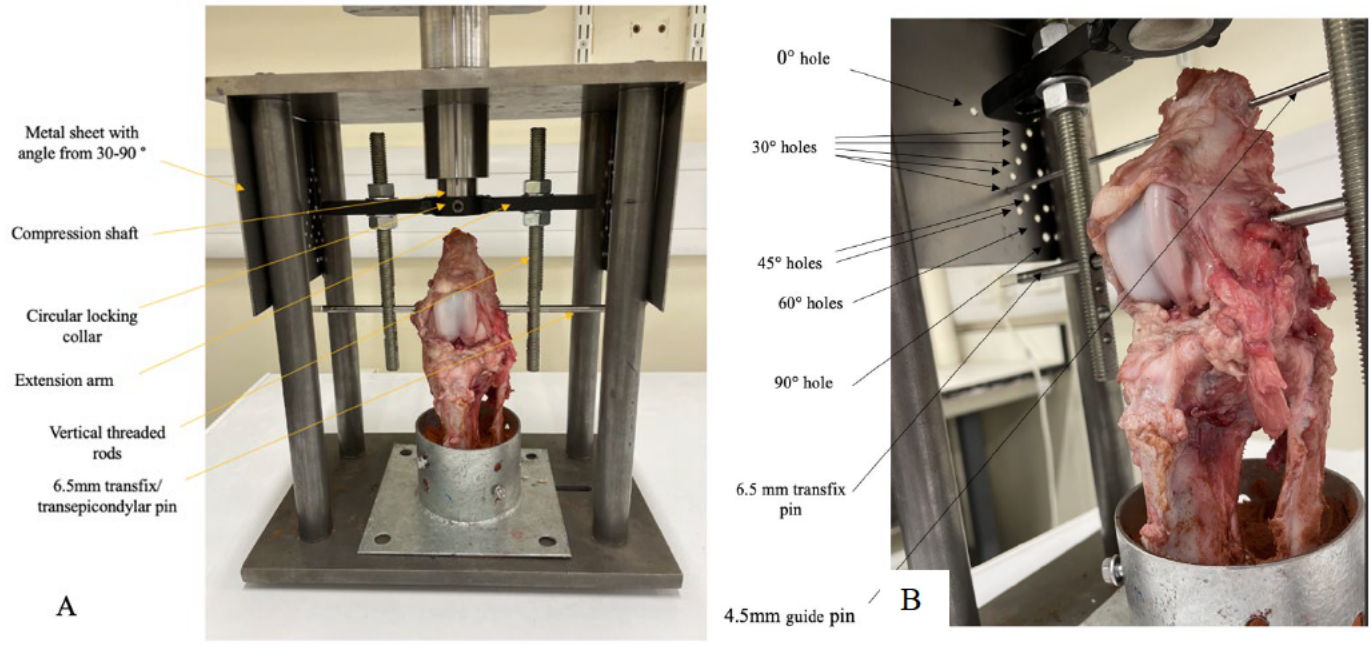

Figure 45. Preliminary testing of a left porcine knee within the test rig **(A)** Knee mounted to the custom-made rig through a 6.5 mm transfix pin passing through the transepicondylar axis **(B)** Testing performed at 30° with a 4.5 mm guide pin passing through the 30° hole in the metal sheet through the femur and out the other side

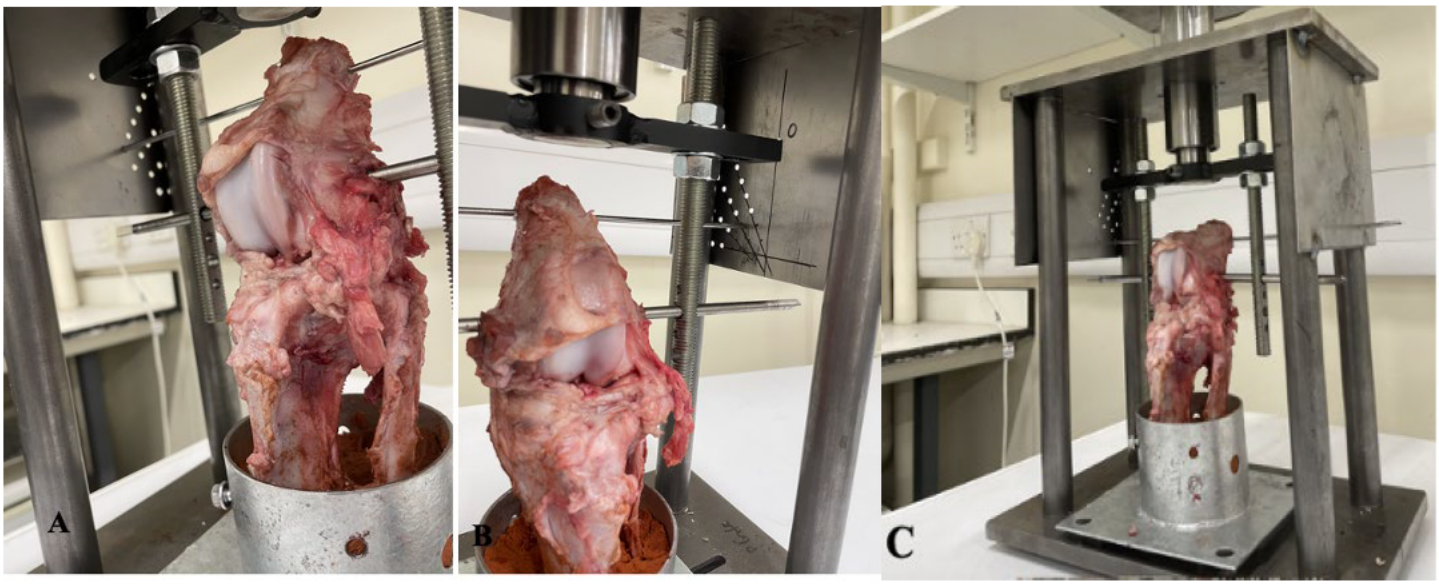

Figure 46. Specimen mounted at different flexion angles **(A)** 30° **(B)** 45° **(C)** 90°.

3.4 Experimental Instruments

Table 1 describes the key surgical instruments that were used for each testing state

Table 1. Surgical instruments that were used within the experiment

Surgical Instruments	Picture	Part of experiment used
#11 and #22 blades and scalpel handle		Dissection of porcine knees
Suturing tools: needle holder, forceps, surgical scissors, mayo needle	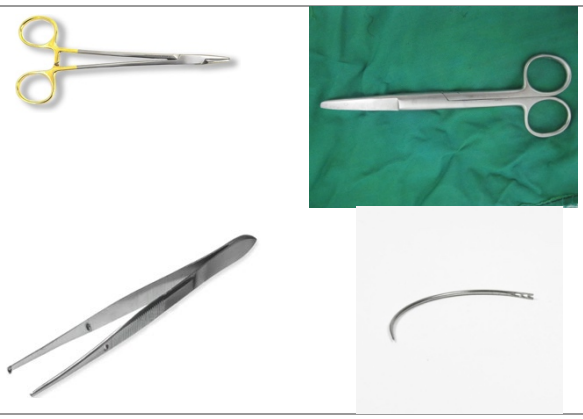	Soft tissue handling, suturing and cutting, knot tying
Orthopaedic power tool with chuck key, with bone drill and k-wire attachments		Drilling the tibia to secure it within the steel cylinder Drilling the femur to create the two transverse tunnels which are then connected to the rig through rods Drilling the tibial tunnels for the meniscal root repair and transtibial centralization state
4.5 mm Kirschner-wire, 6.5mm transfix pin and 3.2mm drill bit		4.5 mm Kirshner-wire pass through proximal femur and into rig to select flexion angles 6.5mm transfix pin pass through distal femur and into rig. Act as load bearing pivot

	 	3.2mm drill bit to drill the tibial tunnels for root repair & transtibial based centralization technique
ACL tibial guide		To locate the anatomical root attachment site so that the angle of drilling for the tibial tunnel from the anteromedial tibial cortex for root repair is in the correct orientation
2mm UltraTape and 1.3mm SutureTape (Smith and Nephew)	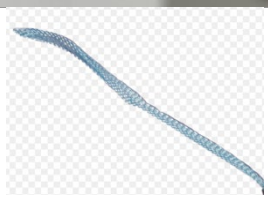	To repair the torn meniscal root and for the transtibial based centralization technique
FirstPass Mini (Smith and Nephew)		Device to pass the UltraTape or SutureTape through the meniscus for repair
Suture Retriever	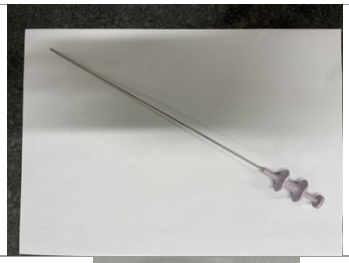	To pass the sutures in the repaired meniscal root and/or in the transtibial centralization technique through the tibial tunnel and outside the anterior tibial cortex
Round TightRope Button (Arthrex)		Sutures that have passed through the tibial tunnels are tied over this on the tibial cortex

1.8 FiberTak Knotless Anchor with curved guide and drill (Arthrex)		Used for the anchor-based centralization system

3.5 Experimental Conditions

Five meniscal conditions were tested: (1) intact (no surgery, best possible state) (n = 12 porcine knees); (2) medial meniscus posterior root tear (worst possible state) (n = 12 porcine knees); (3) anatomical transtibial pull-through root repair (ATPR) (conventional technique) (n = 12 porcine knees); (4) anatomical transtibial pull-through root repair with centralization using 2 knotless anchors (anchor-based centralization) (n = 6 porcine knees); (5) anatomical transtibial pull-through root repair with centralization using a tibial tunnel (transtibial centralization) (n = 6 porcine knees).

3.5.1 Intact state

This is in keeping with the description provided in section 3.2. As described, the MCL required resection to insert the Fujifilm sensitive film, and remained resected in all the subsequent testing states.

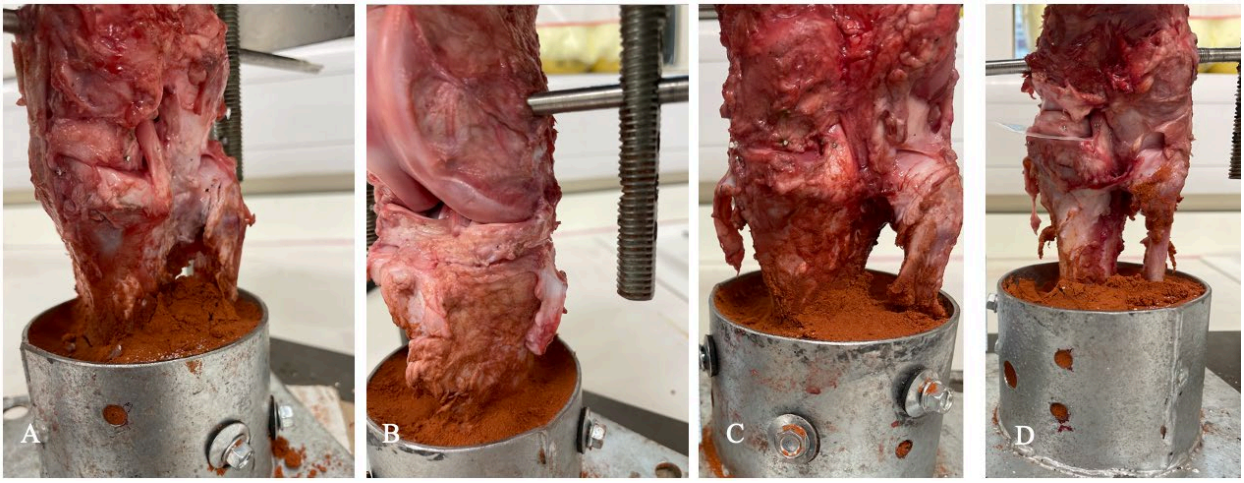

Figure 47. Right porcine knee with intact meniscus within testing phase of experiment **(a)** MCL precluding Fujifilm insertion **(b)** Superficial MCL cut, with meniscofemoral ligament intact **(c)** posterior view of MCL cut **(d)** Insertion of Fujifilm

3.5.2 Medial meniscus posterior root tear state (MMPRT)

The tear was created using a Number 11 scalpel blade (Swann-Morton, Sheffield, England) immediate at the bony root attachment site, which transected the main attachment and the shiny white fibre attachments (Figure 48).

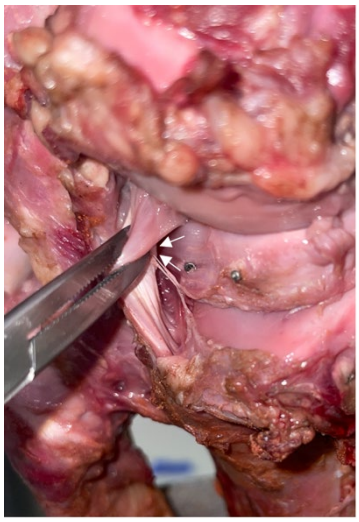

Figure 48. Left porcine knee within testing phase of experiment. PCL lifted up and out to identify the bony root attachment site (white arrows)

3.5.3 Anatomical transtibial pull through repair

The anatomical repair involved marking out the entry and exit site on the anteromedial tibial cortex (1.5 cm medial to the tibial tubercle) and root attachment site of the tibial plateau

respectively with the use of an ACL tibial guide (49a & b). A 3.2 mm orthopaedic power drill under supervision was then used to drill the transtibial tunnel at a 50° inclination angle. The hole exited at the anatomical site (Figure 49c).

Two number 2 UHMPWE sutures (2 mm UltraTape, Smith and Nephew) were each loaded on the FirstPass Mini suture passer (Smith and Nephew) and passed through the medial meniscus posterior root using the two simple stitch technique (Figure 49d). They were placed 5 mm medial to the torn edge and spaced 5 mm apart in the antero-posterior direction.

A suture retriever was passed through the tibial tunnel, captured the free ends of the suture tapes through its eyelet which were then shuttled through the tunnel (Figure 49e & f). Once the meniscus was confirmed to be reduced back into position with appropriate tensioning of the free ends of the tapes (Figure 49g), the tapes were then tied over a round tightrope button (Arthrex) using a surgeon's knot followed by 5 half hitches on alternating posts of the fixation button (Figure 49h). Confirmation of meniscus centralization was then undertaken (Figure 49i).

Figure 49. Anatomical transtibial pull through repair of a right porcine knee within the testing phase of the experiment **(a & b)** Confirmation of transtibial tunnel site with ACL tibial guide **(c)** drill hole exit **(d)** two simple stitch fixation with 2 mm UltraTape (Smith and Nephew) with the aid of First Pass Mini (Smith and Nephew) **(e & f)** Tapes passed through tibial tunnel with the help of suture retriever **(g – i)** tapes tensioned down to ensure adequate meniscus reduction and then tied over a surgical button.

3.5.4 Knotless Anchor based centralization

Centralization was performed using two 1.8 mm Knotless FiberTak Soft Anchors (Arthrex) inserted at the edge of the medial tibial plateau. Based on previous studies, the first anchor was

inserted at the posterior border of the MCL (Amano et al., 2023; Koga et al., 2017). Based on another previous report that identified the medial meniscus to be most extruded at the posterior border of the MCL (Daney et al., 2019), a second anchor was inserted 10 mm posterior to the first (i.e., at the posteromedial region of the medial meniscus). The surgical steps are as per the description in section 2.5.2, and the mattress suture technique for the repair suture of each anchor was performed (Leafblad et al., 2021; Wu et al., 2022) rather than the horizontal plane centralization technique (Koga et al., 2021)

A curved guide with a 1.8 mm drill bit was placed on the edge of the medial tibial plateau at the respective location site for the first or second anchor (Figure 50a & b). The drill bit contains a black mark to which the power tool was tightly secured onto (Figure 50c). A pilot hole was drilled until the drill stopped at the handle of the curved guide. The drill bit was carefully removed whilst the curved guide remained in position, and a 1.8 FiberTak soft anchor was then placed through the curved guide, into the pilot hole and gently tapped down until it was fully seated beneath the medial tibial plateau (Figure 50d). The repair suture passes between the meniscus and capsule from an inferior to superior direction through the capsule and then back down to create a mattress configuration (Figure 50e). The end of the repair suture is then loaded into the fiberlink looped end (Figure 50f). The shuttling suture is then pulled, which causes the repair suture to shuttle into the anchor's locking mechanism ('Chinese finger trap') (figure 50g & h). The shuttling fiberlink exits the knee. The tension is controlled under direct vision, and appropriate amount can be applied to re-tighten the capsule and bring the meniscus back to its anatomical position. The same steps were undertaken for the next knotless anchor.

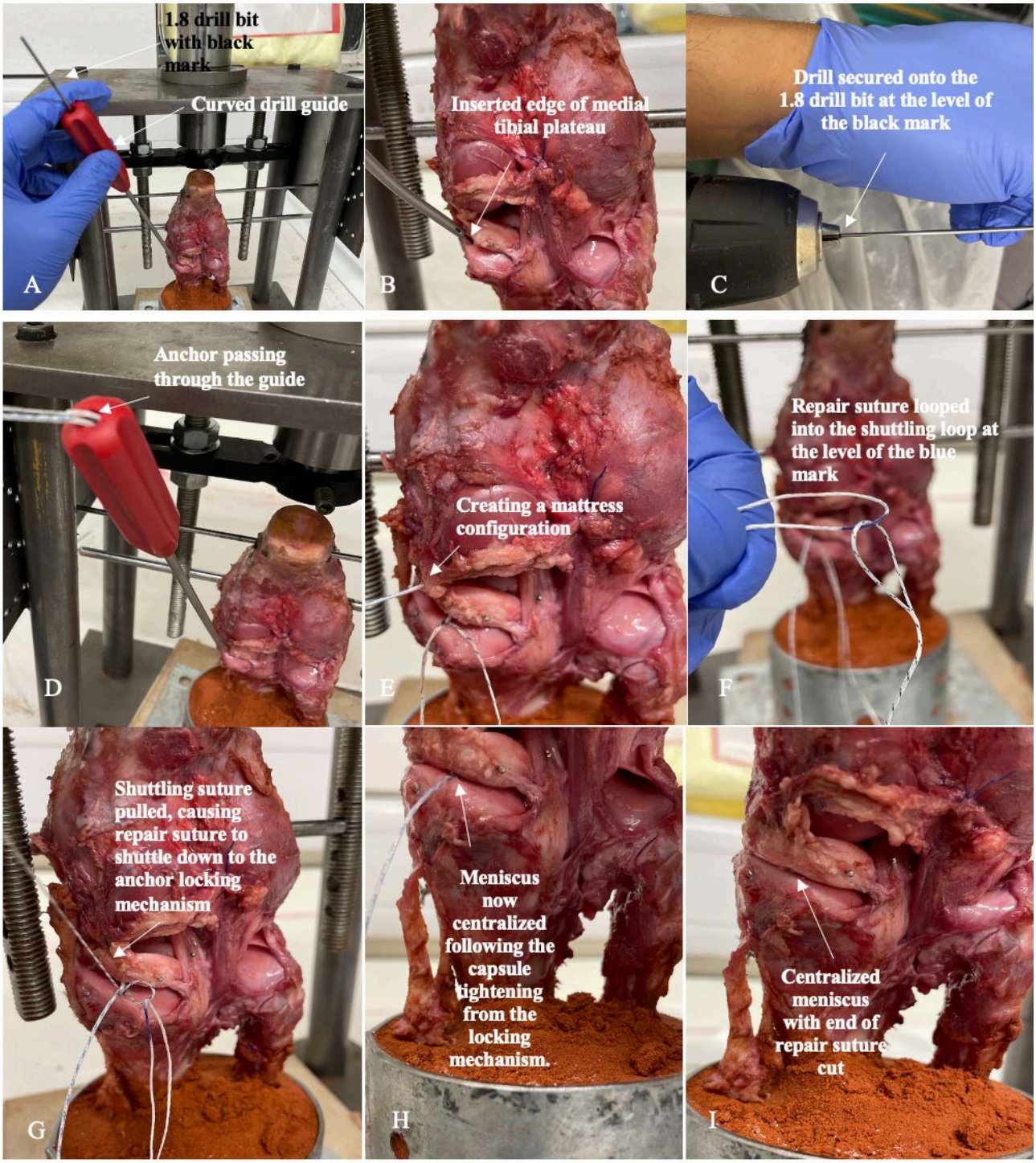

Figure 50. Anchor based centralization for right porcine knee within testing phase of the experiment. The picture depicts the most posterior anchor insertion (10mm posterior to MCL) **(a – d)** Drilling pilot hole through curved guide with soft anchor insertion **(e)** mattress configuration of repair suture at meniscocapsular junction **(f-i)** repair suture shuttled into the anchor locking mechanism using the 'Chinese finger trap' technique, and centralizing the meniscus.

3.5.5 Transtibial centralization

The transtibial centralization technique was performed in line with a previous biomechanical study (Daney et al., 2019). Two 2 mm Ultratapes (Smith and Nephew) were passed through the peripheral meniscus at the mid-point between the posterior root attachment and the posterior border of the MCL (Figure 51a & b). This was in keeping with the apex of the posterior horn of the medial meniscus (Figure 31). The tapes were passed through the meniscus from the tibial to femoral side, and then through the femoral to tibial side to create a double loaded construct (Figure 51b). Within the same location, a 3.2 mm drill bit was used to drill a transtibial tunnel, originating 3 mm inside the articular cartilage border and exiting out of the anteromedial tibial cortex 2 cm medial to the tibial tubercle (Figure 51c & d). The sutures were passed through the eyelet of the suture retriever and through the peripheral tibial tunnel (Figure 51e). With appropriate tensioning, they were finally tied over a round tightrope button (Arthrex) using a surgeon's knot followed by 5 half hitches on alternating posts of the fixation button (Figure 51f). The meniscus was now centralized.

Testing was performed with randomization of the order of the root repair alone and centralization with either 2-anchor based or transtibial centralization. Specifically, the tests were performed in the order of conditions 3 and 4 for 3 knees; conditions 4 and 3 for 3 knees; conditions 3 and 5 for 3 knees, and conditions 5 and 3 for 3 knees.

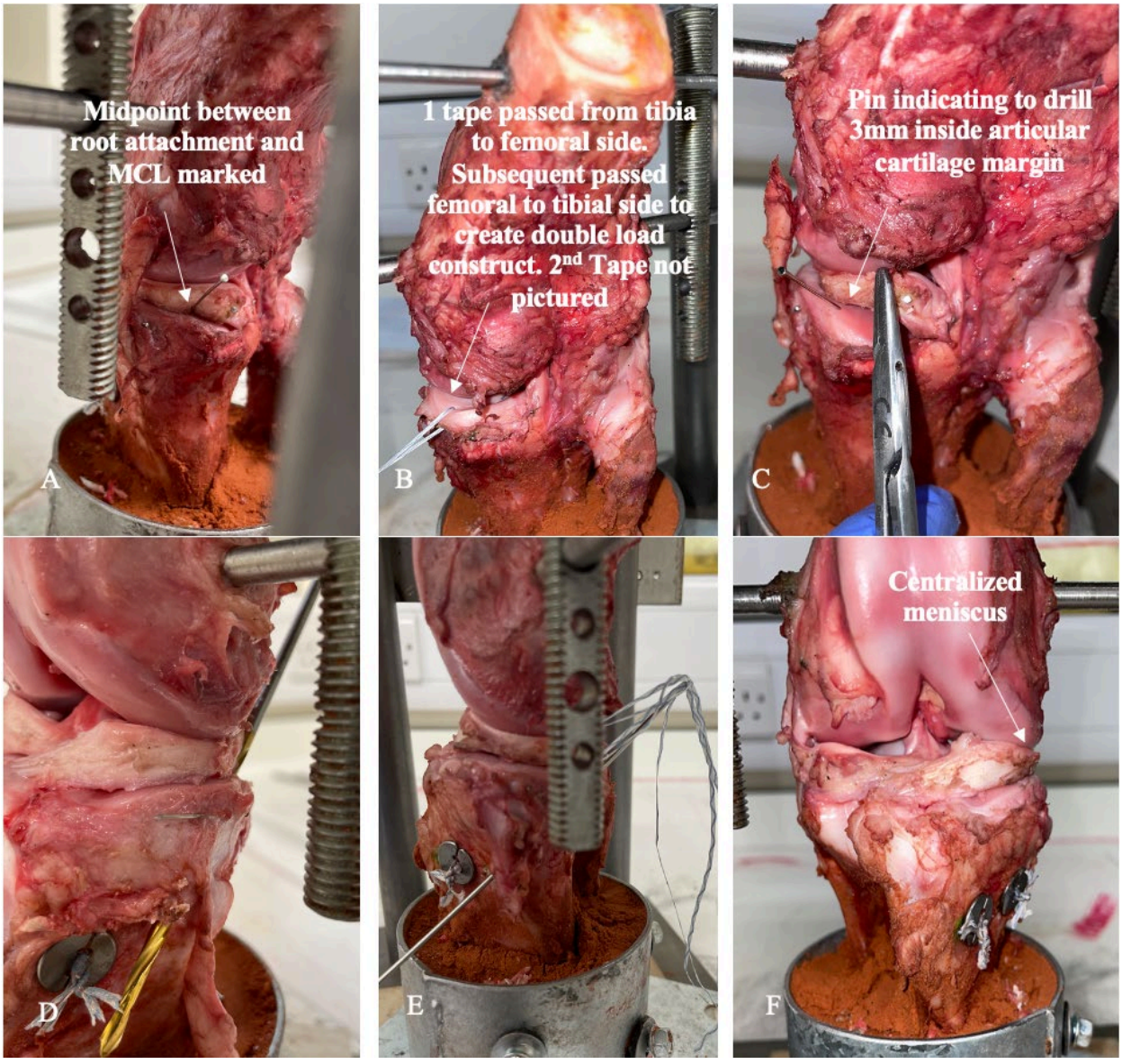

Figure 51. Transtibial based centralization for right porcine knee within testing phase of experiment **(a)** position of transtibial tunnel confirmed **(b)** Tape construct within meniscus **(c-d)** site and execution of peripheral transtibial tunnel **(e)** sutures passed through tunnel with aid of suture retriever **(f)** tibial cortex fixation of transtibial stitch

3.6 Measurement of meniscal extrusion

Two-dimensional motion analysis using digital photography and Image J (version 1.54, Rasband, W.S, U.S. National Institutes of Health, Bethesda, Maryland, USA) software was used to measure medial meniscus extrusion. This software has up to a 98.4% measurement accuracy (Andrialovanirina et al. 2020), with a high test-reliability (Suzuki et. al. 2021), and no difference in precision with digital calipers which have been considered the 'gold standard' (Makki L et al. 2017). Three 2mm markers were attached to the medial meniscus at 3 points: the posterior marker at the centre of the tibial attachment of the PCL (first marker), the medial marker on the posterior border of the MCL (third marker), and one marker in between the two at the posteromedial edge (second marker) (Figure 52). A 2 mm scale bar was added within the field of view. Previous studies have shown a MMPRT generally extrudes posteromedially if it remains undetected or undergoes delayed repair (Lerer et al., 2004; Magee et al., 2008). Furthermore, Daney et al. (2019) reported measuring meniscal extrusion at the level of the posterior aspect of the MCL as performed clinically on coronal MRI scans, best quantifies the degree of extrusion with respect to measurements made in the sagittal or axial planes). These two explanations are why the second and third marker were placed in these positions. MM extrusion was measured for each marker as the difference between the marker position with application of a 200N compression loading and position in the unloaded condition in the intact knee. This is in keeping with a previous study (Amano et al., 2023)

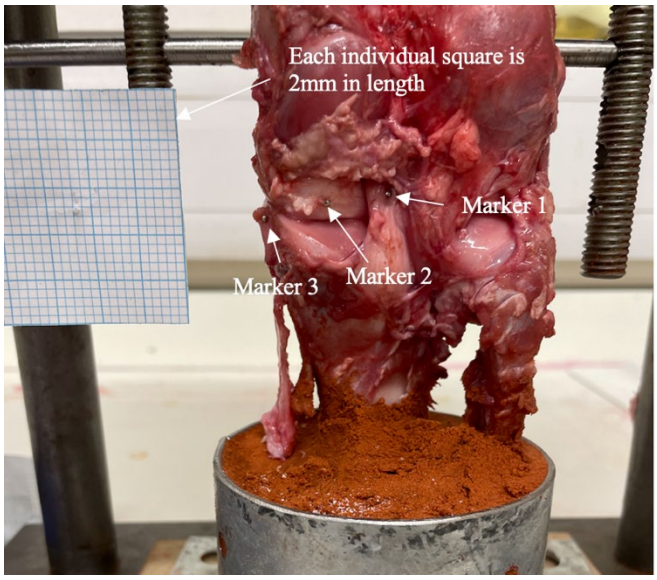

Figure 52. Position of markers to measure meniscal extrusion including 2mm scale bar for calibration within software

Images were imported into Image J. The scale bar was used to calibrate the images to convert the distance between markers from pixels into mm (Figure 53 a). It is important to emphasize that each porcine knee tested underwent their own calibration process on Image J. The images in Figure 53 are examples of one porcine knee during the testing phase of the experiment.

As each small grid on the scale was known to be 2 mm in distance, the 'line selection tool' was used to take a measurement of this grid, which gave a length in number of pixels (Figure 53b). Three measurements were taken to get a mean for the number of pixels for 2mm (Figure 53c & d). The mean length was 36.752 pixels for this particular knee (Figure 53e). Following this, conversion from pixels to mm can now proceed. One selects 'analyse', followed by 'set scale' to set the measurements. The average pixel length was inputted, along with the number 2 for the 'known distance' and 'units' were in mm. This calculated '18.376 pixels equated to 1 mm'. 'Global' was ticked so the method could be set to all images for that knee tested (Figure 53f). Measurement in mm of the distances between markers could now be performed.

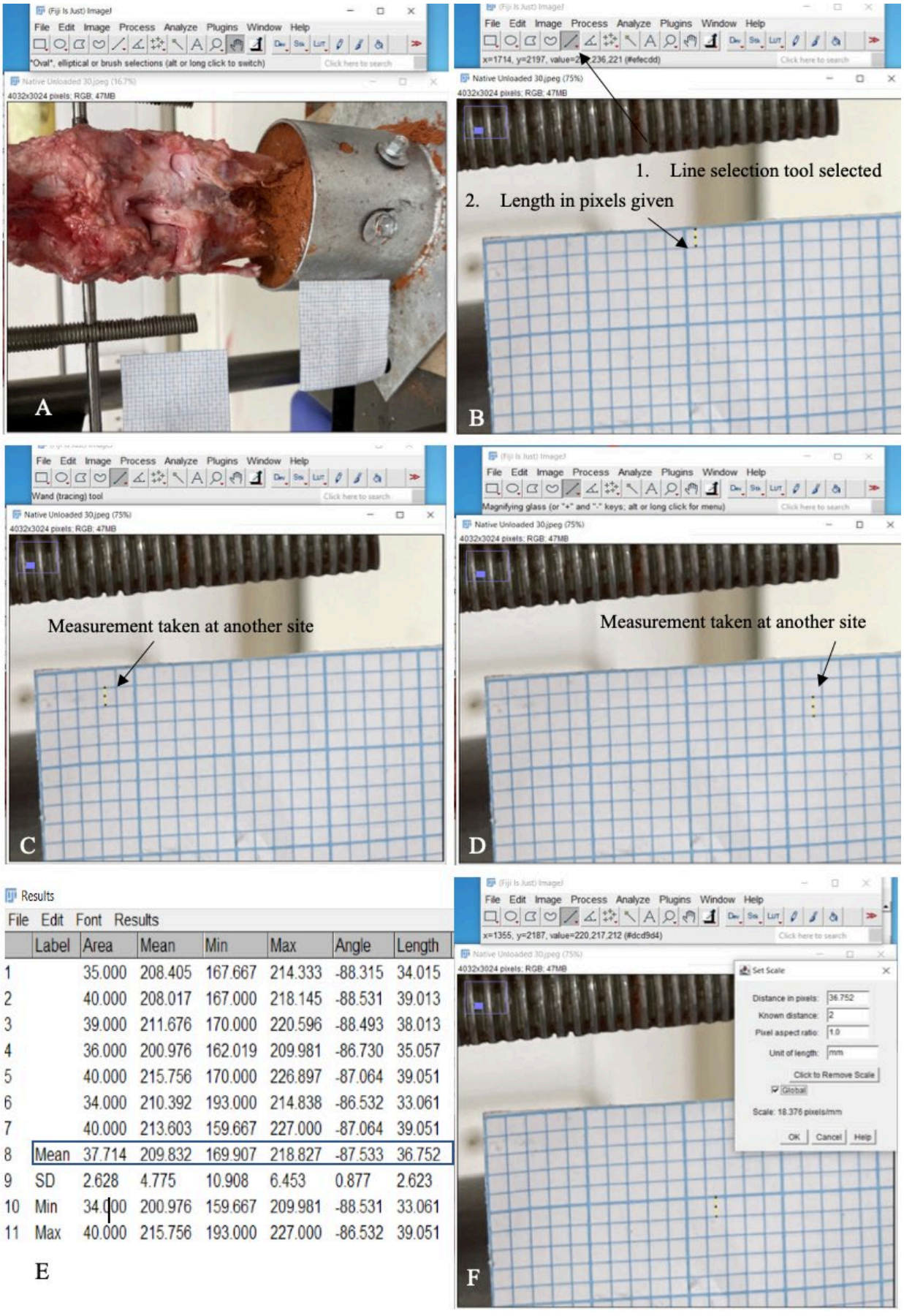

Figure 53. Calibration on Image J of a porcine knee within the testing phase of experiment. **(a-d)** multiple pixel measurements taken from the 2mm scale bar to give **(e)** an average pixel length which then provided **(f)** a measurement of the distance in mm

For each testing state for the porcine knee examined, three measurements were taken between markers 1 and 2, and markers 2 and 3, and an average calculated. Figure 54 provides an example between markers 1 and 2.

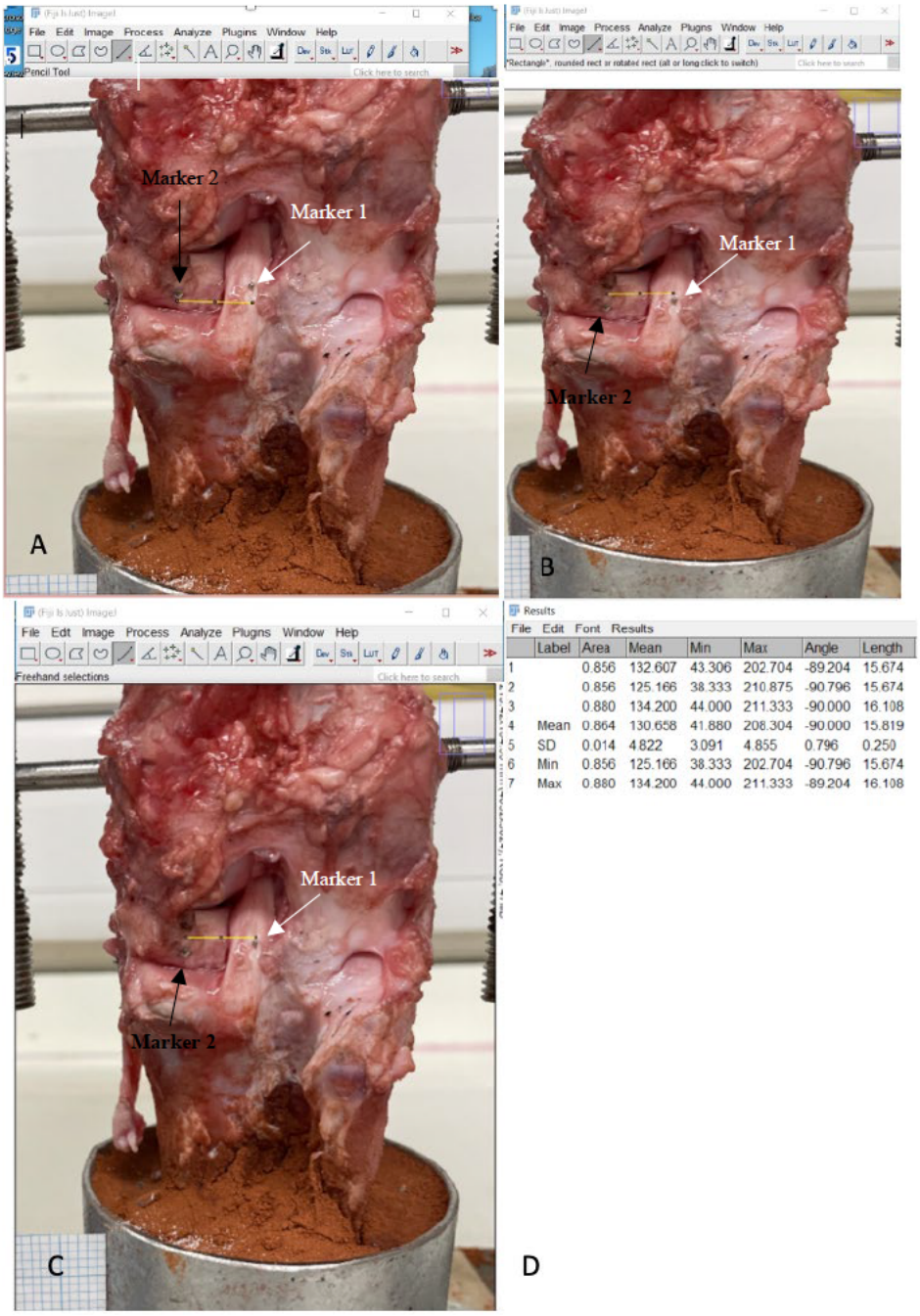

Figure 54. Measurement between marker 1 (white arrow) and 2 (black arrow) of a native knee unloaded at 30°. **(a-c)** Three measurements taken and **(d)** a mean was calculated

3.7 Contact area and force measurements

Tibiofemoral contact mechanics were measured with the use of Fuji prescale pressure-sensitive film (Tokyo, Japan). Following the protocols previously described in Section 2.6.2, the packets were cut to size and sealed to prevent the incursion of moisture up to three to seven days prior to the test date (Liggins et al., 1992; Muriuki et al., 2011).

Prior to load application, the Fujifilm was inserted between the anteromedial and posteromedial arthrotomies described, and positioned beneath the meniscus, covering the tibial plateau. Load was applied for two minutes to comply with the manufacturer's recommendations to allow accurate quantification of the pressures. For each loading condition, one packet of low-pressure range and one packet of super low pressure range Fujifilm were used. A total of twelve trials were performed using Fuji film for intact, MMPRT and ATPR states at each flexion angle. Six trials were performed for transtibial and two knotless anchor centralizations.

After loading, the imprinted Fujifilm was digitally photographed and imported into a customised MATLAB programme (Mathworks, Natwick, Massachusetts) based on the optical density of the scanned Fujifilm and a fifth-order polynomial developed from Fuji film calibration data. The MATLAB programme was sourced, but with the codes modified, from a study assessing tyre/road contact measurements using low and super low Fujifilm sensitive film (de Sande., 2007)

3.7.1 MATLAB coding for pressure maps

A written MATLAB file was required to create the pressure maps for each testing state. The file required the following information once the images were uploaded on MATLAB:

a. **Calibration data** for both super-low and low-range Fujifilm. This included the corresponding pixel values and colour densities. This is provided in the manufacturer guidelines. In the case of super-low range films, pressure range is 0.5 – 2.5 MPa with corresponding pixel values and colour density as detailed in Table 2:

Table 2. Density with according to mean pixel value for super-low range films

Colour Density	Mean Pixel Value
0.1	244
0.3	217
0.5	187
0.7	163
0.9	145
1.1	119
1.3	96
1.5	89

b. **The expected pressure ranges** for both super-low and low-range films. This is described in Figure 32.

c. **Specific visualization preferences.** This was regarding preference to either a combined colour map for both films or separate visualizations for each. Combined was chosen for the thesis, enabling visualization of the pressure map with a proper colour bar, reflecting the correct pressure ranges for each film.

The written file generated for pressure maps was used for all testing states and an example is shown in Appendix 1.

Within this file, functions to include *imread* enabled the calculation whilst *rgb2gray* converted the file into a grayscale for easier processing. Based on the calibration data, the pixel values

were interpolated to pressure values for both films. After the pressure maps were combined, if there were regions in the low-pressure maps with no contact, they were replaced with corresponding regions from the super low-pressure map. This ensured the coverage of the full range of 0.5 to 10 MPa in a single map. The colour maps were displayed under 'turbo' intensity.

3.7.2 MATLAB coding for contact area (mm^2)

A written MATLAB file was required to create the contact area for each testing state. The file required the following information once the images were uploaded on MATLAB:

a. **Pixel size.** This could only be calculated by providing the physical dimensions of the area covered by the image (width (mm) and height (mm)).

As physical dimensions between images differ, a separate written file had to be written for each testing state. An example of the contact area written file for an intact meniscus at 60° flexion under 200N load application is provided in Appendix 2, where the width and height are 18 mm and 40 mm, respectively.

This generates the pixel size (see Appendix 2) which can then help to calculate the contact area:

'Contact area (mm^2): pixel area (mm^2) x number of contact pixels'
'(pixel area mm^2) = pixel width (mm) x pixel height (mm)'

The contact pixels are the 'contact threshold', and this is adjusted based on the definition of minimum and maximum pressure and contact. In keeping with previous studies, it was set here

as 50 (Allaire et al., 2008; Muriuki et al., 2011). Another code was written based on this (Appendix 3), which provided an area of 711.89 mm^2 for this specific testing example.

3.8 Statistical Analyses

A one-way repeated measures ANOVA was applied to analyse the differences in mean values between the dependent variables (medial meniscus extrusion, peak contact pressure and area) recorded during tests across all flexion angles among the five meniscal conditions (independent variable). The root repair was selected as the reference condition to identify statistically significant differences with meniscus extrusion with the other testing conditions. The intact knee was used as a reference.

A prior power analysis (power 0.8, $\alpha = 0.05$) with five groups and an estimated detectable difference of 2.0 for meniscal extrusion based on previous studies (Amano et al., 2023) determined that a sample size of at least five subjects in each group was required for valid comparison. The sample size within this study included twelve subjects each in the intact, MMPRT and ATPR group, and six subjects each in both centralization groups.

Although group sizes differed, the variances were roughly equal. In view of this the Tukey-Kramer test was performed for post hoc comparisons between all pairwise combinations of knee states.

A p-value of less than 0.05 was considered to be statistically significant. All data are presented as means with standard deviations, and with 95% confidence intervals where described. The statistic software IBM SPSS V.29 (International Business Machines Corporation, Armonk. NY, IBM Corp, 2024) was used for all plots and analyses.

CHAPTER 4

4. Results

4.1 Medial meniscus extrusion

4.1.1 30 degrees

Analyses of the second marker (at the posteromedial edge of the MM) showed that following a tear, the meniscus extruded by 6.07 mm. This was significantly reduced with ATPR (meniscal extrusion (ME): 2.53 mm, $p < 0.001$), ATPR with transtibial centralization (ME: 2.46. mm, $p < 0.001$), and ATPR with two-anchor centralization (ME: 2.58 mm; 95% CI, $p < 0.001$). Similar results were also observed at the third marker (at the posterior border of the MCL) (ME: 3.41 mm (MMPRT) vs. 1.33 mm (ATPR) vs. 1.36 mm (ATPR with TT centralization) vs. 1.35 mm (ATPR with two-anchor centralization); $p < 0.001$). There were no differences between the surgical groups in reducing extrusion. This is summarised in Table 3 and Figure 55.

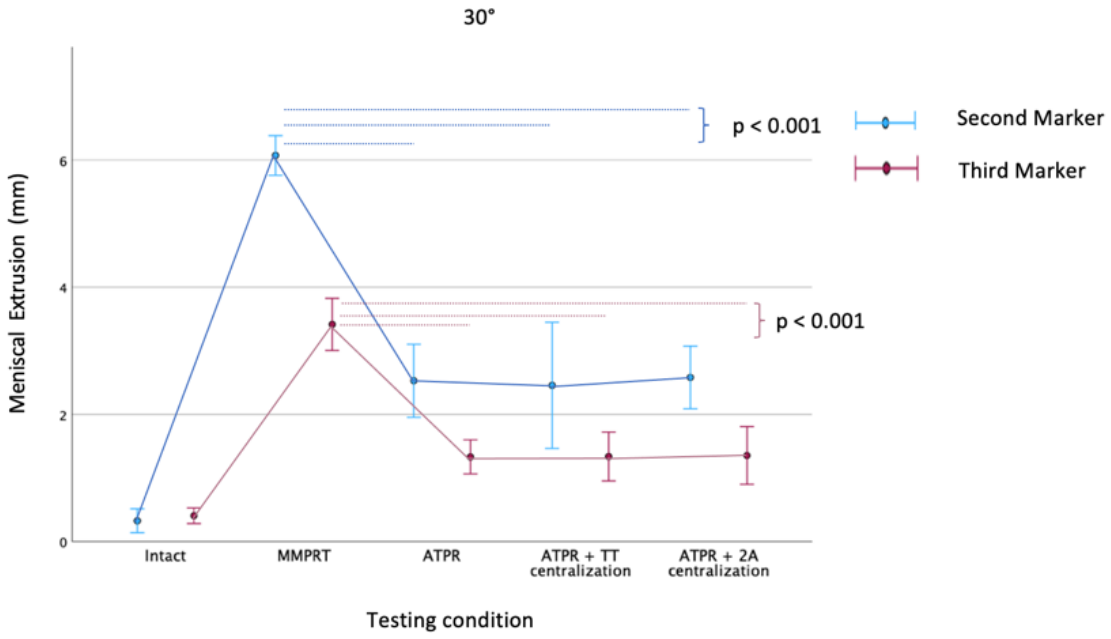

Figure 55. The extent of medial meniscus extrusion at two markers of the medial meniscus in each condition at 30 degrees. The mean values with 95% confidence intervals are shown. All labelled significant differences are $p < 0.05$. MMPRT, medial meniscus posterior root tear; ATPR, anatomical transtibial pull through repair; TT, transtibial; 2A, 2 anchors

	Knee Position	Knee condition					p - value
		Intact	MMPRT	ATPR	ATPR + Transtibial centralization	ATPR + 2 anchor centralization	
Marker 2	30°	0.33 ± 0.30[a] (0.14 - 0.51)	6.07 ± 0.49 (5.76 - 6.38)	2.53 ± 0.90[a] (1.95 - 3.10)	2.46 ± 0.94[a] (1.46 - 3.45)	2.58 ± 0.47[a] (2.09 - 3.07)	< 0.001
	45°	0.84 ± 0.21[a] (0.71 - 0.97)	8.38 ± 0.87 (7.83 - 8.94)	2.79 ± 0.93[a] (2.20 - 3.38)	2.56 ± 0.37[a] (1.79 - 2.56)	2.64 ± 0.20[a] (2.43 - 2.85)	< 0.001
	60°	0.82 ± 0.23[a] (0.68 - 0.97)	13.62 ± 0.77 (13.1 - 14.1)	4.39 ± 0.66[a] (3.97 - 4.80)	2.68 ± 0.28[abc] (2.38 - 2.98)	4.09 ± 0.58[a] (3.49 - 4.69)	< 0.001
	90°	1.09 ± 0.44[a] (0.81 - 1.37)	17.08 ± 0.66 (16.66 - 17.5)	4.75 ± 0.53[a] (4.41 - 5.09)	2.99 ± 0.19[abc] (2.78 - 3.19)	4.36 ± 0.67[a] (3.66 - 5.07)	< 0.001
Marker 3	30°	0.41 ± 0.19[a] (0.28 - 0.53)	3.41 ± 0.64 (3.0 - 3.8)	1.33 ± 0.42[a] (1.06 - 1.60)	1.36 ± 0.37[a] (0.95 - 1.72)	1.35 ± 0.43[a] (0.90 - 1.81)	< 0.001
	45°	0.60 ± 0.39[a] (0.35 - 0.85)	4.81 ± 0.53 (4.47 - 5.15)	2.29 ± 0.97[a] (1.67 - 2.90)	2.15 ± 0.25[a] (1.88 - 2.41)	2.18 ± 0.81[a] (1.33 - 3.03)	< 0.001
	60°	0.67 ± 0.34[a] (0.46 - 0.89)	6.15 ± 0.71 (5.70 - 6.60)	2.75 ± 0.37[a] (2.51 - 2.98)	2.43 ± 0.27[a] (2.14 - 2.71)	2.66 ± 0.23[a] (2.41 - 2.90)	< 0.001
	90°	0.92 ± 0.33[a] (0.71 - 1.14)	12.34 ± 1.16 (11.6 - 13.07)	3.60 ± 0.50[a] (3.29 - 3.92)	2.62 ± 0.20[ab] (2.41 - 2.84)	2.95 ± 0.24[a] (2.71 - 3.2)	< 0.001

Table 3. The extent of meniscal extrusion at two markers of the medial meniscus under each condition. Marker 2 was placed at the posterior border of the MCL. Marker 3 was placed 10mm behind marker 2, at the posteromedial edge of the MCL. The mean values with standard deviation are presented, with 95% confidence intervals in brackets. [a] Statistically significant, comparison to torn state ($p < 0.001$). [b] Statistically significant, comparison to ATPR (**ATPR + Transtibial centralization:** $p < 0.001$ at 60° and 90° for marker 2, $p = 0.04$ at 90° for marker 3). [c]Statistically significant, comparison to ATPR + 2 A centralization (ATPR + Transtibial centralization: $p < 0.001$ at 60° and 90° for marker 2). MMPRT, medial meniscus posterior root tear

4.1.2 45 degrees

Analyses of the second marker showed that following a tear, the meniscus extruded by 8.38 mm. This was significantly reduced with ATPR (ME: 2.79 mm, $p < 0.001$), ATPR with transtibial centralization (ME: 2.56 mm, $p < 0.001$), and ATPR with two-anchor centralization

(ME: 2.64 mm; 95% CI, p < 0.001). Similar results were also observed at the third marker (ME: 4.81mm (MMPRT) vs. 2.29 mm (ATPR) vs. 2.15 mm (ATPR with TT centralization) vs. 2.18 mm (ATPR with two-anchor centralization); p < 0.001). There were no differences between the surgical groups in reducing extrusion. This is summarised in Table 3 and Figure 56.

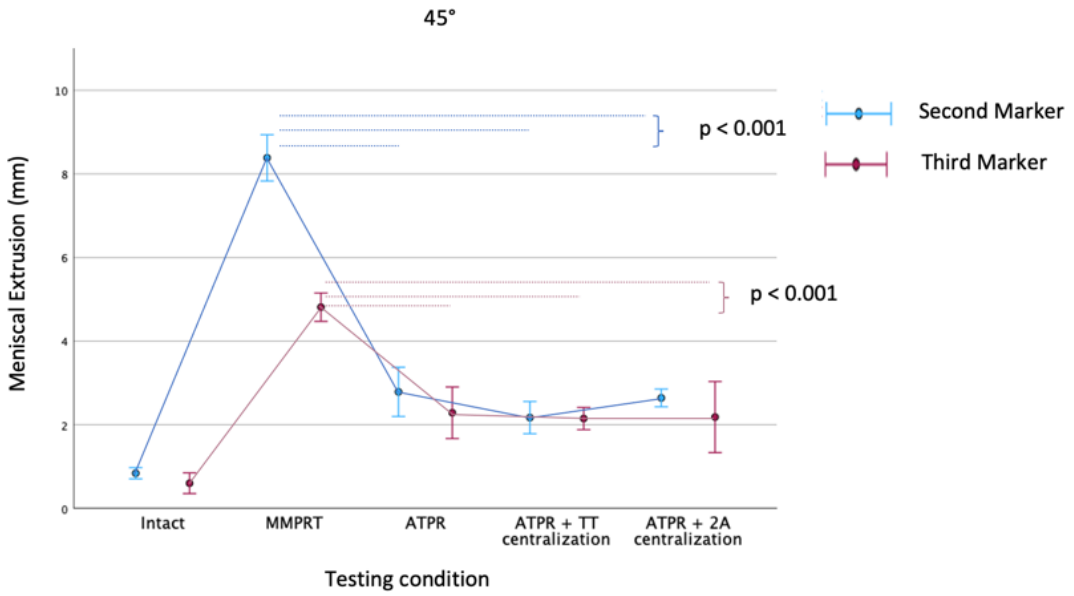

Figure 56. The extent of medial meniscus extrusion at two markers of the medial meniscus in each condition at 45 degrees. The mean values with 95% confidence intervals are shown. All labelled significant differences are p < 0.05.

4.1.3 60 degrees

Analyses of the second marker showed that following a tear, the meniscus extruded by 13.62 mm. This was significantly reduced with ATPR (ME: 4.39 mm, p < 0.001), ATPR with transtibial centralization (ME: 2.68 mm, p < 0.001), and ATPR with two-anchor centralization (ME: 4.09 mm; 95% CI, p < 0.001). Similar results were also observed at the third marker (ME: 6.15mm (MMPRT) vs. 2.75 mm (ATPR) vs. 2.43 mm (ATPR with TT centralization) vs. 2.66 mm (ATPR with two-anchor centralization); p < 0.001). Furthermore, at marker 2, extrusion was significantly better reduced when ATPR with transtibial centralization was

performed compared to either ATPR on its own ($p < 0.001$) or with two knotless anchor centralization ($p < 0.001$). There was no difference between surgical techniques however at

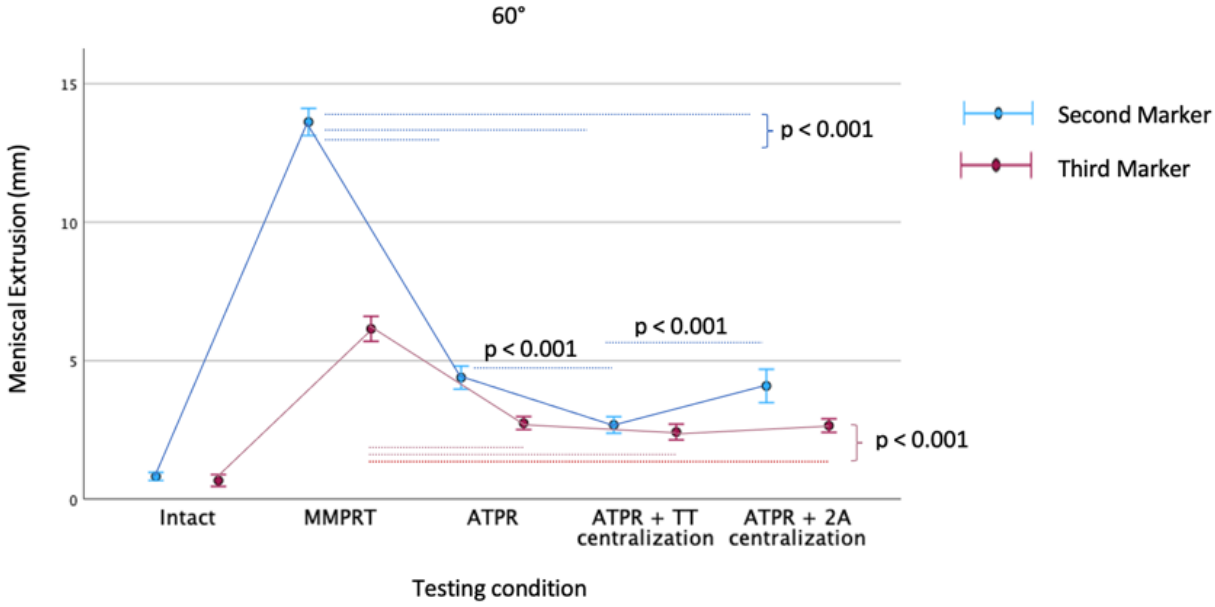

Figure 57. The extent of medial meniscus extrusion at two markers of the medial meniscus in each condition at 60 degrees. The mean values with 95% confidence intervals are shown. All labelled significant differences are $p < 0.05$.

4.1.4 90 degrees

Analyses of the second marker showed that following a tear, the meniscus extruded by 17.08 mm. This was significantly reduced with ATPR (ME: 4.75 mm, $p < 0.001$), ATPR with transtibial centralization (ME: 2.99 mm, $p < 0.001$), and ATPR with two-anchor centralization (ME: 4.36 mm; 95% CI, $p < 0.001$). Similar results were also observed at the third marker (ME: 12.34 mm (MMPRT) vs. 3.60 mm (ATPR) vs. 2.62 mm (ATPR with TT centralization) vs. 2.95 mm (ATPR with two-anchor centralization); $p < 0.001$). Similar to 60 degrees, at marker 2, extrusion was significantly reduced when ATPR with transtibial centralization was performed compared to either ATPR on its own ($p < 0.001$) or with two knotless anchor centralization ($p < 0.001$). Furthermore, ATPR with transtibial centralization performed better than isolated ATPR at marker 3 ($p = 0.04$). This is summarised in Table 3 and Figure 58.

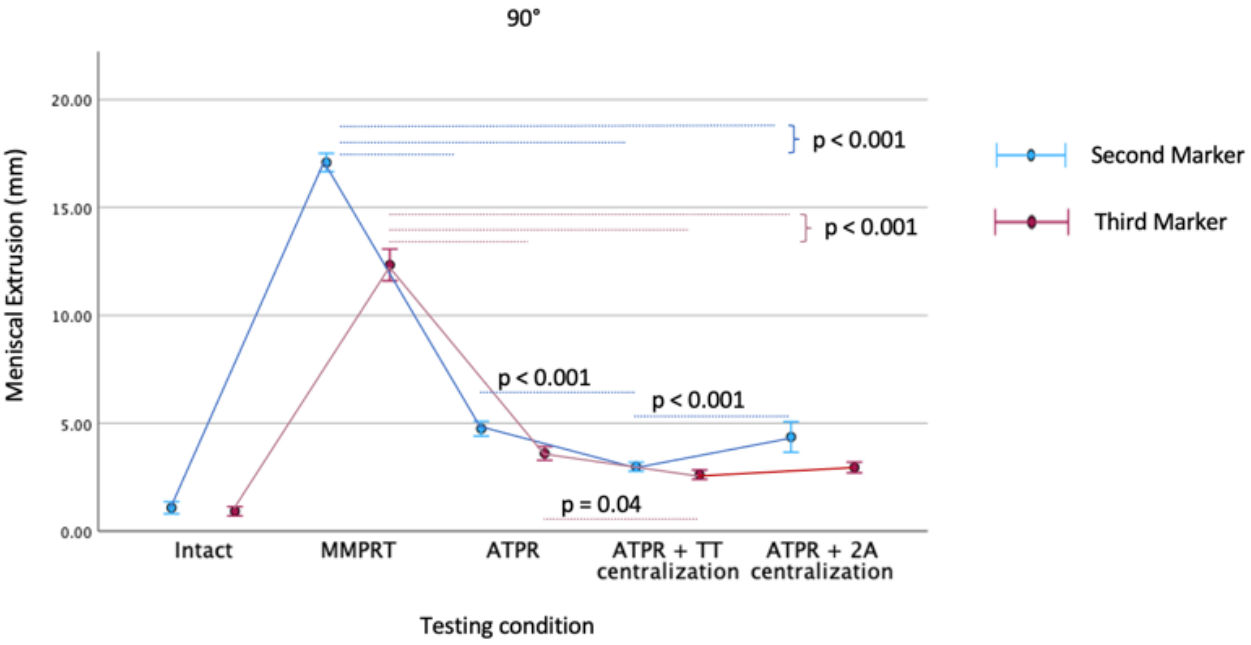

Figure 58. The extent of medial meniscus extrusion at two markers of the medial meniscus in each condition at 90 degrees. The mean values with 95% confidence intervals are shown. All labelled significant differences are $p < 0.05$.

4.2 Contact area of the medial compartment

4.2.1 Load distribution on mapping system

In the intact condition, the load distribution was concentrated on the whole medial meniscus by application of the 200 N compressive loading and shifted from the middle to the posterior meniscus as the knee flexion angle increased (Figure 59a). With a MMPRT, the meniscus remained within the joint at 30°, but started to extrude as flexion angle increased, with the load now mainly concentrated at the tibial cartilage (Figure 59a).

Following repair, with or without either centralization technique, the load distribution was similar to that of the intact state (Figure 59a & b). This included load re-distributing to the

anterior and middle portions of the meniscus at the low to mid-flexion angles (30 °to 60°) and towards the posterior portion at 90°.

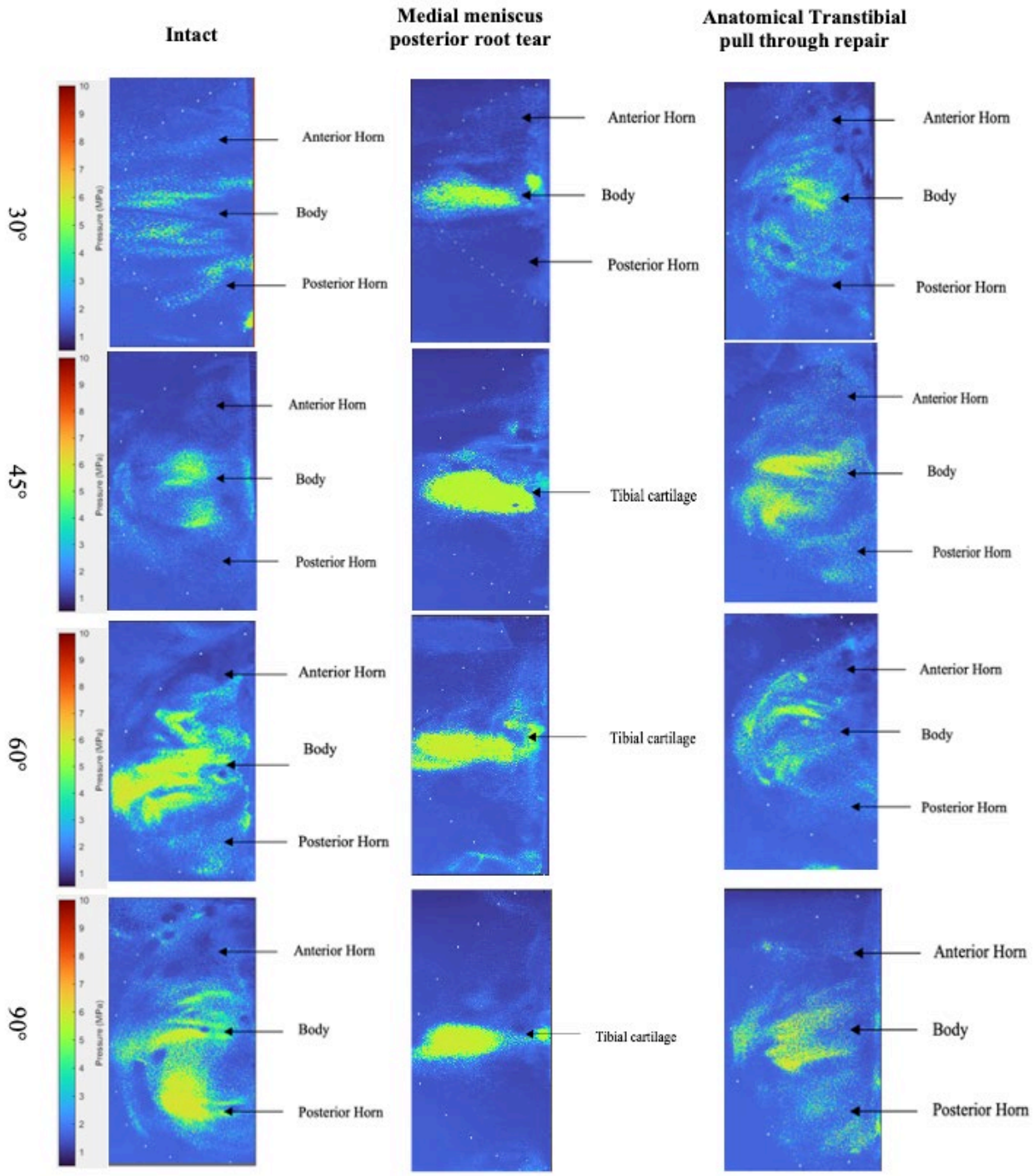

Figure 59 Load distribution analysed on MATLAB following conversion of the Fujifilm prescale films. **(a)** Representative load distribution at axial compression of 200N at various flexion angles for intact, root torn and root repaired state.

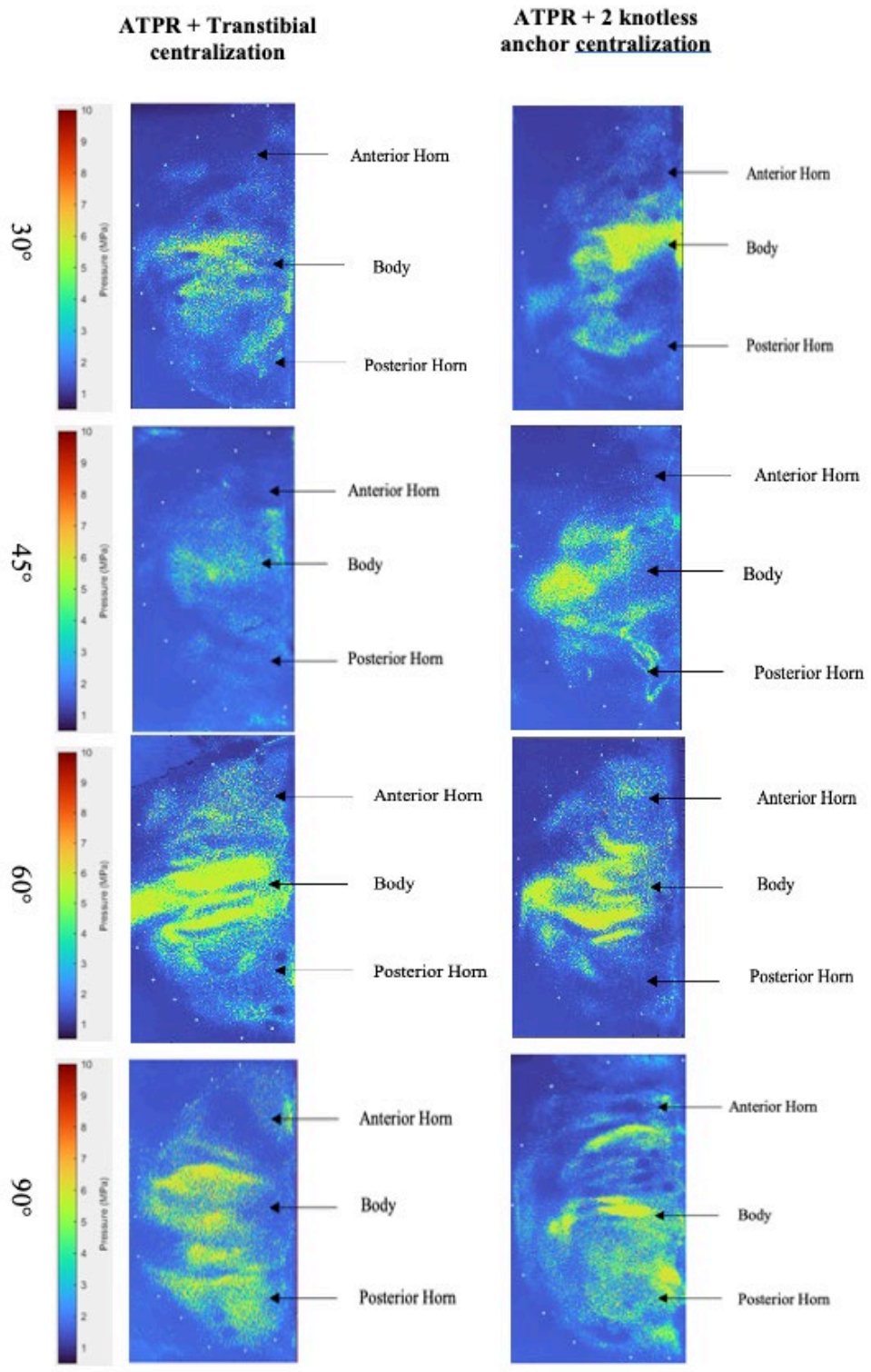

Figure 59 (b) Representative load distribution at axial compression of 200 N at various flexion angles for intact, root torn and root repaired state.

4.2.2 Statistical values

4.2.2.1 30 degrees

There was no difference in contact area between MMPRT (514.58mm^2), intact state (594.13 mm^2), and repaired states to include ATPR (579.24 mm^2), ATPR with transtibial centralization (591.90 mm^2), and ATPR with 2 anchor centralization (585.49 mm^2) ($p = 0.07$). All repaired states restored contact area to that of the intact state ($p > 0.05$) (Table 4 and Figure 60).

4.2.2.2 45 degrees

MMPRT led to a significantly reduced contact area (529.33 mm^2) compared to the intact (654.27 mm^2), ATPR (614.79 mm^2), ATPR with transtibial centralization (635.54 mm^2), and ATPR with 2 anchor centralization (624.40 mm^2) ($p < 0.001$). All repaired states restored contact area to that of the intact state ($p > 0.05$) (Table 4 and Figure 60).

4.2.2.3 60 degrees

MMPRT led to a significantly reduced contact area (524.53 mm^2) compared to the intact (697.18 mm^2), ATPR (601.01 mm^2), ATPR with transtibial centralization (693.31 mm^2), and ATPR with 2 anchor centralization (603.13 mm^2) ($p < 0.001$). Both the intact and ATPR with transtibial centralization had significantly greater contact area to that of an isolated root repair ($p < 0.001$ and $p = 0.008$ respectively), and a root repair with two-anchor centralization ($p = 0.007$ and $p = 0.011$ respectively). There were no differences between the intact state and ATPR with transtibial centralization ($p > 0.05$) (Table 4 and figure 60).

4.2.2.4 90 degrees

MMPRT led to a significantly reduced contact area (478.37 mm^2) compared to the intact (638.77 mm^2), ATPR (563.97 mm^2), ATPR with transtibial centralization (638.68 mm^2), and

ATPR with 2 anchor centralization (598.73 mm^2) ($p < 0.001$). Both the intact and ATPR with transtibial centralization had significantly greater contact area to that of an isolated root repair ($p = 0.006$ and $p = 0.037$, respectively). There were no differences in contact area between the centralization techniques and the intact state ($p > 0.05$) (Table 4 and Figure 60).

Knee position	Mean contact area (mm^2)					p - value
	Intact	MMPRT	ATPR	ATPR + Transtibial centralization	ATPR + 2 anchor centralization	
30°	594.13 ± 65.0 (552.86 - 635.40)	514.58 ± 30.62 (495.13 - 534.03)	579.24 ± 41.80 (552.68 - 605.80)	591.90 ± 42.82 (546.96- 636.83)	585.49 ± 33.85 (549.96 - 621.01)	= 0.07
45°	654.27 ± 64.12[a] (613.53 - 695.0)	529.33 ± 69.69 (485.06 - 573.61)	614.79 ± 32.88[a] (593.90 - 635.68)	635.54 ± 77.30[a] (554.42 - 716.66)	624.40 ± 70.04[a] (550.90 - 697.91)	< 0.001
60°	697.18 ± 37.31[abc] (673.47 - 720.88)	524.53 ± 54.71 (489.77 - 559.29)	601.01 ± 57.95[a] (564.19 - 637.83)	693.31 ± 54.95[abc] (635.64 - 750.97)	603.13 ± 58.20[a] (542.06 - 664.21)	< 0.001
90°	640.77 ± 56.84[ab] (602.66 - 674.88)	478.37 ± 30.36 (459.08 - 497.66)	563.97 ± 54.24[a] (529.51 - 598.43)	619.68 ± 55.16[ab] (580.80 - 696.57)	598.73 ± 55.32[a] (540.67 - 656.79)	< 0.001

Table 4. Mean contact area in the medial compartment at various flexion angles under each testing condition. The mean values with standard deviation are presented, with 95% confidence intervals in brackets [a]Statistically significant, comparison to torn state ($p < 0.001$). [b] Statistically significant, comparison to ATPR (**Intact:** $p < 0.001$ and $p = 0.006$ at 60° and 90° respectively; **ATPR + Transtibial centralization:** $p = 0.008$ and $p = 0.037$ at 60° and 90° respectively. [c]Statistically significant, comparison to 2A centralization (**Intact**: $p = 0.007$ at 60°; **ATPR + Transtibial centralization:** $p = 0.011$ at 60°). MMPRT, medial meniscus posterior root tear

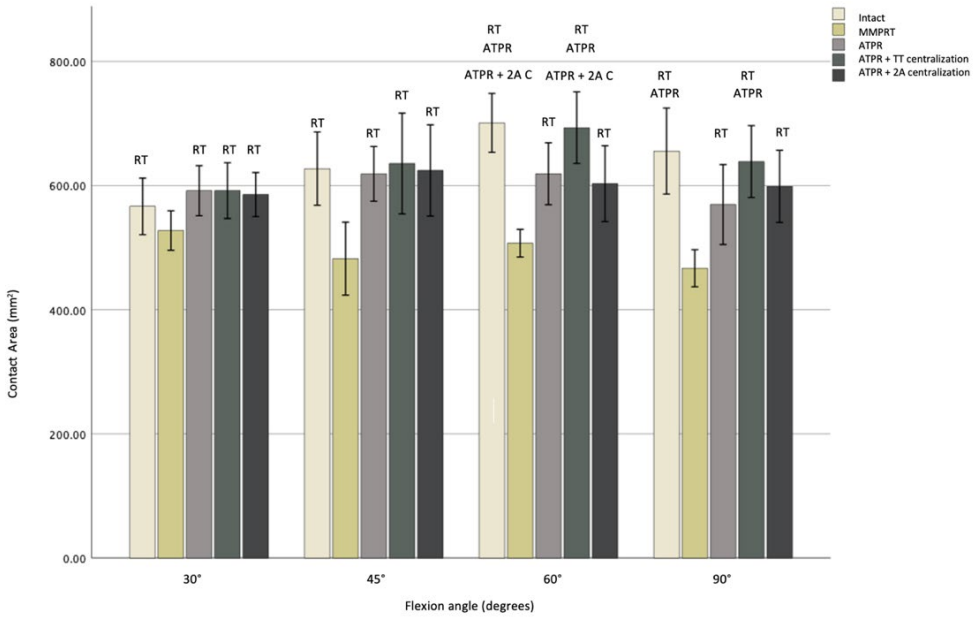

Figure 60. Medial compartment contact area with different medial meniscal root tear and repair states. Each bar chart presents mean + 95% confidence interval. Abbreviations in the bar chart: RT, significant from root tear condition; ATPR, significant from anatomical repair; ATPR + 2 AC, significant from anatomical repair with two anchor centralization

4.3 Peak contact pressure of the medial compartment

4.3.1 30 degrees

MMPRT led to a significantly increased peak contact pressure (5.52 MPa) compared to the intact (4.13 MPa), ATPR (4.64 MPa), ATPR with transtibial centralization (4.36 MPa), and ATPR with 2 anchor centralization (4.49 MPa) ($p < 0.001$). All repaired states restored contact pressure to that of the intact state (anatomic repair, $p = 0.13$; repair with transtibial centralization, $p = 0.90$; repair with 2 anchor centralization, $p = 0.63$) (Table 5 and Figure 61).

4.3.2 45 degrees

MMPRT led to a significantly increased peak contact pressure (6.44 MPa) compared to the intact (4.55 MPa), ATPR (5.6 MPa), ATPR with transtibial centralization (4.97 MPa), and ATPR with 2 anchor centralization (5.07 MPa) ($p < 0.001$). Both the intact and ATPR with transtibial centralization had significantly reduced peak contact pressure to that of an isolated root repair ($p < 0.001$ and $p = 0.02$ respectively). There were no differences in contact pressure between the centralization techniques and the intact state (transtibial centralization, $p = 0.179$; two anchor centralization, $p = 0.57$) (Table 5 and Figure 61).

4.3.3 60 degrees

MMPRT led to a significantly increased peak contact pressure (6.93 MPa) compared to the intact (5.16 MPa), ATPR (5.99 MPa), ATPR with transtibial centralization (5.20 MPa), and ATPR with 2 anchor centralization (5.23 MPa) ($p < 0.001$). The intact state and ATPR with either transtibial or 2 anchor centralization had significantly reduced peak contact pressure to that of an isolated root repair ($p < 0.001$, $p = 0.03$ and $p = 0.03$ respectively). There were no differences in contact area between the centralization techniques and the intact state (transtibial centralization, $p = 0.90$; two anchor centralization, $p = 0.85$) (Table 5 and Figure 61).

4.3.4 90 degrees

MMPRT led to a significantly increased peak contact pressure (6.64 MPa) compared to the intact (4.98 MPa), ATPR (5.41 MPa), ATPR with transtibial centralization (5.02 MPa), and ATPR with 2 anchor centralization (5.15 MPa) ($p < 0.001$). All repaired states restored contact pressure to that of the intact state (anatomic repair, $p = 0.4$; repair with transtibial centralization, $p = 0.88$; repair with 2 anchor centralization, $p = 0.85$) (Table 5 and Figure 61).

Knee position	Peak contact pressure (MPa)					p - value
	Intact	MMPRT	ATPR	ATPR + Transtibial centralization	ATPR + 2 anchor centralization	
30°	4.13 ± 0.61[a] (3.74 - 4.52)	5.52 ± 0.58 (5.15 - 5.89)	4.64 ± 0.46[a] (4.25 - 4.93)	4.36 ± 0.32[a] (4.03- 4.69)	4.49 ± 0.35[a] (4.11 - 4.86)	< 0.001
45°	4.55 ± 0.37[ab] (4.31 - 4.78)	6.44 ± 0.34 (6.22 - 6.65)	5.6 ± 0.38[a] (5.36 - 5.84)	4.97 ± 0.58[ab] (4.37 - 5.58)	5.07 ± 0.18[a] (4.88 - 5.27)	< 0.001
60°	5.16 ± 0.42[ab] (4.89 - 5.42)	6.93 ± 0.57 (6.6 - 7.3)	5.99 ± 0.60[a] (5.61 - 6.39)	5.20 ± 0.65[ab] (4.98 - 5.52)	5.23 ± 0.55[ab] (4.65 - 5.81)	< 0.001
90°	4.98 ± 0.60[a] (4.60 - 5.37)	6.64 ± 0.47 (6.34 - 6.94)	5.41 ± 0.66[a] (4.99 - 5.83)	5.02 ± 0.75[a] (4.23 - 5.81)	5.15 ± 0.45[a] (4.68 - 5.62)	< 0.001

Table 5. Mean peak contact pressure in the medial compartment at various flexion angles under each testing condition. The mean values with standard deviation are presented, with 95% confidence intervals in brackets [a]Statistically significant, comparison to torn state ($p < 0.001$). [b] Statistically significant, comparison to ATPR (**Intact:** $p < 0.001$ at 45° and 60°; **ATPR + Transtibial centralization**: $p = 0.02$ and $p = 0.03$ at 45° and 60° respectively; **ATPR + 2A centralization:** $p = 0.03$ at 60°). MMPRT, medial meniscus posterior root tear

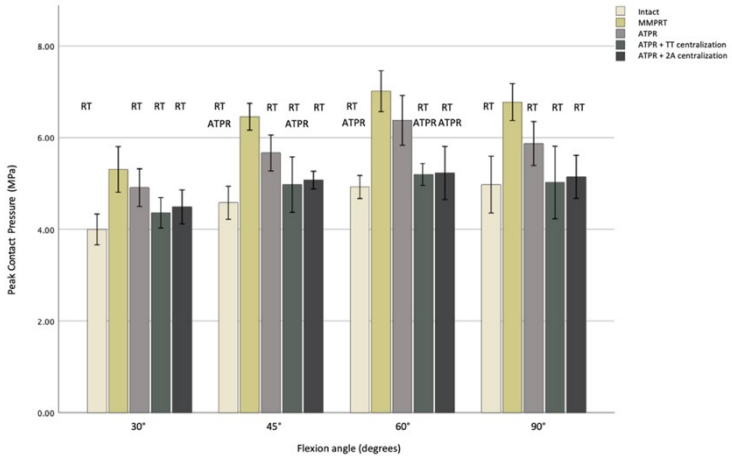

Figure 61. Medial compartment peak contact pressure with different medial meniscal root tear and repair states. Each bar chart presents mean + 95% confidence interval Abbreviations in the bar chart: RT, significant from root tear condition; ATPR, significant from anatomical repair; ATPR + 2 AC, significant from anatomical repair with two anchor centralizations

CHAPTER 5

5. Discussion

This study showed several important findings. Surgical fixation with isolated anatomical transtibial pull-through repair (ATPR), and ATPR in conjunction with either a transtibial or two knotless anchor centralization technique improves meniscal function in terms of extrusion, peak contact pressure and contact area following a medial meniscus posterior root tear. Furthermore, the results of this study showed that the transtibial centralization restored contact pressure and area to the intact meniscus at all flexion angles. Augmentation with two-knotless anchors revealed similar findings except for contact area at 60° of flexion. An isolated root repair was unable to restore contact area to the intact state at 60° and 90° of flexion, and peak contact pressure at 45° and 60°.

Between the fixation techniques, augmentation with the transtibial centralization performed better than both an isolated anatomical repair and one with a two-anchor centralization at certain flexion angles. It was more effective than both techniques in reducing extrusion at the posteromedial edge of the meniscus at 60° and 90° of flexion, and in improving meniscal contact area at the same flexion angles. There were no differences between the centralization techniques at any angle for peak contact pressure. Both performed better than an isolated repair in reducing contact pressure at 60°, with the transtibial stitch also playing a beneficial role at 45°.

In summary, ATPR with a transtibial centralization showed the best improvement, closely followed by the two-anchor technique in reducing meniscal extrusion and restoring tibiofemoral contact mechanics. This was particularly the case at the mid to high flexion angles (60-90°).

Multiple biomechanical studies on root repairs for MMPRTs reveal superior properties of suture anchor repair when compared to transtibial-pull through (Cerminara et al., 2014; Feucht et al., 2014; Saengpetch et al., 2023), with meniscal healing compromised from the micromotion created from the long meniscus-suture construct passing through the tibial tunnel, and the resultant difficulty in providing adequate tension (Kim et al., 2011). In contrast, suture anchor repair allows direct refixation of the root tear at its tibial insertion, eliminating the need for tibial drilling. Based on these explanations, similar biomechanical results may have been expected when comparing the centralization techniques used in this study. However, this was not the case owing to important differences in the anatomy of the respective meniscus-suture constructs. With transtibial centralization, a double-loaded suture construct is created through a portion of meniscus (apex of the posterior horn) that captures the circumferential and radially oriented 'tie' fibres within its deeper zone that provides its structural integrity (Peterson et al., 1998). Although such fibre arrangement can additionally be captured with the transtibial root repair, it will likely also capture circumferential collagen fibres within the root ligament and transition zone that are predominantly arranged in a parallel manner (Smith et al., 2015). This can weaken the repair integrity at the meniscus-suture interface, potentially leading to meniscal micromovement and non-anatomical healing (Robinson et al., 2018). This can partially be resolved by ensuring the capture of the shiny white fibres, which provide 37.4% of the strength of the native root attachment (Ellman et al., 2014). Furthermore, using UHMWPE tapes for the repair construct will hold the root down more broadly allowing a more even distribution of load (Ahn et al., 2009; Bisson et al., 2010; Yokoi et al., 2017), potentially minimizing the stress on the weaker circumferential fibres that are captured. However, these techniques were absent in the studies that showed superiority of suture anchor repair for meniscal root tears (Cerminara et al., 2014; Feucht et al., 2014; Saengpetch et al., 2023), and is thus a potential avenue for

future investigation. Nevertheless, in view of the variation of the meniscus anatomy based on its location, the biomechanical behaviour of the centralization tunnel, with respect to micromotion, can be assumed to be different to that of the root repair tunnel.

Unlike the transtibial stitch which penetrates the meniscus, the knotless anchor centralization technique involves the passage of sutures through the meniscocapsular junction and tensioning to re-tighten the capsule to position the meniscus back to its anatomical position. This proved to be successful in reducing extrusion at the lower flexion angles (30 - 45°). However, the femoral roll back at higher flexion angles causes the meniscus to bear more weight in the posterior direction (Yamamoto et al., 2021; Yao et al., 2008). Any resultant movement will cause posteromedial extrusion, which is thought to be the physiological direction owing to the bony anatomy of the tibial plateau, neighbouring PCL, and geometry of the medial tibial plateau and femoral condyles (Johannsen et al., 2012; Lerer et al., 2004; Magee et al., 2008). Directly holding the repaired meniscal tissue in place across a wider surface area would help to counter such extrusion at higher flexion angles (LaPrade et al., 2015c). These features are more consistent with the transtibial centralization technique, with better suture tension control of the repaired construct to that of the two-anchor technique. This was underlined in its greater contact area at 60°, and extrusion correction at 60° and 90°.

Whilst fixation techniques can be modified to optimize the transtibial pull through root repair, it should be acknowledged that suture micromotion within the tunnel owing to its long construct will remain a potential pitfall for extrusion. Despite the addition of a centralization tunnel posteromedially to counteract this, its combination with the biomechanically superior suture anchor root repair is yet to be explored. Thus, future biomechanical studies are required to compare a variety of combinations of root repair (suture anchor and transtibial pull-through)

and centralization (transtibial stitch and knotless anchors) techniques to ultimately determine the most stable construct in restoring the normal loading profile of the knee.

Daney et al. (2019) showed no differences between ATPR and ATPR with transtibial centralization across all flexion angles for extrusion and tibiofemoral contact mechanics. Although the fixation techniques were similar, two UHMWPE tapes (2mm UltraTape, Smith & Nephew) were used in this research compared to the single UHMWPE suture in the aforementioned study. Tapes have higher load to failure and stiffness compared to their suture counterpart (Bachmaier et al., 2024; Matthews et al., 2020; Nakama et al., 2019; Robinson et al., 2018; Takahashi et al., 2023), and the use of two in this study enhanced these biomechanical properties further (Rosslenbroich et al., 2013). In addition, their larger widths through a 4.5 mm size tunnel that is conventionally drilled in practice will help to minimise the 'bungee effect' from the longitudinal motion of the suture within the tunnel (Cerminara et al., 2014). These factors provide further peripheral stabilization to an extruded meniscus and may explain why ATPR with transtibial centralization was found to perform better than ATPR alone at certain flexion angles.

The results for root repair with two knotless anchor centralizations in comparison to isolated root repair were significantly different to that of Amano et al. (2023). Amano et al. showed that whilst an isolated root repair reduced extrusion better at 60° & 90°, its conjunction with a two-anchor centralization improved meniscal contact area at 30° & 60° and reduced contact pressure at 30°. This study found that the transtibial root repair with two knotless anchors only performed better than the isolated repair for reducing contact pressure at 60°. These differences can potentially be explained by the fixation techniques that were implemented. In the Amano et al. study, a non-anatomical transtibial root repair (NATPR) was performed with the tunnel

placed 4 mm lateral to the tear site. This positional variation in tunnel location on the plateau and site of tear on the meniscal root can compromise meniscal tension, impairing its ability to absorb hoop stresses (Starke et al., 2010). If the tunnel was moved more medially to sit directly under the tear to maintain adequate tension, it will unfortunately shorten the functional circumferential length of the meniscus with subsequent medial migration of the root attachment (Padalecki et al., 2014). In this study, the tear and tunnel position were created at the attachment site to keep tension close to the native state. By improving the root repair in this respect, the results would more likely conform to the inverse relationship expected between peak contact pressure and area amongst the various fixation methods, and reflect the desired technique advocated in practice. Furthermore, this may narrow the differences between the two fixation methods to an insignificant level which can explain why the results were mostly similar across all outcomes and flexion angles. However, this would underline further the superiority of the transtibial centralization where, despite ATPR optimisation, significant differences were still observed in the contact area and pressure at the various flexion angles earlier described. When comparing the knotless anchor centralizations, a mattress suture technique was perfromed at the repair suture for each anchor (Lafblad et al., 2021; Wu et al., 2022), whilst Amano et al. performed a horizontal plane technique in which the repair suture of each anchor was shuttled in the loop of the adjacent anchor. Whilst a horizontal plane enables more controlled and matched tension within the meniscocapsular tissue to keep the meniscus in situ, the mattress technique has the benefit of maintaining its resistance to extrusion if one of the anchors were to fail as they work independently to one another. However, no study to date has compared these configurations, and this is an area for further investigation.

The results of this study suggest that adding a transtibial centralization stitch to an ATPR could be beneficial clinically to reduce an extruded meniscus and restore the loading profile of the

knee. However, this does not account for the biological factors such as soft tissue status, muscle contractions, proprioception, healing and cartilage status. Furthermore, most post-operative rehabilitation protocols involve 4-6 weeks of light loading before full weight bearing (Koga et al., 2020; Krych et al., 2024; Mochizuki et al., 2021). Thus, investigating the combination of these factors with the fixation methods will provide a clearer answer to the repair construct providing the most robust resistance to mechanical stress, and the one that provides the higher ceiling for meniscal healing. There is no clinical comparative study to date comparing isolated root repair to those in conjunction with the centralization techniques described. Nor are there studies comparing the centralization techniques. This is now required.

Limitations

This study has several limitations. As earlier noted, porcine knees were used to conduct the experiment, and tibiofemoral contact mechanics after surgical fixation of MMPRTs in pigs may not entirely correspond to those of human knees. Variations in its anatomy to human cadaveric models are described in section 2.2. However, much similarity exists, particularly for the medial meniscus to include its extensive meniscocapsular attachments along its peripheral border, containing the posterior meniscotibial ligament, posterior oblique ligament, deep medial collateral ligament, and the semi-membranosus muscle (Mameri et al. 2022). Furthermore, porcine menisci have been shown to have similar biomechanical properties to human menisci and are, therefore an accepted model for the study of meniscal repairs (Feucht et al., 2015a; Kim et al., 2016; Mitchell et al., 2016; Robinson et al., 2018).

A static axial load was applied, which does not replicate the variable loading experienced in the knee during gait or other physical activities. However, this loading scheme was consistent and reproducible, which allowed for reliable comparisons between conditions, and has been

used by numerous similar studies (Amano et al., 2023; Kohno et al., 2020; Kubota et al., 2022; Ozeki et al., 2020), allowing for a more direct comparison to the literature. The lack of cyclical loading is a weakness in this study, but one expects that this would reveal an even greater negative effect between the isolated ATPR and ATPR with the centralization techniques. It is hoped that it would not have a negative effect on the centralized knees, but this is a distinct possibility.

No kinematic analysis of the knee joint was performed, to include axial loading with the knee in internal/external rotation, valgus/varus and with anterior tibial translation. From previous studies, increased external tibial torsion of up to 6° can occur with a medial meniscus posterior root tear, causing lateral compartment changes owing to the impaction of the lateral tibial spine on the corresponding femoral condyle (Allaire et al., 2008). This can pathologically load the lateral menisci, and so exploring the effects of medial sided centralization on the lateral meniscus is required.

A certain level of knee dissection was necessary to obtain intra-articular pressure measurements. However, previous authors have disarticulated the knee, performed extensive arthrotomies, and osteotomies to gain access to the knee (LaPrade et al. 2014a; Lee et al., 2006; Padalecki et al., 2014), to which we kept to a minimum in this study. As a result, any potential shifting of the femur during testing will have been diminished. Nevertheless, the MCL required resection for the insertion of the Fujifilm, and this could have affected the rotational stability of the knee joint. However, the effect would be to decrease the contact area and increase contact pressure and extrusion, tending to minimize the potential differences between the intact state, torn state, and repaired states. Amano et al also resected the MCL for pressure film insertion during their centralization experiment on meniscal root tears (Amano et al., 2023), and again

this remained resected through all testing states. Future studies are required to address alternative options to that of MCL resection. Furthermore, it may have been technically easier to place the film between the meniscus and femur to preserve the MCL, but previous studies have shown it to slip frequently and give spurious data (Marzo et al., 2008).

Unlike their human counterparts, porcine knees are unable to fully extend beyond 30° (Olah et al., 2021). Many biomechanical studies on porcine knees have tested knee states from 30° onwards (Amano et al., 2023; Kohno et al., 2022; Kubota et al., 2020; Morales-Avalos et al., 2023; Saengpetch et al., 2023; Seo et al., 2009). Therefore, the results of this biomechanical study should be interpreted with caution when compared to human knees with full extension. However, much of the load during extension is focused on the anterior meniscal root (Espejo-Reina et al., 2023), and only when the flexion angle increases does it become more concentrated on the medial meniscus posterior root (Yamamota et al., 2021). Therefore, testing the repaired states within the porcine knees at higher angles, which was performed in this experiment (60-90°), will provide more relevance to clinical practice.

The piezoresistive Tekscan Pressure Sensor (Tekscan, Boston, MA) is commonly used in biomechanical practice, allowing continuous data collection through several load configurations (Luo et al., 1998; Otto et al., 1999; Wilson et al., 2003). In the current study, Fujifilm prescale film (Tokyo, Japan) was used. This is a static passive technology whereby its colour intensity is proportional to the applied load. It only provides a measure of tibiofemoral contact mechanics at one time under one set of circumstances. Harris et al. (1999) reported that Fujifilm can under-estimate contact mechanics compared to the Tekscan across all flexion angles, but this difference is reduced with the use of super-low films. Furthermore, the

underestimation will occur across all testing conditions, thereby minimizing any potential differences between them.

Conclusion

The anatomic transtibial pull-out repair with transtibial centralization better restores the tibiofemoral contact mechanics compared to that of the knotless-anchor centralization technique. This is particularly the case for contact area at 60°. Furthermore, it also better restored extrusion to that of the knotless-anchor centralization technique at 60° and 90°. This suggests that when there are concerns of residual pathological extrusion following a root repair for a medial meniscus posterior root tear, the addition of a transtibial centralization will be more biomechanically stable. Future comparative trials are now required to determine its effect in clinical practice.

References

Adams JG, McAlindon T, Dimasi M, Carey J, Eustace S. Contribution of meniscal extrusion and cartilage loss to joint space narrowing in osteoarthritis. Clin Radiol. 1999;54(8):502-6.

Ahmed AM, Burke DL. In-vitro measurement of static pressure distribution in synovial joints—part 1: tibial surface of the knee. J Biomech Eng 1983; 105(3): 216–225.

Ahn JH, Wang JH, Yoo JC, Noh HK, Park JH. A pull-out suture for transection of the posterior horn of the medial meniscus: using a posterior trans-septal portal. Knee Surg Sports Traumatol Arthrosc 2007;15:1510–1513

Ahn JH, Wang JH, Lim HC, et al. Double transosseous pull out suture technique for transection of posterior horn of medial meniscus. Arch Orthop Trauma Surg 2009;129(3):387–392

Allaire R, Muriuki M, Gilbertson L, Harner CD. Biomechanical consequences of a tear of the posterior root of the medial meniscus: similar to total meniscectomy. J Bone Joint Surg Am. 2008;90(9):1922-1931.

Amano Y, Ozeki N, Matsuda J, Nakamura T, Nakagawa Y, Sekiya I, Koga H. Augmentation of a Nonanatomical Repair of a Medial Meniscus Posterior Root Tear With Centralization Using Three Knotless Anchors May Be Associated With Less Meniscal Extrusion and Better Compressive Load Distribution in Mid-Flexion Compared With Non-Anatomical Root Repair Alone in a Porcine Knee Model. Arthroscopy. 2023;39(12):2487-2498

Andrews SHJ, Adesida AB, Abusara Z, Shrive NG. Current concepts on structure-function relationships in the menisci. Connect Tissue Res. 2017;58(3-4):271-281.

Andrialovanirina N, Ponton D, Behivoke F, Mahafina J. A powerful method for measuring fish zie of small-scale fishery catches using Image J. Fisheries Research. 2020;223:105425

Arnoczky SP. Gross and vascular anatomy of the meniscus and its role in meniscal healing, regeneration and remodeling. In: Mow VC, Arnoczky SP, Jackson DW, eds. Knee Meniscus: Basic and Clinical Foundations. New York, NY: Raven Press; 1992:1-14

Aspden RM, Yarker YE, Hukins D. Collagen orientations in the meniscus of the knee joint. Journal of anatomy. 1985;140(Pt 3):371.

Athanasiou KA, Sanchez-Adams J. Engineering the Knee Meniscus. San Rafael, CA: Morgan & Claypool Publishers; 2009.

Avanzi P, Cardoni G, Zorzi C. Arthroscopic Superior Capsular Reconstruction (ASCR): All Soft Anchors Technique. Arthrosc Tech. 2023;12(3):e343-e34

Bachmaier S, Krych AJ, Smith PA, Feucht MJ, LaPrade RF, Wijdicks CA. Biomechanical Performance of Transtibial Pull-Out Posterior Horn Medial Meniscus Root Repair Is Improved With Knotless Adjustable Suture Anchor-Based Fixation. Orthop J Sports Med 2024;12(4):23259671241239575

Banovetz MT, Roethke LC, Rodriguez AN, LaPrade RF. Meniscal Root Tears: A Decade of Research on their Relevant Anatomy, Biomechanics, Diagnosis, and Treatment. Arch Bone Jt Surg. 2022;10(5):366-380

Baratz ME, Fu FH, Mengato R. Meniscal tears: the effect of meniscectomy and of repair on intraarticular contact areas and stress in the human knee. A preliminary report. Am J Sports Med. 1986;14(4):270-275

Becher C, Huber R, Thermann H, Paessler HH, Skrbensky G. Effects of a contoured articular prosthetic device on tibiofemoral peak contact pressure: a biomechanical study. Knee Surg Sports Traumatol Arthrosc. 2008;16(1):56-63.

Berthiaume MJ, Raynauld JP, Martel-Pelletier J, Labonté F, Beaudoin G, Bloch DA, Choquette D, Haraoui B, Altman RD, Hochberg M, Meyer JM, Cline GA, Pelletier JP. Meniscal tear and extrusion are strongly associated with progression of symptomatic knee osteoarthritis as assessed by quantitative magnetic resonance imaging. Ann Rheum Dis. 2005;64(4):556-63.

Bertsch C, Rosenbaum D, Claes L. Intra-articular and plantar pressure distribution of the ankle joint complex in relation to foot position. Unfallchirurg. 2001;104:426–433.

Bin S-I, Kim J-M, Shin S-J. Radial tears of the posterior horn of the medial meniscus. Arthroscopy. 2004;20(4):373-378

Bisson LJ, Manohar LM. A biomechanical comparison of the pullout strength of No. 2 FiberWire suture and 2-mm FiberWire tape in bovine rotator cuff tendons. Arthroscopy 2010;26(11):1463–68

Boksh K, Haque A, Sharma A, Divall P, Singh H. Use of Suture Tapes Versus Conventional Sutures for Arthroscopic Rotator Cuff Repairs: A Systematic Review and Meta-Analysis. Am J Sports Med 2022;50(1):264-272

Boksh K, Shepherd DET, Espino DM, Ghosh A, Aujla R, Boutefnouchet T. Centralization reduces meniscal extrusion, improves joint mechanics and functional outcomes in patients undergoing meniscus surgery: A systematic review and meta-analysis. Knee Surg Sports Traumatol Arthrosc. 2024a. doi: 10.1002/ksa.12410. Online ahead of print.

Boksh K, Martins A, Elbashir M, Aujla R, Boutefnouchet T. Modified Mason-Allen vs Two Simple Stitch Fixation for Medial Meniscus Posterior Root Tears: A Systematic Review and Meta-analysis. Am J Sports Med. 2024b;52(7):1877-1887

Bonasia DE, Pellegrino P, D'Amelio A, Cottino U, Rossi R. Meniscal root tear repair: why, when and how? Orthop Rev. 2015;7(2):5792.

Brantigan OC, Voshell AF. The mechanics of the ligaments and menisci of the knee joint. J Bone Joint Surg Am. 1941;23:44-66.

Brindle T, Nyland J, Johnson DL. The meniscus: review of basic principles with application to surgery and rehabilitation. J Athl Train. 2001;36(2):160–169

Brown TD, Shaw DT. In vitro contact stress distributions on the femoral condyles J Orthop Res. 1984;2:190-199

Bullough PG, Munuera L, Murphy J, Weinstein AM. The strength of the menisci of the knee as it relates to their fine structure. J Bone Joint Surg Br. 1970;52(3):564-567

Burgess R, Elder S, McLaughlin R, Constable P. In vitro biomechanical evaluation and comparison of FiberWire, FiberTape, OrthoFiber, and nylon leader line for potential use during extraarticular stabilization of canine cruciate deficient stifles. Vet Surg 2010;39(2):208–215

Carreau JH, Sitton SE, Bollier M. Medial meniscus root tear in the middle aged patient: a case based review. Iowa Orthop J. 2017;37:123-132.

Cerminara AJ, LaPrade CM, Smith SD, Ellman MB, Wijdicks CA, LaPrade RF. Biomechanical evaluation of a transtibial pull-out meniscal root repair: challenging the bungee effect. Am J Sports Med. 2014;42(12):2988-2995.

Chang PS, Radtke L, Ward P, Brophy RH. Midterm outcomes of Posterior Medial Meniscus Root Tear: A Systematic Review. Am J Sports Med. 2022;50(2):545-553

Chung KS, Choi CH, Bae TS, Ha JK, Jun DJ, Wang JH, Kim JG. Comparison of Tibiofemoral Contact Mechanics After Various Transtibial and All-inside Fixation Techniques for Medial Meniscus Posterior Root Radial Tears in a Porcine Model. Arthroscopy. 2018;34(4):1060-1068

Chung KS, Ha JK, Ra HJ, Kim JG. A meta-analysis of clinical and radiographic outcomes of posterior horn medial meniscus root repairs. Knee Surg Sports Traumatol Arthrosc. 2016;24(5):1455-1468.

Chung KS, Ha JK, Ra HJ, Nam GW, Kim JG. Pullout fxation of posterior medial meniscus root tears: correlation between meniscus extrusion and midterm clinical results. Am J Sports Med. 2017;45(1):42–9.

Conte S, Bergeron R, Gonyou H, Brown J, Rioja-Lang FC, Connor L, Devillers N. Measure and characterization of lameness in gestating sows using force plate, kinematic, and accelerometer methods1. J Anim Sci. 2014;92(12):5693–703.

Cooper DE, Arnoczky SP, Warren RF. Meniscal repair. Clin Sports Med. 1991;10(3):529–548

Costa CR, Morrison WB, Carrino JA. Medial meniscus extrusion on knee MRI: is extent associated with severity of degeneration or type of tear? AJR Am J Roentgenol. 2004;183(1):17-23.

Crawford MD, Hellwinkel JE, Aman Z, Akamefula R, Singleton JT, Bahney C, LaPrade RF. Microvascular anatomy and intrinsic gene expression of menisci from young adults. Am J Sports Med. 2020;48(13):3147–3153.

Crema MD, Roemer FW, Felson DT, Englund M, Wang K, Jarraya M, Nevitt MC, Marra MD, Torner JC, Lewis CE, Guermazi A. Factors associated with meniscal extrusion in knees with or at risk for osteoarthritis: the Multicenter Osteoarthritis study. Radiology. 2012;264(2):494-503.

Cruz RS, Ferrari BT, Mestsavaht L, LaPrade RF. Understanding posterior medial meniscus root lesions: from basic science to treatment. Rev Bras Ortop 2017;52(4):463-472

Daney BT, Aman ZS, Krob JJ, Storaci HW, Brady AW, Nakama G, Dorrnan GJ, Provencher MT, LaPrade RF.. Utilization of Transtibial Centralization Suture Best Minimizes Extrusion and Restores Tibiofemoral Contact Mechanics for Anatomic Medial Meniscal Root Repairs in a Cadaveric Model. Am J Sports Med. 2019;47(7):1591-1600

Dean RS, DePhillipo NN, Monson JK, LaPrade RF. Peripheral Stabilization Suture to Address Meniscal Extrusion in a Revision Meniscal Root Repair: Surgical Technique and Rehabilitation Protocol. Arthrosc Tech. 2020;9(8):e1211-e1218

Debieux P, Jimenze AE, Novaretti JV, Kaleka CC, Kriscenski DE, Astur DC, Obopilwe E, Tamburini LM, Muench LN, Cote MP, Cohen M, Coyner KJ. Medial meniscal extrusion greater than 4 mm reduces medial tibiofemoral compartment contact area: a biomechanical analysis of tibiofemoral contact area and pressures with varying amounts of meniscal extrusion. Knee Surg Sports Traumatol Arthrosc. 2021;29(9):3124-3132

DePalma AF. Diseases of the Knee. Philadelphia, PA: JB Lippincott Co; 1954.

DePhillipo N, Moatshe G, Chahla J, Aman ZS, Storaci HW, Morris ER, Robbins CM, Engebretsen L, LaPrade RF. Quantitative and qualitative assessment of the posterior medial meniscus anatomy: defining meniscal ramp lesions. Am J Sports Med. 2018;47(2):372–378.

De Sande, BV. Assessment of Fuji pre-scale films in tyre/road contact surface measurements. Engineering. 2007;1-66

Ellman MB, LaPrade CM, Smith SD, Rasmussen MT, Engebretsen L, Wijdicks CA, LaPrade RF. Structural Properties of the Meniscal Roots. Am J Sports Med. 2014;42(8):1881-1887.

Engelsohn E, Umans H, Difelice GS. Marginal fractures of the medial tibial plateau: possible association with medial meniscal root tear. Skeletal Radiol. 2007;36(1):73–6.

Espejo-Reina A, Prado-Novoa M, Espejo-Baena A, Estebanez B, Perez-Blanca A. Improved tibiofemoral contact restoration after transtibial reinsertion of the anterior root of the lateral meniscus compared to in situ repair: a biomechanical study. Int Orthop. 2023;47(10):2419-2427.

Feucht MJ, Grande E, Brunhuber J, Burgkart R, Imhoff AB, Braun S. Biomechanical evaluation of different suture techniques for arthroscopic transtibial pull-out repair of posterior medial meniscus root tears. Am J Sports Med. 2013;41:2784–2790

Feucht MJ, Grande E, Brunhuber J, Rosenstiel N, Burgkart R, Imhoff AB, Braun S. Biomechanical comparison between suture anchor and transtibial pull-out repair for posterior medial meniscus root tears. Am J Sports Med. 2014;42(1):187-193.

Feucht MJ, Grande E, Brunhuber J, Rosenstiel N, Burgkart R, Imhoff AB, Braun S. Biomechanical evaluation of different suture materials for arthroscopic transtibial pull-out repair of posterior meniscus root tears. Knee Surg Sports Traumatol Arthrosc 2015a;23(1):132-139

Feucht MJ, Kühle J, Bode G, Mehl J, Schmal H, Sudkamp NP, Niemeyer P. Arthroscopic transtibial pullout repair for posterior medial meniscus root tears: a systematic review of clinical, radiographic, and second-look arthroscopic results. Arthroscopy. 2015b;31(9):1808-1816.

Fox AJS, Bedi A, Rodeo SA. The basic science of human knee menisci: structure, composition, and function. Sports Health. 2012;4(4):340–51

Frank JM, Moatshe G, Brady AW, Dornan GJ, Coggins A, Muckenhirn KJ, Slette EL, Mikula JD, LaPrade R. Lateral meniscus posterior root and meniscofemoral ligaments as stabilizing structures in the ACL-deficient knee: a biomechanical study. Orthop J Sports Med. 2017;5(6):2325967117695756.

Fukubayashi T., Kurosawa H. The contact area and pressure distribution pattern of the knee. Acta Orthop. Scand. 1980;51:871–879.

Fuss FK. Anatomy and function of the cruciate ligaments of the domestic pig (Sus scrofa domestica): a comparison with human cruciates. J Anat. 1991 Oct;178:11-20.

Gale DR, Chaisson CE, Totterman SMS, Schwartz RK, Gale ME, Felson D. Meniscal subluxation: association with osteoarthritis and joint space narrowing. Osteoarthritis Cartilage. 1999;7(6):526-532.

Gee SM, Posner M. Meniscus anatomy and basic science. Sports Med Arthrosc Rev. 2021;29(3):e18–e23.

Geeslin AG, Civitarese D, Turnbull TL, Dornan GJ, Fuso FA, LaPrade RF. Influence of lateral meniscal posterior root avulsions and the meniscofemoral ligaments on tibiofemoral contact mechanics. Knee Surg Sports Traumatol Arthrosc. 2016;24(5):1469-1477

Ghosh P, Ingman AM, Taylor TK. Variations in collagen, non-collagenous proteins, and hexosamine in menisci derived from osteoarthritic and rheumatoid arthritic knee joints. J Rheumatol. 1975;2:100-107.

Han SB, Shetty GM, Lee DH, Chae DJ, Seo SS, Wang K.H. Unfavorable results of partial meniscectomy for complete posterior medial meniscus root tear with early osteoarthritis: a 5- to 8-year follow-up study. Arthroscopy. 2010;26(10):1326–1332

Harris ML, Morberg P, Bruce WJ, Walsh WR. An improved method for measuring tibiofemoral contact areas in total knee arthroplasty: A comparison of K-scan sensor and Fuji film. J Biomech. 1999;32(9):951-958

Hathila SB, Sarvaiya BJ, Vaniya VH, Kulkarni M. A cadaveric study indicating clinical significance of relation between area of menisci with corresponding tibial plateau and that of distance between anterior horn and posterior horn of menisci. Int J Anat Res. 2019;7(1.2):6198–6203.

Hiranaka T, Furumatsu T, Okazaki Y, et al. Clinical evaluation of suture materials for transtibial pullout repair of medial meniscus posterior root tear. Knee Surg Relat Res 2022;34:389

Homan MD, Braaten JA, Banovetz MT, Kennedy NI, LaPrade RF. Meniscal root tears: repair and salvage techniques. Joint of Cartilage and Joint Preservation. 2023;3(1):100098

Hwang BY, Kim SJ, Lee SW, Lee HE, Lee CK, Hunter DJ, Jung KA. Risk factors for medial meniscus posterior root tear. Am J Sports Med. 2012;40(7):1606-1610

Johannsen AM, Civitarese DM, Padalecki JR, Goldsmith MT, Wijdicks CA, LaPrade RF. Qualitative and quantitative anatomic analysis of the posterior root attachments of the medial and lateral menisci. Am J Sports Med. 2012;40(10):2342-7.

Kaplan DJ, Alaia EF, Dold AP, Meislin RJ, Strauss EJ, Jazrawi LM, Alaia MJ. Increased extrusion and ICRS grades at 2-year follow-up following transtibial medial meniscal root repair evaluated by MRI. Knee Surg Sports Traumatol Arthrosc. 2018. 26(9):2826-2834

Kean CO, Brown RJ, Chapman J. The role of biomaterials in the treatment of meniscal tears. PeerJ. 2017;5:e4076

Kennedy MI, Strauss M, LaPrade RF. Injury of the meniscus root. Clin Sports Med. 2020;39(1):57–68.

Kim DH, Lee GC, Kim HH, Cha DH. Correlation between meniscal extrusion and symptom duration, alignment, and arthritic changes in medial meniscus posterior root tear: research article. Knee Surg Relat Res. 2020;32(1):2.

Kim JH, Chung JH, Lee DH, Lee YS, Kim JR, Ryu KJ. Arthroscopic suture anchor repair versus pullout suture repair in posterior root tear of the medial meniscus: a prospective comparison study. Arthroscopy. 2011a;27(12):1644–53.

Kim SB, Ha JK, Lee SW, et al. Medial meniscus root tear refixation: comparison of clinical, radiologic, and arthroscopic findings with medial meniscectomy. Arthroscopy. 2011b;27(3):346-354.

Kim Y, Joo Y, Noh C, Park I. The optimal suture site for the repair of posterior horn root tears: biomechanical evaluation of pullout strength in porcine menisci. Knee Surg Relat Res. 2016;28(2):147–152

Koga H, Muneta T, Yagishita K, Watanabe T, Mochizuki T, Horie M, Nakamura T, Okawa A, Sekiya I. Arthroscopic centralization of an extruded lateral meniscus. Arthrosc Tech. 2012;1:e209-e212

Koga H, Muneta T, Watanabe T, Mochizuki T, Horie M, Nakamura T, Otabe K, Nakagawa Y, Sekiya I. Two-Year Outcomes After Arthroscopic Lateral Meniscus Centralization. Arthroscopy. 2016;32(10):2000-2008

Koga H, Watanabe T, Horie M, Katagiri H, Otabe K, Ohara T, Katakura M, Sekiya I, Muneta T. Augmentation of the pullout repair of a medial meniscus posterior root tear by arthroscopic centralization. Arthrosc Tech 2017;6:e1335–e1339.

Koga H, Nakamura T, Katagiri H, Nakagawa Y, Ozeki N, Ohara T, Shioda M, Kohno Y, Amemiya M, Sekiya I. Two-Year Outcomes After Meniscoplasty by Capsular Advancement With the Application of Arthroscopic Centralization Technique for Lateral Compartment Knee Osteoarthritis. Am J Sports Med. 2020;48(13):3154-3162

Koga H, Nakamura T, Nakagawa Y, Ozeki N, Ohara. T, Shioda M, Kohno Y, Amemiya M, Sekiya I. Arthroscopic Centralization Using Knotless Anchors for Extruded Medial Meniscus. Arthrosc Tech. 2021;10(3):e639-e645

Koh JL, Yi SJ, Ren Y, Zimmerman TA, Zhang LQ. Tibiofemoral Contact Mechanics with Horizontal Cleavage Tear and Resection of the Medial Meniscus in the Human Knee. J Bone Joint Surg Am. 2016;98(21):1829-1836

Kohno Y, Koga H, Ozeki N, Matsuda J, Mizuno M, Katano H, Sekiya I. Biomechanical analysis of a centralization procedure for extruded lateral meniscus after meniscectomy in porcine knee joints. J Orthop Res. 2022;40(5):1097-1103

Kubota R, Koga H, Ozeki N, Matsuda J, Kohno Y, Mizuno M, Katano H, Sekiya I. The effect of a centralization procedure for extruded lateral meniscus on load distribution in porcine knee joints at different flexion angles. BMC Musculoskelet Disord. 2020;21(1):205

Kurosawa H, Fukubayashi T, Nakajima H. Loadbearing mode of the knee joint: physical behavior of the knee joint with or without menisci. Clin. Orthop. 1980;283-290.

Krause WR, Pope MH, Johnson RJ, Wilder DG. Mechanical changes in the knee after meniscectomy. J Bone Joint Surg Am. 1976;58:599-604.

Krych AJ, Reardon PJ, Johnson NR, Mohan R, Peter L, Levy BA, Stuart MJ. Non-operative management of medial meniscus posterior horn root tears is associated with worsening arthritis and poor clinical outcome at 5-year follow-up. Knee Surg Sports Traumatol Arthrosc. 2017;25(2):383–9.

Krych AJ, Johnson NR, Mohan R, Dahm DL, Levy BA, Stuart MJ. Partial meniscectomy provides no benefit for symptomatic degenerative medial meniscus posterior root tears. Knee Surg Sports Traumatol Arthrosc. 2018;26(4):1117–22.

Krych AJ, Bernard CD, Kennedy NI, Tagliero AJ, Camp CL, Levy BA, Stuart MJ. Medial versus lateral meniscus root tears: is there a difference in injury presentation, treatment decisions, and surgical repair outcomes? Arthroscopy 2020;36:1135-1141.

Krych AJ, Boos AM, Lamba A, Smith PA. Clinical Outcome of Meniscus Centralization with Medial Meniscus Root Repair for the Extruded Medial Meniscus. Arthroscopy. 2024;40(5):1578-1587

LaPrade CM, Ellman MB, Rasmussen MT, James EW, Wijdicks CA, Engebretsen L, et al. Anatomy of the anterior root attachments of the medial and lateral menisci: a quantitative analysis. Am J Sports Med. 2014a;42(10):2386-92.

LaPrade CM, Jansson KS, Dornan G, Smith SD, Wijdicks CA, LaPrade RF. Altered tibiofemoral contact mechanics due to lateral meniscus posterior horn root avulsions and radial tears can be restored with in situ pull-out suture repairs. J Bone Joint Surg Am. 2014b;96(6):4710-479

LaPrade CM, James EW, Cram TR, Feagin JA, Engebretsen L, LaPrade RF. Meniscal root tears: a classification system based on tear morphology. Am J Sports Med. 2015a;43(2):363-369.

LaPrade CM, Foad A, Smith SD, Turnbull TL, Dornan GJ, Engebretsen L, Wijdicks CA, LaPrade RF.. Biomechanical consequences of a nonanatomic posterior medial meniscal root repair. Am J Sports Med. 2015b;43(4):912-20.

LaPrade CM, LaPrade MD, Turnbull TL, Wijdicks CA, LaPrade RF. Biomechanical evaluation of the transtibial pull-out technique for posterior medial meniscal root repairs using 1 and 2 transtibial bone tunnels. Am J Sports Med. 2015c;43(4):899-904.

LaPrade RF, Floyd ER, Carlson GB, Moatshe G, Chahla J, Monson JK. Meniscal root tears: Solving the silent epidemic. Journal of Arthroscopic Surgery and Sports Medicine. 2021a;2(1):47-57.

LaPrade RF, Chahla J. Evidence-based management of complex knee injuries: restoring the anatomy to achieve best outcomes. St. Louis: Elsevier; 2021b

LaPrade RF, LaPrade CM, Ellman MB, Turnbull TL, Cerminara AJ, Wijdicks CA. Cyclic displacement after meniscal root repair fixation: a human biomechanical evaluation. Am J Sports Med. 2015d;43(4):892–898.

LaPrade RF, LaPrade CM, James EW. Recent advances in posterior meniscal root repair techniques. J Am Acad Orthop Surg. 2015e;23(2):71-76.

LaPrade RF, Matheny L, Moulton S, James E, Dean C. Posterior meniscal root repairs: outcomes of an anatomic transtibial pull-out technique. Am J Sports Med. 2017;45:884–891

Leafblad ND, Smith PA, Stuart MJ, Krych AJ. Arthroscopic Centralization of the Extruded Medial Meniscus. Arthrosc Tech. 2021;10(1):e43-e48

Lee DR, Reinholz AK, Till SE, Lu Y, Camp CL, DeBerardino TM, Stuart MJ, Krych AJ. Current Reviews in Musculoskeletal Medicine: Current Controversies for Treatment of Meniscus Root Tears. Curr Rev Musculoskelet Med. 2022;15(4):231-243

Lee DW, Jang SH, Ha JK, Kim JG, Ahn JH. Meniscus root refixation technique using a modified Mason-Allen stitch. Knee Surg Sports Traumatol Arthrosc. 2013;21(3):654-7.

Lee DW, Kim MK, Jang HS, Ha JK, Kim JG. Clinical and radiologic evaluation of arthroscopic medial meniscus root tear refixation: comparison of the modified Mason-Allen stitch and simple stitches. Arthroscopy. 2014;30:1439–1446

Lee J, Lim Y, Kim K, Kim K, Song J. Arthroscopic pullout suture repair of posterior root tear of the medial meniscus: radiographic and clinical results with a 2-year follow-up. Arthroscopy. 2009;25:951–958

Lee SK, Yang BS, Park BM, Yeom JU, Kim JH, Yu JS. Medial meniscal root repair using curved guide and soft suture anchor. Clin Orthop Surg. 2018;10(1):111–5.

Lee SJ, Aadalen KJ, Malaviya P, Lorenz EP, Hayden JK, Farr J, Kang RW, Cole BJ. Tibiofemoral contact mechanics after serial medial meniscectomies in the human cadaveric knee. Am J Sports Med. 2006;34 (8), 1334–1344

Lerer DB, Umans HR, Hu MX, Jones MH. The role of meniscal root pathology and radial meniscal tear in medial meniscal extrusion. Skeletal Radiol. 2004;33(10):569-574.

Li W, Shepherd DET, Espino DM. Frequency dependent viscoelastic properties of porcine brain tissue. J Mech Behav Biomed Mater. 2020;102:103460

Liggins AB, Finlay JB. Recodring contact areas and pressures in joint interfaces. In: Little EG, editor. International Conference on Experimental Mechanics: technologoy transfer between high tech engineering and biomechanics. Limerick, Ireland: Elsevier Science Publishers BV. 1992, 71 - 88

Liggins AB, Hardie WR, Finlay JB. The spatial and pressure resolution of fuji pressure-sensitive film. Experimental Mechanics. 1995;35:166-173

Luo ZP, Berglund LJ, An KN. Validation of F-scan pressure sensor system: a technical note. J Rehabil Res Dev. 1998;35:186–191.

Magee T. MR findings of meniscal extrusion correlated with arthroscopy. J Magn Reson Imaging. 2008;28(2):466-470.

Mahmood H, Shepherd DET, Espino DM. Surface damage of bovine articular cartilage-off-bone: the effect of variations in underlying substrate and frequency. BMC Musculoskelet Disord. 2018;;19(1):384.

Makki L, Ferguson DJ, Stapelberg R. Measuring irregularity index: Comparing study cast caliper method with 2D dimensional ImageJ photogrammetry and 3D STL image measurement. APOS Trends in Orthodontics. 2017;7(6):260-266

Mameri ES, Dasari SP, Fortier LM, Verdejo FG, Gursoy S, Yanke AB, Chahla J. Review of meniscus anatomy and biomechanics. Curr Rev Musculoskelet Med. 2022;15(5):323-335

Markes AR, Hodax JD, Ma CB. Meniscus form and function. Clin Sports Med. 2020;39(1):1–12.

Martens TA, Hull ML, Howell SM. An in vitro osteotomy method to expose the medial compartment of the human knee. J Biomech Eng. 1997;119(4):379-385.

Martinelli L, Hurschler C, Rosenbaum D. Comparison of capacitive versus resistive joint contact stress sensors. Clin Orthop Relat Res. 2006;447:214-220
Marzo JM. Medial meniscus posterior horn avulsion. J Am Acad Orthop Surg. 2009;17(5):276-283.

Matthews JR, Wang J, Zhao J, Kluczynski MA, Bisson LJ. The influence of suture materials on the biomechanical behavior of suture-meniscal specimens: a comparative study in a porcine model. Knee Surg Relat Res 2020;32:42

McDermott ID, Amis AA. The consequences of meniscectomy. J Bone Jt Surg Br. 2006;88(12):1549–1556.

Mitchell R, Pitts R, Kim YM, Matava MJ. Medial meniscal root avulsion: a biomechanical comparison of 4 different repair constructs. Arthroscopy. 2016;32(1):111-119.

Mochizuki Y, Kawahara K, Samejima Y, Kaneko T, Ikegami H, Musha Y. Short-term results and surgical technique of arthroscopic centralization as an augmentation for medial meniscus extrusion caused by medial meniscus posterior root tear. Eur J Orthop Surg Traumatol. 2021;31(6):1235-1241

Moon HK, Koh YG, Kim YC, Park YS, Jo SB, Kwon SK. Prognostic factors of arthroscopic pull-out repair for a posterior root tear of the medial meniscus. Am J Sports Med. 2012;40(5):1138-43

Morales-Avalos R, Diabb-Zavala JM, Mohamed-Noriega N, Vilchez-Cavazos F, Perelli S, Padilla-Medina JR, Torres-Gaytán AG, Huesca-Pérez HA, Erosa-Villarreal RA, Monllau JC. Effect of Injury to the Lateral Meniscotibial Ligament and Meniscofibular Ligament on Meniscal Extrusion: Biomechanical Evaluation of the Capsulodesis and Centralization Techniques in a Porcine Knee Model. Orthop J Sports Med. 2023;11(11):23259671231212856

Mow V, Fithian D, Kelly M. Fundamentals of articular cartilage and meniscus biomechanics. In: Ewing JW, ed. Articular Cartilage and Knee Joint Function: Basic Science and Arthroscopy. New York, NY: Raven Press; 1989:1-18

Mueller BT, Moulton SG, O'Brien L, LaPrade RF. Rehabilitation following meniscal root repair: A clinical commentary. journal of orthopaedic & sports physical therapy. 2016;46(2):104-113.

Muir H. The structure and metabolism of mucopolysaccharides (glycosaminoglycans) and the problem of the mucopolysaccharidoses. Am J Med. 1969;47(5):673-690.

Muriuki MG, Tuason DA, Tucker BG, Harner CD. Changes in tibiofemoral contact mechanics following radial split and vertical tears of the medial meniscus an in vitro investigation of the efficacy of arthroscopic repair. J Bone Joint Surg Am. 2011;93(12):1089-1195

Nakagawa Y, Ozeki N, Koga H. A narrative review of lateral meniscus root tears and extrusion: techniques and outcomes. Ann Jt. 2022;15;7:15.

Nakama GY, Aman ZS, Storaci HW, Kuczmarski AS, Krob JJ, Strauss MJ. Different Suture Materials for Arthroscopic Transtibial Pull-out Repair of Medial Meniscal Posterior Root Tears: A Human Biomechanical Study. Orthop J Sports Med. 2019;7(9):2325967119873274

Nakamura T, Linde MA, Marshall BD, Koga H, Muneta T, Smolinski P, Fu FH. Arthroscopic centralization restores residual knee laxity in ACL-reconstructed knee with a lateral meniscus defect. Knee Surg Sports Traumatol Arthrosc. 2019;27(11):3699–704.

Neogi DS, Kumar A, Rijal L, Yadav CS, Jaiman A, Nag HL. Role of nonoperative treatment in managing degenerative tears of the medial meniscus posterior root. J Orthop Traumatol. 2013;14(3):193–199.

Nicholas SJ, Golant A, Schachter AK, Lee SJ. A new surgical technique for arthroscopic repair of the meniscus root tear. Knee Surg Sports Traumatol Arthrosc 2009;17(12):1433–1436

Okimura S, Mae T, Tachibana Y, Iuchi R, Nakata K, Yamashita T, Shino K. Biomechanical comparison of meniscus suture constructs for pullout repair of medial meniscus posterior root tears. J Exp Orthop. 2019;6(1):17

Oláh T, Cai X, Michaelis JC, Madry H. Comparative anatomy and morphology of the knee in translational models for articular cartilage disorders. Part I: Large animals. Ann Anat. 2021;235:151680

Ostermeier S, Holst M, Hurschler C, Windhagen H, Stukenborg-Colsman C. Dynamic measurement of patellofemoral kinematics and contact pressure after lateral retinacular release: an in vitro study. Knee Surg Sports Traumatol Arthrosc. 2007;15(5):547–554

Otto JK, Brown TD, Callaghan JJ. Static and dynamic response of a multiplexed-array piezoresistive contact sensor. Experimental Mechanics. 1999;39:317–323.

Ozeki N, Koga H, Matsuda J, Kohno Y, Mizuno M, Katano H, Tsuji K, Saito T, Muneta T, Sekiya I. Biomechanical analysis of the centralization procedure for extruded lateral menisci with posterior root deficiency in a porcine model. J Orthop Sci. 2020;25(1):161-166

Ozkoc G, Circi E, Gonc U, Irgit K, Pourbagher A, Tandogan RN. Radial tears in the root of the posterior horn of the medial meniscus. Knee Surg Sports Traumatol Arthrosc. 2008;16(9):849–854.

Pache S, Aman ZS, Kennedy MI, Nakama G, Moatshe G, Ziegler C, LaPrade R. Meniscal root tears: current concepts review. Arch Bone Jt Surg. 2018;6:250–259.

Padalecki JR, Jansson KS, Smith SD, Dornan GJ, Pierce CM, Wijdicks CA, LaPrade RF. Biomechanical consequences of a complete radial tear adjacent to the medial meniscus posterior root attachment site: in situ pull-out repair restores derangement of joint mechanics. Am J Sports Med. 2014;42(3):699-707

Park HJ, Chang MJ, Cho HJ, Hong E, Kim TW, Chang CB, Bae TS, Kwak DS, Kang SB. Medial meniscus posterior root repair restores contact pressure and contact area to its native state even after opening-wedge high tibial osteotomy: A cadaveric biomechanical study. Arthroscopy. 2023;39(3):638-646

Pasic N, Storaci H, Guzman R, Debaun M, Maruyama M, Hall K, Salazar BP, Dragoo JL. A Biomechanical Comparison of All-Inside Versus Transtibial Meniscus Root Repair Techniques. Am J Sports Med. 2023;51(9):2366-2373.

Patel R, Eltgroth M, Souza R, Zhang CA, Majumdar S, Link TM, Motamedi D. Loaded versus unloaded magnetic resonance imaging (MRI) of the knee: effect on meniscus extrusion in healthy volunteers and patients with osteoarthritis. Eur J Radiol Open. 2016;3:100–107

Pereira H, Fatih Cengiz I, Gomes S, Espregueira-Mendes J, Ripoll PL, Monllau JC, Reis RL, Oliveira JM. Meniscal allograft transplants and new scaffolding techniques. EFORT Open Rev. 2019;4(6):279–295.

Petersen W, Forkel P, Feucht MJ, Zantop T, Imhoff AB, Brucker PU. Posterior root tear of the medial and lateral meniscus. Arch Orthop Trauma Surg. 2014;134:237–255

Petersen W, Tillmann B. Collagenous fibril texture of the human knee joint menisci. Anat Embryol (Berl). 1998;197:317-324.

Proffen BL, McElfresh M, Fleming BC, Murray MM. A comparative anatomical study of the human knee and six animal species. Knee. 2012;19(4):493-499

Robinson JR, Frank EG, Hunter AJ, Jermin PJ, Gill HS. The Strength of Transosseous Medial Meniscal Root Repair Using a Simple Suture Technique Is Dependent on Suture Material and Position. Am J Sports Med 2018;45(4):924-932

Robinson JR, Hernandez BA, Taylor C, Gill HS. Knotless Anchor Fixation for Transosseous Meniscal Root Repair Using Suture Tape Is Inferior Compared With Button or Screw Fixation: A Biomechanical Study. Orthop J Sports Med. 2020;8(4):2325967120912185

Rosenbaum D, Eils E, Hillmann A. Changes in talocrural joint contact stress characteristics after simulated rotationplasty. J Biomech. 2003;36:81–86.

Rosslenbroich SB, Borgmann J, Herbort M, Raschke MJ, Peterson W, Zantop T. Root tear of the meniscus: biomechanical evaluation of an arthroscopic refixation technique. Arch Orthop Trauma Surg. 2013;133(1):111-115

Saengpetch N, Noowan S, Boonrod A, Jaruwanneechai K, Sumanont S, Vijittrakarnrung C. Comparison of medial tibiofemoral joint mechanics between all-suture anchors and transtibial pullout technique for posterior medial meniscal root tears. J Orthop Surg Res. 2023;18(1), 591

Salata MJ, Gibbs AE, Sekiya JK. A systematic review of clinical outcomes in patients undergoing meniscectomy. Am J Sports Med. 2010;38(9):1907–16.

Saltzman BM, Habet NA, Rao AJ, Trofa DP, Corpus KT, Yeatts NC, Odum SM, Garcia JCC, Varkey DT, Piasecki DP, Fleischli JE. Biomechanical Evaluation of an All-Inside Posterior Medial Meniscal Root Repair Technique Via Suture Fixation to the Posterior Cruciate Ligament. Arthroscopy, 2020;36(9):2488-2497

Schillhammer CK, Werner FW, Scuderi MG, Cannizzaro JP. Repair of lateral meniscus posterior horn detachment lesions: a biomechanical evaluation. Am J Sports Med. 2012;40(11):2604–2609.

Seo JH, Li G, Shetty GM, Kim JH, Bae JH, Jo ML, Kim JS, Lee SJ, Nha KW. Effect of repair of radial tears at the root of the posterior horn of the medial meniscus with the pullout suture technique: a biomechanical study using porcine knees. Arthroscopy. 2009;25(11):1281–1287.

Seedhom BB, Hargreaves DJ. Transmission of the load in the knee joint with special reference to the role in the menisci: part II. Experimental results, discussion and conclusion. Eng Med. 1979;8:220-228.

Shi Q, Wang H, He K, Tao M, Cheng CK. Comparison of the morphology of the anterior cruciate ligament and related bony structures between pigs and humans. Front Vet Sci. 2022;18;9:1045785.

Simonian PT, Sussmann PS, van Trommel M, Wickiewicz TL, Warren RF. Popliteomeniscal fasciculi and lateral meniscal stability. Am J Sports Med. 1997;25(6):849–853.

Śmigielski R, Becker R, Zdanowicz U, Ciszek B. Medial meniscus anatomy—from basic science to treatment. Knee Surg, Sports Traumatol, Arthrosc. 2014;23(1):8–14

Smith NA, Costa ML, Spalding T. Meniscal allograft transplantation: rationale for treatment. Bone Joint J. 2015;97(5):590-594

Starke C, Kopf S, Grobel KH, Becker R. The effect of a nonanatomic repair of the meniscal horn attachment on meniscal tension: a biomechanical study. Arthroscopy. 2010;26(3):358-365.

Suzuki T, Hashisdate H, Fujisawa Y, Yatsunami M, Ota T, Shimizu N, Betsuyaku T. Reliability of measurement using Image J for reach distance and movement angles in the functional reach test. J Phys Ther Sci. 2021;33(2):112-117.

Svensson F, Felson D, Turkiewicz A, Guermazi A, Roemer FW, Neuman P, Englund M. Scrutinizing the cut-off for “pathological” meniscal body extrusion on knee MRI. Eur Radiol. 2019;29(5):2616–2623

Tagliero AJ, Kurian EB, LaPrade MD, Song BM, Saris DBF, Stuart MJ, et al. Arthritic progression secondary to meniscus root tear treated with knee arthroplasty demonstrates similar outcomes to primary osteoarthritis: a matched case-control comparison. Knee Surg Sports Traumatol Arthrosc. 2021;29(6):1977–82.

Takahashi T, Takeshita K. Biomechanical Comparison of Two Different Sutures for the Tensile Strength of the Pullout Repair of Posterior Meniscal Root Tear. Cureus 2023;15(7):e42378

Takroni T, Laouar L, Adesida A, Elliott JAW, Jomha NM. Anatomical study: comparing the human, sheep and pig knee meniscus. J Exp Orthop. 2016;3(1)35

Thambyah A, Goh JC, De SD. Contact stresses in the knee joint in deep flexion. Med Eng Phys 2005; 27(4): 329–335.

Thompson WO, Thaete FL, Fu FH, Dye SF. Tibial meniscal dynamics using three-dimensional reconstruction of magnetic resonance imaging. Am J Sports Med. 1991;19:210-216.

Ueki H, Kanto R, DiNenna M, Linde MA, Fu FH, Smolinski P. Arthroscopic centralization reduces extrusion of the medial meniscus with posterior root defect in the ACL reconstructed knee. Knee Surg Sports Traumatol Arthrosc. 2023;31(2):543-550

van der Lelij TJN, Gerritsen LM, van Arkel ERA, Munnik-Hagewoud R, Zuurmond RG, Keereweer S et al The role of patient characteristics and the effects of angiogenic therapies on the microvasculature of the meniscus: a systematic review. Knee. 2022;38: 91–106

Vyas D, Harner CD. Meniscus root repair. Sports Med. Arthrosc. 2012;20(2):86-94

Walker PS, Erkman MJ. The role of the meniscus in force transmission across the knee. Clin Orthop Relat Res. 1975;109:184-192.

Wang Y, Wluka AE, Pelletier JP, Martel-Pelletier J, Abram F, Ding C, Cicuttini FM. Meniscal extrusion predicts increases in subchondral bone marrow lesions and bone cysts and expansion of subchondral bone in osteoarthritic knees. Rheumatology (Oxford). 2010;49(5):997-1004.

Wieser K, Farshad M, Vlachopoulos L, Ruffieux K, Gerber C, Meyer DC. Suture slippage in knotless suture anchors as a potential failure mechanism in rotator cuff repair. Arthroscopy. 2012;28:1622–1627.

Wilson DR, Apreleva MV, Eichler MJ, Harrold FR. Accuracy and repeatability of a pressure measurement system in the patellofemoral joint. J Biomech. 2003;36:1909–1915.

Wirz D, Becker R, Li SF, Friederich NF, Muller W. Validation of the Tekscan system for statistic and dynamic pressure measurements of the human femorotibial joint. Biomed Tech (Berl). 2002;47(7-8): 195-201

Wu SH, Yeh TT, Hsu WC, Wu ATH, Li G, Chen CH, Lee CH, Wu JL. Biomechanical comparison of four tibial fixation techniques for meniscal root sutures in posterior medial meniscus root repair: A porcine study. J Orthop Translat. 2020; 17(24):144-149

Wu TY. Arthroscopic medial meniscus posterior root repair with centralization using knotless suture anchors. Arthrosc Tech. 2022;11(4):e661–e668

Yamamoto T, Taneichi H, Seo Y, Yoshikawa K. MRI-based kinematics of the menisci through full knee range of motion. J Orthop Surg (Hong Kong). 202;29(2):23094990211017349

Yao JQ, Seedhom BB. A new technique for measuring contact areas in human joints--the '3S technique'. Proc Inst Mech Eng H. 1991;205(2):69-72.

Yao J, Lancianese SL, Hovinga KR, Lee J, Lerner AL. Magnetic resonance image analysis of meniscal translation and tibio-menisco-femoral contact in deep knee flexion. J Orthop Res. 2008;26(5):673-84.

Yokoi H, Mae T, Iuchi R, Take Y, Tachibana Y, Shimomura K, Ohori T, Shino K, Yoshikawa H, Nakata K.. Novel flat and wide meniscal repair material improves the ultimate load of knot breakage in a porcine trans-capsular meniscal repair model. J Exp Orthop. 2017;4(1):41

Zdanowicz U, Śmigielski R, Espejo-Reina A, Espejo-Baena A, Madry H. Anatomy and vascularisation. Berlin: Springer Berlin Heidelberg; 2016. pp. 15–21

Appendix 1 – MATLAB written file for pressure maps for the low and super low Fujifilm pressure films

```
image_file_super_low = enter knee state.png'; % Super Low Pressure Image
image_super_low_rgb = imread(image_file_super_low);
image_super_low_gray = rgb2gray(image_super_low_rgb);

image_file_low = 'enter knee state.png'; % Low Pressure Image
image_low_rgb = imread(image_file_low);
image_low_gray = rgb2gray(image_low_rgb);

% Super Low Pressure Fujifilm (0.5 to 2.5 MPa)
pixel_values_super_low = [244, 217, 187, 163, 145, 119, 96, 89]; % Example data
pressure_values_super_low = [0.5, 0.75, 1, 1.25, 1.5, 1.75, 2, 2.5]; % Pressure range for super low

% Low Pressure Fujifilm (2.5 to 10 MPa)
pixel_values_low = [244, 217, 187, 163, 145, 119, 96, 89]; % Example data
pressure_values_low = [2.5, 3.5, 4.5, 5.5, 6.5, 7.5, 8.5, 10]; % Pressure range for low pressure

% Super Low Pressure
image_super_low_double = double(image_super_low_gray);
pressure_image_super_low = interp1(pixel_values_super_low, pressure_values_super_low,
image_super_low_double, 'linear', 'extrap');

image_low_double = double(image_low_gray);
pressure_image_low = interp1(pixel_values_low, pressure_values_low, image_low_double, 'linear', 'extrap');

combined_pressure_map = pressure_image_super_low;
combined_pressure_map(isnan(pressure_image_super_low)) =
pressure_image_low(isnan(pressure_image_super_low));

figure;
imagesc(combined_pressure_map);
colorbar;
title('Combined Pressure Map: Super Low and Low Pressure Fujifilm');
xlabel('X Pixels');
ylabel('Y Pixels');
caxis([0.5 10]); % Combined pressure range from 0.5 to 10 MPa

colormap(turbo); % Use the 'turbo' colormap for better color differentiation

c = colorbar;
c.Label.String = 'Pressure (MPa)';
```

Appendix 2 – MATLAB written file for contact area for each testing state part 1

```
image_file = 'intact meniscus 60 loaded .png'; % Replace with the actual image path
image = imread(image_file);

[image_height_pixels, image_width_pixels, ~] = size(image);

physical_width_mm = 18; % mm
```

```
physical_height_mm = 40; % mm

pixel_size_width_mm = physical_width_mm / image_width_pixels; % Width in mm/pixel
pixel_size_height_mm = physical_height_mm / image_height_pixels; % Height in mm/pixel

fprintf('Pixel Size (Width): %.5f mm/pixel\n', pixel_size_width_mm);
fprintf('Pixel Size (Height): %.5f mm/pixel\n', pixel_size_height_mm);

fprintf('Image Resolution: %d x %d pixels\n', image_width_pixels, image_height_pixels);
```

pixel size (width): 0.09474mm/pixel
Pixel size (height): 0.12658 mm/pixel =
Image resolution: 190 x 316 pixels

Appendix 3 – MATLAB written file for contact area for each testing state part 2

```
image_file = 'intact meniscus 60 loaded.png'; % Replace with the actual image path
image = imread(image_file);

image_gray = rgb2gray(image);

contact_threshold = 50;

contact_mask = image_gray > contact_threshold;

pixel_size_mm2 = 0.09474 * 0.12658; % Width (mm/pixel) * Height (mm/pixel)

contact_area_mm2 = num_contact_pixels * pixel_size_mm2; % Contact area in mm²

figure;
imshow(contact_mask);
title('Contact Area Mask');

fprintf('Contact Area: %.2f mm²\n', contact_area_mm2)
```

Contact area: 711.89 mm^2